広島大学学位請求論文

Structure biological study on the peptidyl-prolyl *cis-trans* isomerization mechanism

（プロリンペプチド結合異性化機構の構造生物学的研究）

2014 年

広島大学大学院理学研究科
数理分子生命理学専攻

徐　宁

目　次

１．主論文

Structure biological study on the peptidyl-prolyl *cis-trans* isomerization mechanism
(プロリンペプチド結合異性化機構の構造生物学的研究)
著者　Ning Xu
(徐　宁)

２．公表論文

(1) The C113D mutation in human Pin1 causes allosteric structural changes in the phosphate binding pocket of the PPIase domain through the tug of war in the dual-histidine motif
(ヒト Pin1 タンパク質 C113D 変位は二重ヒスチジンモチーフ中の綱引きによりアロステリックに PPIase ドメインのリン酸基結合ポケット構造を変化させる)
著者　Xu,N., Tochio,N., Wang,J., Tamari,Y., Uewaki,J., Utsunomiya-Tate,N., Igarashi,K., Shiraki,T., Kobayashi,N., and Tate,S.
(徐　宁, 栃尾尚哉，王　静，玉利　佑，上脇準一，楯（宇都宮）直子，五十嵐和彦，白木琢磨，小林直宏，楯　真一)
(学会誌) *Biochemistry*, **53** (34), (2014), 5568-5578.

主論文

Structure biological study on the peptidyl-prolyl *cis-trans* isomerization mechanism

Contents

Page

Abbreviations

NMR: Nuclear magnetic resonance

pSer/pThr-Pro: phosphorylated Serine/Threonine-Proline

FKBP: FK506-binding protein

E. coli: Escherichia coli

ITC: Isothermal titration calorimetry

H/D exchange: Hydrogen/deuterium exchange

CD: Circular dichroism

hNOE: heteronuclear overhauser effect

PCR: Polymerase chain reaction

PEI: Polyethylenimine

PEG: Polyethylene glycol

IPTG: Isopropyl ß-D-1-thiogalactopyranoside

PDB: Protein data bank

BMRB: Biological magnetic resonance bank

EXSY: Exchange spectroscopy

Chapter I

General Introduction

Protein posttranslational modifications are essential in mediating protein biological functions in living cells [1, 2]. Protein posttranslational modifications include phosphorylation [3, 4], peptidyl-prolyl *cis-trans* isomerization and so on [5-7]. Peptidyl-prolyl (X-Pro, X means any amino acid) has *cis* and *trans* configurations in proteins [8]. In *cis* configuration, the dihedral angle (ω) formed by Cα-C-N-$C\alpha_{+1}$ is about 0º, while ω is close to 180º in *trans* configuration. *Trans* configuration has less energy than *cis* [9] and thus *trans* configuration of the peptidyl-prolyl is dominant in proteins. However, there are still about 5.2-6.5% X-Pro peptide bonds with *cis* configuration in proteins [10-12]. Previous studies have demonstrated that peptidyl-prolyl *cis-trans* isomerization has a very important role in regulating numerous cellular processes containing protein folding, ligand selection, ion-channel gating, phage infection, structural stability maintenance, cellular signal transduction and so on [9, 13-15]. Given the significance of peptidyl-prolyl *cis-trans* isomerization, the detailed biological functions and catalytic mechanisms for peptidyl-prolyl *cis-trans* isomerization will be discussed in the following sections.

1. The biological functions of peptidyl-prolyl *cis-trans* isomerization

Peptidyl-prolyl cis-trans isomerization in protein folding

Proline residue has only one hydrogen atom connected with nitrogen. When X-Pro peptide bond is formed, proline nitrogen has no hydrogen and cannot role as hydrogen bond donor in proteins. Therefore, proline acts as a disruptor for protein secondary structure [16]. In α-helix, hydrogen bond is formed by the amide group of one residue and the carbonyl oxygen of the sequentially fourth residue. Obviously, proline cannot exist in the middle of α-helix and often locates as the first residue of α-helix. In ß-sheet, proline only roles as hydrogen bond acceptor. Proline often exists in ß-turn [17, 18], which is used to connect the α-helix and ß-sheet in the protein.

Due to the specialty of the proline residue in protein structure, peptidyl-prolyl *cis-trans* isomerization is critical for protein folding [19, 20]. Ribonuclease A has some folding phases and four prolines [19, 21-24]; thus, it is often used to study the relationship between peptidyl-prolyl *cis-trans* isomerization and protein folding. P93 and P114 are in the *cis* configuration of Ribonuclease A [25]. *Trans* configuration of P93 and P114 will alleviate the protein conformational folding ability, especially P93 with *trans* configuration resulted in drastic reduced folding rate [19, 21, 26]. Additionally, the conformational change for P117 from *trans* to the *cis* configuration in Ribonuclease A also affected the rate of protein folding [19, 21]. These studies have shown that peptidyl-prolyl with own unique arrangement is necessary for protein folding. Previous studies revealed that folding of some other proteins were also affected by peptidyl-prolyl *cis-trans* isomerization, such as Ribonuclease T1 [27, 28]. Wedemeyer and colleagues suggested that peptidyl-prolyl *cis-trans* isomerization destroyed the formation of hydrogen

bonds that was thought to be critical for protein structure and thus changed the protein folding rate [19].

Peptidyl-prolyl cis-trans isomerization in ligand selection

Proline is commonly found in loops of proteins [29]. Some protein loops interact with ligands [30]. Therefore, it is possible that the proline is involved in interacting with ligands. The interaction between protein and ligands is dependent on hydrogen bonds, van der Waals forces, and other forces [31, 32]. Peptidyl-prolyl *cis-trans* isomerization could induce local structural and hydrogen bonds changes, thus may affect the protein-ligand interaction. Peptidyl-prolyl *cis-trans* isomerization may be one potential mechanism for regulating the protein-ligand interaction.

Src homology 2 (SH2) domain belongs to interleukin-2 tyrosine kinase (Itk) that participates in immune response [33-35]. NMR spectrum of SH2 domain showed that some residues sequentially or spatially close to P287 had both *cis* and *trans* configurations [33]; when P287 residue was replaced by glycine, NMR spectrum showed that P287G mutant had only one conformation [33]. Solution structure of SH2 domain showed that P287 was located in the loop of SH2, and indeed P287 had both *cis* and *trans* configurations in conformers [33]. Previous studies demonstrated that SH2 with P287 in the *cis* configuration preferred to interact with neighboring SH3 domain [36, 37] while SH2 with P287 in *trans* configuration favored the motif with phosphotyrosine [36]. It is proposed that peptidyl-prolyl *cis-trans* isomerization roles to mediate ligand selection as the molecular switch [33].

Peptidyl-prolyl cis-trans isomerization in ion-channel gating

Ion channels are located at the cell membrane to regulate the ions to transfer into or out of cells. Living cells have more than 300 kinds of ion channels [38, 39], which are regulated by temperature [40, 41], pH [42-44] and other signals. Ion channels could be provided as one target for disease therapy [45, 46].

5-Hydroxytryptamine type 3 (5-HT3) receptor as an ion channel could be regulated by neurotransmitter [47]. There is a proline named P 8* existing in one loop connecting transmembrane helices [48]. NMR spectrum showed that some residues close to P 8* had both *cis* and *trans* configurations; mutation for P 8* resulted in functional loss of 5-HT3 receptor [49], which implied peptidyl-prolyl conformational change in this loop was related with ion-channel gating function [47]. It is proposed that when 5-HT3 receptor is in the open state for function, P 8* is in the *cis* configuration; while P 8* exists in *trans* configuration in the closed state of 5-HT_3 receptor [47]. Peptidyl-prolyl *cis-trans* isomerization provides a unique insight to improve our understanding for ion-channel gating on the atomic level.

Peptidyl-prolyl cis-trans isomerization in phage infection

Filamentous phage fd is one unusual virus that could infect *Escherichia coli (E. coli)* [50]. Gene-3-protein is found in the tip of phage, which was thought to be involved in infection for *E.coli* [50]. Gene-3-protein has two domains, named N1 and N2 domains that are connected by one hinge [51]. P213 is found in this hinge [51]. P213 residue was considered to affect N1 and N2 domains

interaction which was suggested to be important for infectious ability [52, 53]. It is proposed that when P123 is in the *cis* configuration, N1 and N2 domains will be close to each other, and the phage has no infectious ability; when P123 is isomerized from *cis* to *trans* configuration, N1 and N2 domains will be far from each other, and the phage is functional [13, 53]. Hence, P213 *cis-trans* isomerization is proposed to regulate the infectious ability of the phage [53].

Peptidyl-prolyl cis-trans isomerization in protein structural stability

Proteins execute biological functions depending on their unique structures. The structural stability is needful for the roles of proteins in cells. Previous studies have revealed there is a balance between structural stability and protein function [54]. Proteins with reduced structural stability are harmful to physiological processes, which could cause monogenic disease [55], Parkinson's disease and so on [56]. Peptidyl-prolyl *cis-trans* isomerization has impact on protein structural stability [13].

Up to now, the importance of peptidyl-prolyl *cis-trans* isomerization for structural stability is testified in many proteins, such as *Staphylococcus aureus* nuclease [57], G protein-coupled receptor kinase 2 (GRK2) [58]. GRK2 could phosphorylate the G protein-coupled receptor that is related with cellular growth, development and so on [59-61]. GRK2 has S670-P671 motif where S670 could be phosphorylated to form pS670-P671 [58]. Human Pin1 promotes the degradation of GRK2 with pS670-P671 motif [58]. Pin1 is momentous for performing *cis-trans* isomerization of pSer/pThr-Pro motif [62].

Thus, it is reliable that peptidyl-prolyl *cis-trans* isomerization affects structural stability of GRK2.

Peptidyl-prolyl cis-trans isomerization in cellular signal transduction

Cellular functions are precisely regulated by kinds of proteins. These proteins form the huge network in the cells. Protein-protein interaction and protein-ligand interaction will transmit the outer simulative signals into the cells and thus cells response correctly. Proteins in cellular signal transduction pathways are affected by many factors, for example, peptidyl-prolyl *cis-trans* isomerization [13, 63, 64].

Crk as a signaling protein is found to be overexpressed in many cancers [65, 66]. Crk has two SH3 domains connected by one loop containing some proline residues [67]. Peptide bond between G237 and P238 plays an important role in regulating direction of both SH3 domains [67]. When peptidyl-prolyl of G237-P328 occupies *cis* conformation, both SH3 domains interact with each other, resulting in no functional state. Contrast, in the case of *trans* configuration, both SH3 domains are not close to each other, and Crk protein recovers the ligand binding affinity [67, 68]. Therefore, peptidyl-prolyl *cis-trans* isomerization mediates Crk protein function and thus controls the cellular signal transduction.

2. The catalytic mechanisms of peptidyl-prolyl *cis-trans* isomerization

Based on the above description, we know peptidyl-prolyl *cis-trans* isomerization is significant in living cells. Therefore, it is necessary to uncover the mechanism of peptidyl-prolyl *cis-trans* isomerization. It is known that carbon-nitrogen prolyl bond has partial double bond characteristics [69, 70]. The high barrier energy results in the slow process for *cis-trans* isomerization [71, 72]. The peptidyl-prolyl *cis-trans* isomerization is accelerated by peptidyl-prolyl *cis-trans* isomerases. Enzymes with isomerase activity are separated into cyclophilins, FK506 binding proteins (FKBPs), phosphotyrosyl phosphatase activator (PTPA) and parvulins [73-76]. The detailed catalytic mechanism regulated by isomerases remains controversial. In order to explain peptidyl-prolyl *cis-trans* isomerization, nucleophilic attack mechanism and twisting amide bond mechanism were hypothesized for isomerases. Nucleophilic attack mechanism was facilitated through the formation of covalent bond between active site cysteine residue and substrate carbonyl carbon; however, twisting amide bond mechanism was not assisted by the formation of the covalent bond [77-81]. Some peptidyl-prolyl *cis-trans* isomerases might adopt the twisting amide bond mechanism [82-84]. We will discuss peptidyl-prolyl *cis-trans* isomerization mechanism based on cyclophilins, FKBPs, PTPA and parvulin subfamilies in the following sections.

Cyclophilins

Cyclophilins are widely found in many species, including mammals, bacteria and so on [85]. Here cyclophilin A (CyPA) is chosen as a representative for cyclophilins to discuss the peptidyl-prolyl *cis-trans* isomerization mechanism.

CyPA is known for binding cyclosporine A (CsA), which is a cyclic peptide inhibiting the lymphocyte activation [86-88]. Human cyclophilin A (hCyPA) could isomerize the peptidyl-prolyl bond in Itk and HIV-1 capsid proteins [36, 89]. Fischer and colleagues thought cysteine residues in CyPA possessed a role in catalytic process as a nucleophile [86]. hCyPA has four cysteines, C52, C62, C115 and C161, respectively [90]. According to the nucleophilic attack mechanism [86], these four cysteines should interact with CsA covalently; however, replacement of every cysteine with alanine did not affect the affinity for CsA, which indicated that the role of cysteine thiol as a nucleophilic group in the catalysis was not taken [90]. The positions of four cysteines were not conserved in yeast CyP sequence whilst yeast CyP still had the detectable catalytic activity [90, 91]. Thus, it is speculated that cysteine residues have another role in CyPA instead of nucleophile. Values from secondary deuterium isotope effects for cyclophilin showed that carbonyl carbon did not rehybridize from sp^2 to sp^3 in the catalytic process, which eliminated nucleophilic attack mechanism [92-94]. It was hypothesized that twisting amide bond mechanism was accepted for hCyPA [81, 95] and R55 of hCyPA was suggested to role as hydrogen bond donor for proline nitrogen to facilitate the peptidyl-prolyl *cis-trans* isomerization [96], which was evidenced by that the replacement of R55 with alanine resulted in inactive catalytic function [97]. The role of cysteine residues in hCyPA remains elusive. To analyze the detailed function of cysteine residues will improve the understanding for peptidyl-prolyl *cis-trans* isomerization.

FK506 binding proteins

FK506 binding proteins (FKBPs) are known for binding FK506 that is a chemical molecule could inhibit lymphocyte activation [98-101]. Besides peptidyl-prolyl *cis-trans* catalytic function, FKBP of archaea had chaperone-like activities [102], which implied that FKBP might have dual function in the living cells. FKBP-12 is one human FKBP, interacting with Smad7-Smurf1 [103], which indicates peptidyl-prolyl *cis–trans* isomerization may possess a role in regulating Smad7–Smurf1 complex. Complex crystal structure of FKBP and FK-506 demonstrated five hydrogen bonds existed between them [104]. The ketone carbonyl in the FK506 was perpendicular to the peptide bond plane, different from the unbound form of FK506, indicating the twisting amide mechanism may be accepted [104]. However, the position of R55 in cyclophilin was not found in FKBPs. It is speculated that the amide group of the residue following proline acts as hydrogen bond donor to form intramolecular hydrogen bond with proline nitrogen to facilitate the isomerization [81].

Phosphotyrosyl phosphatase activator

Phosphotyrosyl phosphatase activator (PTPA) regulates and activates PP2A and PP2A-like enzymes through isomerizing peptidyl-prolyl bond [105]. PTPA proteins are extensively discovered in various species, scattering from yeast to human [106, 107]. Crystal structures of human PTPA (hPTPA), yeast PTPA1 (Ypa1) and yeast PTPA2 (Ypa2) have demonstrated that hPTPA, Ypa1 and Ypa2 have the similar folds, comprising of α-helix without ß-sheet [108],

however, other three kinds of PPIases have ß-sheets in their structural core [84, 104, 109]. Complex crystal structure of Ypa1 and peptide demonstrates that peptide addition leads to forming Ypa1 protein dimer, and peptide is located in hydrophobic groove formed by dimer interaction [108]. The communication mode of PTPA and substrate is significantly different from other PPIases [108], especially ATP or analogues are not dispensable for PP2A activation [106, 107]. Although PTPA shows the importance and specialty, however, to date, the catalytic mechanism remains elusive.

Parvulins

Parvulin was first discovered in *E.coli* [110], and other parvulin proteins were found subsequently in human [111], plant [112]. So far, about 10 kinds of parvulin protein have the published structures deposited in PDB: Pin1 [113], Par14 [114, 115] from human, Pin1At from *Arabidopsis thaliana* [116], Par10 [117], SurA [118] from *E. coli*, Ess1 from *Candida albicans* [119], PrsA-PPIases from *Bacillus subtilis* [120] *and Staphylococcus aureus* [121], PinA from *Cenarchaeum symbiosum* [122], and TbPin1 from *Trypanosoma brucei* [123]. According to favored substrate specificity, the above 10 kinds of PPIases are divided into two parts: Pin1-type parvulin (Pin1, TbPin1 and Pin1At) that prefers phosphorylated substrate with pSer/pThr-Pro motif [113, 123, 124]; the other is non Pin1-type (Par14, Par10, SurA, PinA, and both PrsA-PPIases) prefers non-phosphorylated substrate [112, 121, 122, 125]. Comparison shows that parvulin proteins have significant structural changes among them. Pin1At, TbPin1, PinA, Par14, Par10 have only catalytic PPIase domain

relative to other parvulin proteins [114-117, 121, 122]. The fold of catalytic PPIase domains of all parvulins are same, comprising of four α-helices and four ß-sheets; two ß-sheets are in the center of the structure and surrounded by four α-helices [113-123]. In the structure of PrsA from *Staphylococcus aureus*, it was the first time that Heikkinen and colleagues found there was a charge relay system between His-His motif located in the structural core [121]. Based on the high resolution of Par14 crystal structure, it was concluded that extended Cys/Asp-His-His-Thr/Ser motif and corresponding hydrogen bonds were conserved in all the parvulin proteins with isomerase activity [126]. However, the detailed role of tetrad motif in the parvulins is still not known.

Human Pin1 is representative in parvulins. Pin1 consisting of 163 residues was first discovered in yeast research [111]. Pin1 protein is composed of two domains connected by a long linker, and one domain is N-terminal WW domain that is in charge of binding short proline-rich motifs of substrates; the other one is C-terminal PPIase domain whose catalytic mechanism attracted much attention in the past years [113]. The isolated WW domain showed disappeared isomerization ability, whilst the separated PPIase domain had 90% catalytic ability relative to the full-length Pin1 protein [127]. Pin1 prefers substrate with the pSer/pThr-Pro motif [113], however, due to low binding ability of PPIase domain for substrate, to date; there is no published structure for PPIase domain with natural substrates containing pSer/pThr-Pro motif to study the catalytic mechanism. In view of the complex crystal structure of Pin1 and short Ala-Pro peptide, nucleophilic addition mechanism was proposed for catalysis [113], similar with cyclophilin [86]. Pin1 has one cysteine in the

active site, called C113 [113]. Ranganathan and colleagues thought that the thiol of cysteine would attack the carbonyl carbon and form covalent bond between them to facilitate the isomerization of motif [113]. However, more and more evidences are against nucleophilic addition mechanism of Pin1. The cysteine does not seem to be essential as evidenced by that C113S and C113D mutant did not abolish catalytic activity [128]. Behrsin and colleagues suggested that C113 only maintained the overall electronegative environment for the substrate, which might prevent the formation of carbon-nitrogen double bond in the substrate [128]. However, this mechanism cannot explain the severely decreased catalytic activity of C113S and C113D because carboxyl in aspartic acid, hydroxyl in serine also could function to supply the electronegative environment for the isomerization process. One complex crystal structure of Pin1 and a specially devised inhibitor where carbonyl group was replaced by methylene that mimicked the twisted state of the substrate expressed that C113 sulfur was 4.6 angstrom distant from methylene carbon [84]. The structure also showed that the covalent bond between C113-S and carbonyl carbon was not formed in the catalytic process. Additionally, cyclohexyl ketone inhibitors showed weak inhibition of Pin1 [129]; Results from secondary kinetic isotope effects meant carbonyl carbon did not change from sp^2 to sp^3 in the catalytic process, which ruled out the nucleophilic addition mechanism [130]. Twisting amide mechanism was proposed for Pin1 [130]. Twisting amide mechanism was assisted by inter or intra hydrogen bonds. Schroeder and colleagues suggested that H59 $N^{\varepsilon 2}$-H would role as hydrogen bond donor [77]. However, complex crystal structure of Pin1 and

substrate with twisted-amide state demonstrated that there was no hydrogen bond between proline nitrogen and Pin1 atoms, which indicated that the amide group of the residue following proline acts as hydrogen bond donor to promote isomerization.

Based on the above discussion, twisting amide mechanism may be hypothesized for some peptidyl-prolyl *cis-trans* isomerases. Nucleophilic addition mechanism was suggested in the initial studies of CyPA and Pin1 [86, 113]. The reason is that CyPA and Pin1 have cysteine residue in the active site, and thiol group of cysteine could function as nucleophile. To date, nucleophilic addition mechanism was ruled out by mutagenesis, kinetic isotope effects. However, the role of cysteine in PPIases remains elusive. Replacement of cysteine resulted in decreased catalytic activity. Hence, it is necessary to uncover the role of cysteine in PPIases, and it will help us improve the understanding for detailed catalytic mechanism of PPIases.

Chapter II

The C113D mutation in human Pin1 causes allosteric structural changes in the phosphate binding pocket of PPIase domain through the tug-of-war in the dual histidine motif

Summary

Pin1 peptidyl-prolyl isomerase (PPIase) catalyzes specifically pSer/pThr-Pro motif. The peptidyl-prolyl *cis–trans* isomerization mechanism has been studied by various approaches, including X-ray crystallography, site directed mutation to identify the functionally relevant residues, and kinetic isotope effect on the isomerization. However, it still remains elusive. Preceding studies proposed that C113 in Pin1 has a catalytic role in the conformational transition process through its nucleophilic attack or hydrogen bonding to substrate carbonyl moiety. The fact that C113D mutant Pin1 does not abolish the activity challenges the importance of C113 as a catalyst. To facilitate our understanding on the Pin1 isomerization process, the structures and dynamics of the wild-type and C113D mutant Pin1 PPIase domains comprising the residues 51–163 were compared. We found that the C113D mutation disturbed the hydrogen bonds among the conserved histidine residues, H59 and H157 ("dual histidine motif"); H59 imidazole forms a tighter hydrogen bond to H157 in the wild type, whilst it has a stronger hydrogen bond to D113 in C113D

mutant. C113D mutation unbalanced the tug-of-war for H59, which eventually resulted in the altered active loop structure having basic triad residues (K63, R68 and R69) engaging in the phosphate binding. The active loop distortion could explain the severely reduced substrate binding of C113D mutant. This work demonstrated that C113 had a role in maintaining the catalytic site in an active fold, which has been never described before.

1. Introduction

Pin1 is a highly conserved peptidyl-prolyl isomerase (PPIase) that specifically catalyzes the *cis–trans* isomerization of pSer/pThr-Pro substrates, thereby regulating protein functions [131-133]. Pin1 catalyzes the intrinsically slow conversion of the peptidyl-prolyl bond from *cis* to *trans* and *vice versa,* thus "switches" their conformation, in coupled with protein kinases to Ser/Thr-Pro motif. The Pin1-mediating conformation changes following phosphorylation are believed to constitute novel transduction pathways in various phosphorylation-dependent signaling processes in cells. Disordering of Pin1 function, therefore, leads to pathogenesis of cancer and the protein folding diseases including Parkinson's and Alzheimer's diseases [134-136]. Pin1 interacts with some transcription factors that are phosphorylated in cells essentially roles in maintaining pluripotency of the induced pluripotent stem (iPS) cells and the embryonic stem (ES) cells [137].

Pin1 comprises of two domains; a catalytic domain functioning as PPIase and a WW domain that binds to pSer/pThr-Pro containing substrate [113]. The two domains are shown to interplay when Pin1 acts [138-140], whereas PPIase domain is solely responsible for isomerization activity. In fact, the isolated PPIase domain displays comparable or more activity relative to the full-length Pin1 [141], which assures the isolated PPIase domain can be used for the study of its enzyme mechanism.

Pin1 is a member of the parvulin family composing of a small PPIases. Parvulins are classified into two types in terms of substrate specificity; phosphospecific (Pin1-type) and non-phosphospecific (Par14-type) [142]; the

non-phosphospecific type parvulins consist of only PPIase without WW domain [143]. All parvulins share similar folds and conserved residues in the catalytic site in PPIase [113], which allow the structural comparisons among the parvulin PPIases for assessing the roles of each conserved catalytic site residues. The high-resolution crystal structure of human Par14 showed the four conserved residues have hydrogen bonding network running across the catalytic site [126]. The hydrogen bonding network by the four-residue motif ("catalytic tetrad") in Par14 is supposed to be conserved among all parvulin family PPIases to maintain the folding of the catalytic site [126]. The catalytic tetrad in Pin1 consists of C113-H59-H157-T152 while the Par14 counterpart is D74-H42-H123-T118. The tetrad motif sequence is, thus, represented as Cys/Asp-His-His-Thr/Ser with inclusion of the variation at fourth residue in the parvulins [126].

Pin1 catalytic mechanism on the atomic level is not well understood. The proximity of C113 to the carbonyl in the bound Ala-Pro dipeptide in the Pin1 complex crystal structure deduced the nucleophile attack catalysis by C113 (Figure II-1A) [113]. The cysteine, however, does not seem to be essential, as evidenced by that C113D and C113S mutations did not abolish the activity (Figure II-1B) [128]. Moreover, the corresponding cysteine is replaced by an aspartate in Par14-type PPIases [115, 143]. In an alternative proposition, SH group of C113 makes the hydrogen bond to the carbonyl oxygen in the substrate to disrupt the carbon-nitrogen π-bond of the amide to rotate easily [128]. This mechanism cannot clearly explain the severe activity reduction for C113S that replaces SH with OH, in considering that both groups can work as

hydrogen bond donors. An elaborate study using kinetic isotope effects demonstrated that twisting the amide bond formation lowers the transition energy for isomerization, which is facilitated by hydrogen bonding to prolyl nitrogen from the following residue amide proton in the substrate peptide [130]. The crystal structure of Pin1 with a reduced amide inhibitor bound in the active site showed the compound structure was close to the twisted amide supposed to be in transition state [84].

Molecular dynamics simulation gave the other insights into the *cis–trans* isomerization process. Hamelberg and co-worker applied molecular dynamics simulation to sample the entire conformation ensembles of the Pin1 substrate complex, with the corresponding relative binding free energies, during the *cis–trans* conversion of the substrate [144]. The theoretical work could assess the binding free energies in the substrate–Pin1 complex, which are not accessible experimentally, and showed Pin1 preferentially binds to transition state substrate having $\omega \approx 90°$ over those in *cis* or *trans* states [144]. This observation is consistent with the twisted amide bond mechanism mentioned above [130].

Hamelberg's group has also demonstrated that the PPIase domain of Pin1 in free state samples significantly wider conformations than those for the complexes with *cis* or *trans* peptide substrate [145]. They proposed that Pin1 adopt conformational selection in phosphorylated substrate recognition, with emphasizing the importance of intrinsic structural flexibility of Pin1 PPIase domain [145]. The functional relevance of the structural dynamics of PPIase domain is also emphasized experimentally: the conformation sampling may

change through the contact with WW domain in response to the substrate bound in the domain interface [138-140].

In this work, we explored the mechanism for the reduced activity of C113D Pin1 PPIase mutant with intention to improve our understanding how Pin1 isomerizes. C113D mutant has arose controversial arguments against the proposed mechanisms. C113D mutant has the catalytic tetrad motif, defined as Cys/Asp-His-His-Thr/Ser, but the mutant showed severely reduced activity. Therefore, the proposed role of the hydrogen bonding network among the tetrad in precisely positioning Cys/Asp moiety [126] does not seem valid for Pin1. In addition, the mechanism assuming C113–substrate carbonyl interaction hardly explains that C113D mutant retains activity, although it is reduced; aspartate side chain cannot be a hydrogen bond donor as thiol group is at neutral pH [128]. Exploring why C113D mutant has reduced its activity will, therefore, give us newer insights into the isomerization mechanism of Pin1, which prompted us to work on C113D mutant Pin1 PPIase domain.

The present work has shown that the reduced activity of C113D is primarily ascribed to its reduced binding to phosphate moiety in the substrate. The reduced binding could be explained by the deformed active loop comprising of three basic residues (K63, R68 and R69) that directly bond to phosphate, as evidenced by NMR structures of C113D and wild-type Pin1 PPIases. The hydrogen bonding network among two histidines (H59 and H157) within the tetrad motif was observed in both wild-type and C113D mutant Pin1 PPIase domains. The strengths of the hydrogen bonds, however, changed in the C113D mutation; H59 seems pulled to H157 in the wild type, whilst it

has a stronger hydrogen bond to D113 in C113D mutant. H59 is in the "tug-of-war" of the hydrogen bonding network between the residues at 113 and H157 among the catalytic tetrad. The unbalancing the tug-of-war by the mutation altered the active loop structure presumably by destabilizing the catalytic site fold. The structural destabilization by C113D mutation was apparent, as evidenced by the elevated chemical exchanges seen in the spin relaxation data and the increased H/D exchange rates for most of the residues in C113D mutant. We eventually emphasize that C113 roles in keeping the catalytic site in an active fold.

2. Materials and methods

2-1. Pin1 PPIase purification

The cDNA encoding the peptidyl-prolyl isomerase (PPIase) domain of human Pin1 (residues 51–163) [113] was cloned to the expression vector pET28a (Addgene). The recombinant plasmids were transformed to *Escherishia coli* strain BL21 (DE3) cells (New England Biolabs). The cells were grown in M9 minimum medium at 37°C with 50 μg/ml kanamycin to an A_{600} of 0.6. For preparing the NMR samples, $^{15}NH_4Cl$ and ^{13}C-glucose were used for nitrogen and carbon sources, respectively. The expression of the His_6-tagged protein was induced by adding isopropyl-β-thiogalactopyranoside (IPTG) to a final concentration of 0.5 mM, and the cells were further cultured for 16 h at 18°C. Cells from a 1-liter culture medium were harvested and re-suspended in 100 ml buffer solution (50 mM Tris-HCl, pH 8.0). The cells were broken by sonication and the soluble fraction was collected by the centrifugation at 14,000 rotation per min (rpm) at 4°C for 20 min. Polyethylenimine was put into the supernatant to a final concentration of 0.1% to remove the DNA and RNA contaminants by applying another centrifugation at 14,000 rpm at 4°C for 20 min. The collected supernatant was applied to TALON® column (TAKARA Bio). After the flow through to the column with the buffer solution (50 mM Tris-HCl, pH 8.0), the column was further washed with the 200 ml solution containing 50 mM Tris-HCl, pH 8.0 and 25 mM imidazole. His_6-tagged protein was eluted with the other buffer solution (50 mM Tris-HCl, pH 8.0 and 400 mM imidazole). The collected His_6-tagged protein was subjected to dialysis against 50 mM sodium phosphate buffer, pH 6.0. After the dialysis, 80-unit

thrombin protease solution (GE Healthcare) was put into the protein solution to cleave the His_6-tag from the PPIase domain fragment; the proteolysis reaction was done at 20°C for overnight. The reactant was applied to cation-exchanger column HiTrap SP FF (GE Healthcare) equilibrated with 50 mM sodium phosphate buffer, pH 6.0. PPIase domain was eluted by the NaCl gradient from 0 M to 1 M in 50 mM sodium phosphate buffer, pH 6.0, using BioLogic DuoFlow™ HPLC system (Bio-Rad). The collected fractions containing PPIase were subjected to the extensive dialysis against the desired buffer solutions according to the purposes for use.

Site directed mutation to change C113 to D113 in Pin1 PPIase domain was done by using KOD FX (TOYOBO). The purification of C113D mutant PPIase was carried out according to the same protocol described for the wild-type PPIase.

2-2. NMR spectroscopy and structure determination

The structural determination of the wild-type and C113D PPIases were done according to the standard procedure using isotope labeled samples [146]. A set of standard 3D triple-resonance data was used to assign backbone and side chain resonances. NOEs from ^{15}N edited and ^{13}C edited 3D NOESY spectra were used to generate the distance restraints in the structure calculation. All NMR data were got on a Bruker AvanceII spectrometer equipped with a triple resonance cryogenic probe operating at 700.33 MHz for ^{1}H resonance frequency. Samples concentrations for wild-type and C113D were both 0.8 mM, in 50 mM sodium phosphate (pH 6.6), 100 mM Na_2SO_4, 1 mM DTT, 0.03% NaN_3 and 5

mM EDTA. In the case of the samples in 50 mM Tris-HCl (pH 6.8), 1mM DTT, and 0.03% NaN_3 contained 0.3 mM protein for both the wild-type and the C113D mutant PPIases. All experiments were done at 299 K. NMR data were processed by NMRPipe [147], and the spectral analyses were done using the program suite KUJIRA [148] running with NMRview [149].

Structure calculation was carried out by the program CYANA 2.1 for fully automatic NOE assignments [150, 151]. The backbone dihedral angle restraints were generated by the TALOS+ program [152]. The 40 lowest-energy CYANA structures were subjected to explicit water refinement with XPLOR-NIH [153] with the distance and dihedral restraints. The final 10 XPLOR-NIH structures were validated using the program PROCHECK-NMR [154]. The structural statics for both wild-type and C113D mutant PPIase domains in the presence of sulfate and phosphate ions are provided in table II-1.

The resonance assignments and the structural data for the wild-type and C113D mutant PPIase domains in the presence of sulfate and phosphate ions are deposited in the Biological Magnetic Resonances Bank (BMRB) and the Protein Data Bank (PDB): BMRB accession codes: 11559 and 11560, PDB accession codes: 2RUC and 2RUD. BMRB accession codes for wild-type and C113D mutant PPIases in the absence of sulfate and phosphate ions are 11557 and 11558.

2-3. Isothermal titration calorimetry (ITC) experiments

ITC experiments were carried out at two temperatures, 288 K and 298 K, on a Microcal Auto-iTC200 calorimeter (GE Healthcare). Cdc25C peptide (sequence: EQPLpTPVTDL, pT represents a phosphorylated threonine) was dissolved in 50 mM Tris-HCl buffer solution (pH 6.8). The peptide was titrated into a 200 μl PPIase solution (0.1 mM protein centration, 50 mM Tris-HCl, pH 6.8); 1.5 μl of peptide solution (1.2 mM concentration) was injected at each of the total 25-time titrations. The collected data were analyzed through the software Microcal ORIGIN (GE Healthcare). Cdc25C phosphorylated peptide was purchased from a company (Funakoshi) and used without further purification.

2-4. Isomerization rate measurements

Isomerase activities for wild-type and C113D mutant PPIases were assessed by using 2D ^{1}H-^{1}H EXSY (EXchange SpectroscopY) [138, 155]. The sample contained 2 mM Cdc25C phosphopeptide with 50 μM PPIase, wild-type or C113D. The sample solution contained 50 mM Tris-HCl (pH 6.8), 1 mM DTT, and 0.03% NaN_3. The experiments were done at 295 K on a 700 MHz NMR spectrometer. The exchange times were set to 2, 5, 10, 15, 25, 35, 50 (twice), 75, 100 (twice), 200, 300, and 400 ms. The net exchange rate, k_{EX}, was estimated to fit the equation below (eq. 1) to the ratios of the *trans-to-cis* exchange cross-peaks against the trans diagonal peaks. In estimating the k_{EX} values, the buildup profiles from the signals for pT5 CH_3, pT5 HN and V7 HN were simultaneously used for fitting, as in a global fitting manner.

$$\text{ratio}\,(t_{mix}) = \frac{(1-e^{-(k_{CT}+k_{TC})t_{mix}})k_{TC}}{k_{CT}+k_{TC}\,e^{-(k_{CT}+k_{TC})t_{mix}}} \qquad (1)$$

In eq 1, k_{CT} and k_{TC} are the adjustable parameters in fitting and the net exchange rate, k_{EX}, is defined as $k_{EX} = k_{CT} + k_{TC}$, where k_{CT} and k_{TC} are the exchange rates from *cis-to-trans* and *trans-to-cis*, respectively. Uncertainties in the rate constants were estimated by using Monte Carlo simulations based on the duplicated data.

2-5. NMR spin relaxation experiments and analysis

All backbone ^{15}N R_1 and R_2 relaxation rates and steady-state heteronuclear ^{15}N NOE (hNOE) data were collected at 700 MHz NMR spectrometer at 299 K. Samples had 1.4 mM (wild-type) and 2.0 mM (C113D mutant) protein, respectively, in 50 mM sodium phosphate (pH 6.6), 5 mM EDTA, 100 mM Na_2SO_4, 1 mM DTT, and 0.03% NaN_3. In the case of the samples in 50 mM Tris-HCl (pH 6.8), 1mM DTT, and 0.03% NaN_3 contained 0.3 mM protein for both the wild-type and the C113D mutant PPIases. Each peak intensity was measured by averaging over the signal intensities at the peak center and its eight surrounding points (9-point averaging); each peak center was found by SPARKY 'pc' function (T.D. Goddard and D.G. Kneller, SPARKY 3, University of California, San Francisco). The delays for R_1 measurements were t_{relax} = 10.3 (twice), 153.9, 307.9, 461.8, 615.7 (twice), 769.6, 923.6, 1128.8, 1539.3 ms, while the delays for R_2 were t_{relax} = 0.0, 16.0 (twice), 40.0, 80.0 (twice), 160.0 ms. The spectra for R_1 and R_2 were collected in an interleaved manner. For

measuring hNOEs, we recoded an interleaved pair of spectra in which ^{1}H saturation of 3 s was applied alternatively with the relaxation delay set to 2 s.

R_1 and R_2 relaxation rate constants for each signal were determined through the function fitting using modelXY TCL built-in function of NMRPipe. Uncertainties for R_1 and R_2 were estimated in a Monte Carlo manner based on the duplicated data. The uncertainty for each hNOE value was evaluated using the root mean square deviation (rmsd) value on the spectral area having no peaks, which was gained by the NMRPipe built-in module.

The reduced spectral density functions including $J_{eff}(0)$, $J(\omega_h)$, $J(\omega_N)$ were calculated using the software suites, REALAX version 3.1.5 [156, 157]. Rotational correlation times and the rotation diffusion tensors for the wild-type and C113D mutant were determined by using the program package RotDif [158] on Matlab platform (Mathworks).

2-6. H/D exchange rate measurements

The amide proton-deuteron exchange (H/D exchange) rates were measured with extensively lyophilized samples; the sample solution (wild-type or C113D mutant PPIase in 50 mM sodium phosphate, pH 6.6, 5 mM EDTA, 100 mM Na_2SO_4, 1 mM DTT, and 0.03% NaN_3) was rapidly frozen by liquid nitrogen, then put into a vacuum chamber for about 12 h. To remove remaining protons from the sample, the above lyophilized sample was again dissolved by 100 μL D_2O (over 99.96 atom % deuterium; Sigma-Aldrich) and again lyophilized. The lyophilized sample in a plastic test tube was dissolved by the same volume of D_2O as that evaporated, just prior to a series of 2D ^{1}H-^{15}N HSQC spectra.

NMR measure was initiated within 10 min after dissolving the sample. For the case of the wild-type, one spectrum was collected for 25 min and 24 data were collected sequentially. For the C113D mutant, it took 35 min for one spectrum and the 35 spectra were measured sequentially. There were no apparent structural changes caused by lyophilize to both wild-type and C113D PPIases, which was evidenced by the NMR spectral comparison between the data before and after lyophilization. H/D exchange rate for each peak was determined through the peak intensity change according to the measuring time; time at the end of each spectral collection was used as the H/D exchange delay time for the signals on the corresponding spectrum. In functional fitting to extract the H/D exchange rate, $R_{H->D}$, the incomplete ^{1}HN exchange to ^{2}DN due to the residual protons content in D_2O solution was considered; the function in eq. 2 was, thus, used for fitting to the HN intensity profile;

$$I(t) = I_0 \exp(-R_{H \rightarrow D} t) + I_b \qquad (2)$$

where I_0, I_b, and $R_{H->D}$ are used as the adjustable parameters in fitting calculation.

2-7. R_2 relaxation dispersion experiments

Conformational exchange rates were further elucidated by using R_2 relaxation dispersion experiments using a series of ^{15}N CPMG-HSQC spectra [159]. The effective transverse relaxation rates were measured by changing the delays between 180° pulses for ^{15}N spins in CPMG loop. Total CPMG duration was kept constant at 40 ms. Samples contained 1.4 mM (wild-type) and 2.0 mM (C113D mutant) protein, respectively, in 50 mM sodium phosphate

(pH 6.6), 5 mM EDTA, 100 mM Na_2SO_4, 1 mM DTT, and 0.03% NaN_3. In the case of the samples in 50 mM Tris-HCl (pH 6.8), 1mM DTT, and 0.03% NaN_3 contained 0.3 mM protein for both the wild-type and the C113D mutant PPIases. All the experiments were carried out at 299 K on a Bruker AvanceII 700 MHz NMR spectrometer. Each peak intensity was estimated by the nine-point averaging for each cross peak with a home-written program.

Kinetic parameters were estimated by using a two-state model of the general Carver-Richards equation [160]. Functional fitting to the data was achieved by using a home-written program adopting the differential evolution optimization [161]. Uncertainties were estimated on the basis of duplicate data and Monte-Carlo approach, in which 32 data sets of each residue were generated based on an initial fit of the collected data to which Gaussian noise representing experimental uncertainties of R_2 was added. Exchanging residues were grouped according to their individual R_2 rates, and the residues in each group were subjected to the global fitting to gain the single R_2 value for all the residues in the same group. Uncertainty for the global kinetic parameter was estimated by Monte-Carlo approach.

2-8. Measuring histidine imidazole ^{15}N chemical shift changes according to the D_2O content in solution

The imidazole ^{15}N chemical shifts were measured using ^{1}H-^{15}N HSQC spectra for the sample solution containing 6%, 50% and 100% D_2O. The sample was prepared from the lyophilized protein solution with 50 mM sodium phosphate buffer (pH 6.6) and 100 mM sodium sulfate. To exclusively

eliminate the proton, the lyophilized sample was dissolved by D_2O and then subjected to further lyophilization; the procedure was repeated twice to extensively purge protons in the sample. In the final sample solution containing different amount of D_2O, 5 mM EDTA, 1 mM DTT and 0.03% NaN_3 was added. All data were collected at 299 K on a 700 MHz NMR spectrometer.

2-9. Circular Dichroism (CD) spectroscopy to monitor the heat denaturing processes of the wild-type and C113D mutant

The molar ellipticity at 222 nm was performed to monitor the structural denaturing process with a JASCO-720W spectrometer. Sample solution was consists of 50 mM sodium phosphate (pH 6.0), 100 mM Na_2SO_4, and 1 mM DTT. Protein concentration was adjusted to 2 μM for the cases of the wild-type and C113D mutant. Temperature was changed in the range of 20°C to 80°C, with increasing rate at 1°C/min.

2-10. Maleimide assay for reactivity analyses of the cysteine residues in Pin1

Maleimide assay was performed as described previously [162]. Briefly, proteins (2 μg) were incubated with various concentration of hydrogen peroxide (H_2O_2) in the presence of 1mM TCEP for 30 min at room temperature. Oxidation reaction was terminated by adding TCEP and SDS for the final concentration of 1 mM and 0.5%, respectively. Then, rhodamine-maleimide (Life Technologies) was added to the mixture to 0.2 mM final concentration,

and incubated at room temperature for 30 min. The reaction was stopped by adding SDS-PAGE sample buffer containing ß-mercaptoethanol, and proteins were separated by SDS-PAGE. Rhodamine fluorescence was visualized by image reader, RAS4000 (Fujifilm, Tokyo Japan).

2-11. Mass spectroscopic analyses of the oxidized peptides in Pin1

The wild-type Pin1 was incubated with 0.01% hydrogen peroxide in the presence of 1 mM TCEP for 30 min at room temperature. Proteins were separated from reaction ingredients by desalting column, PD-10 (GE healthcare). After proteins had been completely digested by trypsin, peptides were analyzed by LTQ (Thermo Fisher Scientific) and MASCOT search engine (Matrix Science).

3. Results

3-1. Cis-trans isomerization rates for wild-type and C113D mutant PPIases

C113D mutant Pin1 PPIase showed significant reduction in k_{cat} relative to the wild-type [128]. To further elucidate the role of C113 in the isomerization process, we directly measured the *cis-trans* isomerization rates for the wild-type and C113D mutant PPIase domains using 2D EXSY (Figure II-2A). In the following description, we refer to Pin1 PPIase domain as simply PPIase, unless otherwise noted. Cdc25C phosphorylated peptide was used as substrate. The *cis-to-trans* isomerization rates were 51.6 ±1.9 s^{-1} (wild-type) and 0.7 ± 0.5 s^{-1} (C113D mutant) at 295 K. The rates for *trans-to-cis* exchange were 6.6 ± 2.1 s^{-1} (wild-type) and 0.1 ± 0.0 s^{-1} (C113D mutant). The isomerase activity of C113D was approximately 70-fold lower than that of the wild-type.

3-2. C113D mutant PPIase had limited affinity to the phosphorylated peptide

The binding affinity to phosphorylated peptide was compared with ITC (Figure II-2B). The results demonstrated that C113D mutant PPIase has very limited affinity to the phosphor-peptide, apparently no binding ability was observed; while the wild-type showed the dissociation constant K_D ~ 10 mM. The reduced isomerization rate of C113D mutant is ascribed to its faint substrate affinity.

3-3. Induced structural change by C113D mutation assessed by NMR chemical shifts

Comparison of 2D ^{1}H-^{15}N HSQC spectra for the wild-type (Figure II-3A) and C113D mutant (Figure II-3B and II-3B-1) PPIases showed C113D mutation caused spectral change to a wide-range of residues in the catalytic site (Figure II-4A). Residues K63, R68, and R69 showed significant structural changes, implying the mutation may disturb the distal loop in an allosteric manner (Figure II-4A, right).

S114 and S115, which neighboring to the mutation site, showed a severe reduction in their signal intensities (Figure II-4B); the signal for S114 in C113D was observed at 8.80 ppm (^{1}H) and 120.6 ppm (^{15}N) (Figure II-3B-1) on the spectrum with extremely weak intensity, whereas the S115 signal was not observed. C113D substitution could facilitate their amide proton exchanges with water by proximate positioning of the negatively charged aspartate side chain to the amide groups of S114 and S115 [163].

3-4. Structural changes caused by C113D mutation

Three dimensional structures for the wild-type and C113D mutant were solved by NMR under the same experimental condition (Figure II-5). The overlaid structures for the wild-type and C113D PPIases demonstrated the apparent structural changes are in the helix near the mutation site, and the active site loop (residues K63-T81) (Figure II-6A). In the followings, the observed structural differences will be described in detail.

The structures near the C113 showed subtle but significant changes; the short helix including S114 and S115 was extended in C113D (Figure II-6B). The extended helix could make the amide groups in S114 and S115 stay close to the side chain negative charge of D113 in longer residence time than that for the corresponding residues in the wild-type, which may explain the reduced signal intensities for S114 and S115 in C113D (Figure II-4B).

In closer looking at the active site loop (residues K63-T81) in C113D mutant, the backbone structure changed from the corresponding part in the wild-type to disorient the side chains of the residues K63, R68 and R69, which are called as "basic triad" (Figure II-6C). The crystal structure of a reduced amide-Pin1 complex (PDB code: 3NTP), which structure is considered to mimic the transition state complex with pSer-Pro, the residues in the basic triad have hydrogen bonds to the phosphate moiety in the substrate [84]. The side chain disorientation of the basic triad in C113D mutant may explain the severely reduced binding to the phosphorylated substrate (Figure II-2B).

To support the above discussion on the C113D active loop structure, it should be noted that the active loop keeps the structural rigidity comparable to the secondary structured parts, as evidenced by the hNOE values greater than 0.8, in both the wild-type and C113D mutant (Figure II-12). The structural change observed for the loop is, therefore, significant (Figure II-6C): in general, the accuracy and precision for a segment in NMR structure tend to be spoiled, if the segment has apparent structural flexibility indicated by low hNOE values (typically, < 0.5), but it is not the case for this loop.

The structural determination of the wild-type and C113D mutant PPIases were finished in the solution containing 50 mM sodium phosphate and 100 mM Na_2SO_4. In the sample solution, phosphate or sulfate ions should stay in the phosphate binding pocket formed by the basic triad in both the wild-type and C113D mutant; which were evidenced by the chemical shift changes between the spectra for the proteins in solution with (Figure II-3) and without (Figure II-7) phosphate and sulfate ions (Figure II-8). The basic triad structures in the present wild-type and C113D mutant (Figure II-6C) could surrogate the phosphor-moiety bound state, which may consolidate the functional significance of the structural changes in the basic triad.

The C113D mutation destabilized the neighboring histidine cluster comprising of H59 and H157: the number of NOEs from histidine ring protons have significantly reduced in C113D relative to the wild-type (Figure II-6D). Although the spatial arrangement of the imidazole rings of H59 and H157 in C113D is close to that in the wild-type, their side chain dynamics should be increased in the mutant. NOE intensity depends not only on the inter-proton distance but also the internal motion to fluctuate the inter-proton distance; if the fluctuation on the inter-proton distance is significant, the observed NOE intensity for a coupled protons should be reduced [164].

3-5. Histidine hydrogen bond stabilities elucidated using H/D isotope effect on NMR chemical shifts

In accordance with the destabilization to histidine cluster in the active site, C113D mutation perturbed the hydrogen bonds mediated by H59 and H157,

which was evidenced by using H/D isotope effect on the ^{15}N chemical shifts for their ring moieties. The direct attachment of deuteron to ^{15}N atom changes the ^{15}N chemical shifts according to the "hydron" (referring to proton or deuteron) position in the hydrogen bond; the secondary isotope effect is defined as $\Delta\delta(\mathrm{DN}) = \delta(\mathrm{DN}) - \delta(\mathrm{HN})$, where δ(DN) and δ(HN) denote the ^{15}N chemical shift values when bonded to deuteron and proton, respectively [165].

The tautomeric forms for H59 and H157 in Pin1 PPIase were determined by ^{1}H-^{15}N HSQC using $^{1}H^{\varepsilon 1}$ and $^{1}H^{\delta 2}$ in imidazoles [166]; H59 $N^{\varepsilon 2}$ and H157 $N^{\delta 1}$ were directly bound to proton (Figure II-9). The ^{15}N chemical shifts for $N^{\varepsilon 2}$ (H59) and $N^{\delta 1}$ (H157) showed high-field isotope shifts by binding to deuteron (Figure II-10). The identified tautomeric forms for the histidine imidazole rings were used in the structure calculation to define their ring orientation (Figure II-6D). The imidazole ring flips for H59 and H157 were the same between the wild-type and C113D mutant Pin1 PPIase; their ring orientations were similar to those found in the high-resolution Par14 crystal structure [126]. As expected from the Par14 structure, the hydrogen bonds between $H^{\varepsilon 2}$ (H59) and $H^{\delta 1}$ (H157) can form hydrogen bonds to C113 (D113) side chain S^{γ} (O^{δ}) atom and H59 $N^{\delta 1}$, respectively.

The stability of each hydrogen bond was elucidated based on the chemical exchange rates between the ND and NH states in the solution containing 50% D_2O (Figure II-10). As demonstrated in the parts of the spectra, the signal shapes for $N^{\varepsilon 2}$ (H59) and $N^{\delta 1}$ (H157) observed in 50% D_2O solution were different between the wild-type and C113D mutant, implying the hydrogen bonds in the histidine cluster changed in C113D mutant active site (Figure

II-10). The $N^{\delta 1}$ (H157) in the wild-type PPIase was doublet along the ^{15}N axis, whilst the counterpart signal in the C113D mutant was singlet resonating at the mid of the chemical shifts between $\delta(N^{\delta 1}H)$ and $\delta(N^{\delta 1}D)$ (Figure II-10A). In the case of the $N^{\varepsilon 2}$ (H59), the wild-type showed singlet but the C113D mutant show doublet signal (Figure II-10B). The doublet signals in 50% D_2O solution indicates the slow H/D exchange onto the corresponding ^{15}N nucleus; based on the isotope shift of $\delta(^{15}N)$ around -1.0 ppm (Figure II-10), the H/D exchange rate for the proton on the ^{15}N nucleus showing double is estimated less than 155 s^{-1}. The ^{15}N imidazole nitrogen atoms showing doublet should be engaged in the stable hydrogen bonds.

The imidazole ring orientations determined in the wild-type and C113D mutant could assure the hydrogen bond network connecting the residues C113/D113-H59-H157-T152, is formed across the active site irrespective of mutation, as found in Par14 crystal structure [126]. In assuming the hydrogen bond network, $^{15}N^{\varepsilon 2}$ (H59) doublet in the C113D mutant may indicate a stable hydrogen bond is formed between D113 O^{δ} and H59 $H^{\varepsilon 2}$ in C113D, while $^{15}N^{\delta 1}$ (H157) doublet indicates the stable hydrogen bond formed by $H^{\delta 1}$ (H157) to $N^{\delta 1}$ of H59 in wild-type with reducing the stability of the hydrogen bond by $H^{\varepsilon 2}$ (H59) to C113 side chain oxygen, S^{γ}.

3-6. C113D reduced structural stability as evidenced by enhanced amide H/D exchange

The residue-specific amide H/D exchange rates were measured from a sequentially collected ^{1}H-^{15}N HSQC spectra for both the wild-type and C113D

mutant. The exchange rates were determined for all the residues observed on the first ^{1}H-^{15}N HSQC spectrum just after pouring D_2O into the lyophilized sample powder. Most of the residues in C113D mutant showed enhanced H/D exchange rates relative to the wild-type (Figure II-11), implying C113D mutant PPIase structure is less stable than the wild-type.

3-7. Comparing the reduced spectral density maps between the wild-type and C113D mutant

To further characterize the structural dynamics change caused by C113D mutation, we compared the reduced spectral density functions [167]. The reduced spectral density functions, $J_{eff}(0)$, $J(\omega_h)$, and $J(\omega_N)$, can be mapped for each residue with the rates R_1 and R_2 with hNOE for ^{15}N spin, under the approximation to equate the high-frequency values of the spectral density function $J(\omega_H) = J(\omega_H-\omega_N) = J(\omega_H+\omega_N)$ [167]. The spectral density function $J(\omega_H)$ is denoted as $J(\omega_h)$ in the reduced form, to implicate the above approximation [167]. The reduced spectral density function $J_{eff}(0)$ denotes that, since chemical exchange is not considered explicitly in its derivation. The entire profiles for the reduced spectral densities are compared (Figures II-13 and Figures II-14).

The difference in the $J_{eff}(0)$ values between the wild-type and C113D mutant are plot along the residue number; each difference was calculated as $\Delta J_{eff}(0) = J_{eff}(0)$[C113D] – $J_{eff}(0)$[wild-type] (Figure II-15). The most of the residues in C113D showed larger $J_{eff}(0)$ values than those for the corresponding residues in the wild-type (Figure II-15). This allosteric destabilization effect by C113D seems rather independent on the presence of the phosphate group in the

pocket, as the residues in the active loop showed increased $J_{eff}(0)$ in the mutant in the solution with or without phosphate and sulfate ions (Figure II-15). In general, $J_{eff}(0)$ dominates R_2 relaxation rate, while hNOE is very sensitive to both changes in internal motion described by the correlation time, τ_i, and the generalized order parameter, S^2. Assuming the internal motion of protein backbone is too fast and, thus, independent from the overall rotational motion represented by the correlation time, τ_c, the simple model-free formalism [168] gives the spectral density function as described below, eq. 3.

$$J(\omega) = (1\text{-}S^2)\frac{\tau_{mix}}{1+\omega^2\tau^2_{mix}} + S^2\frac{\tau_c}{1+\omega^2\tau^2_c}$$
$$\tau_{mix} = \tau_i\tau_c / (\tau_i + \tau_c) \qquad (3)$$

The spectral density function of $J(0)$ is, thus, described as in eq. 4.

$$J(0) = (1\text{-}S^2)\tau_i + S^2\tau_c \qquad (4)$$

The spectral density function $J(0)$ is dependent on S^2, τ_i, and τ_c, when the chemical exchange is negligible.

The transverse relaxation rate R_2 contains the rates governed by the nuclear spin-spin relaxation process (R_2^{DD}), chemical shift anisotropy of ^{15}N nuclear spin (R_2^{CSA}), and chemical exchange process (R_{ex}) [167];

$$R_2 = R_2^{DD} + R_2^{CSA} + R_{ex} \qquad (5)$$

Chemical exchange apparent in the backbone ^{15}N spin relaxation process implies that the backbone conformational exchange happening in msec time regime [167].

It is noted that, in deriving the reduced spectral density functions, R_{ex} term is neglected in the R_2 function in eq. 5. However, $J_{eff}(0)$, not the other $J(\omega_h)$ and $J(\omega_N)$, depends on R_2 rate and if the chemical exchange rate, R_{ex}, is significant,

the corresponding $J_{eff}(0)$ value increases accordingly [167]. The hNOE profiles for the wild-type and C113D mutant PPIase are close to each other (Figure II-12), implying that C113D mutation does not apparently affect the structural dynamics in ns – ps time range; τ_i, and S^2 values for the residues in C113D mutant are be very close those for the counterpart residues in the wild-type. The rotational correlation time, τ_c, was estimated for each the wild-type and C113D mutant, in considering rotational diffusion anisotropy [158]: they were $\tau_c = 9.4 \pm 0.4$ ns with rotational diffusion tensor anisotropy 1.3 ± 0.1 (wild-type) and $\tau_c = 9.5 \pm 0.5$ ns with the anisotropy 1.2 ± 0.1 (C113D mutant). In both cases, the axially symmetric rotational diffusion tensor model was adopted with statistical significance. As estimated above, the correlation time, τ_c, does not change by the C113D mutation. The changes in the dynamics parameters τ_c, τ_i, and S^2 are marginal to explain the observed differences in $J_{eff}(0)$, in considering the model-free function $J(0)$ in eq. 4. The increased $J_{eff}(0)$ values for the residues in C113D mutant, therefore, can be traced to the increased chemical exchange terms for R_2 rate (eq. 5); which implies that most part in C113D mutant becomes structurally unstable to show significant conformational exchange apparent in msec time regime.

The changes in $J_{eff}(0)$ values are particularly apparent for the residues in the phosphate binding pocket, especially residues 60–75 (Figure II-15A right), suggesting the binding pocket becomes structurally unstable in C113D mutant. The higher frequency reduced spectral density functions, $J(\omega_h)$ and $J(\omega_N)$, did not show any noticeable changes in their values induced by the mutation,

although those changes were dependent on the existence of phosphate and sulfate ions (Figures II-16 and Figures II-17).

R_2 relaxation dispersion experiments were applied to further characterize the structural dynamics in ms time domains. However, the results were less informative due to the limited number of the residues having detectable R_2 dispersion profiles, as described in the preceding work (Table II-2) [169]. It is noted that the changes in the structural dynamics revealed by the R_2 dispersion profiles were dependent on the co-existence of the phosphate and sulfate ions (Table II-2); the number of residues showing significant R_2 dispersion increased in both the wild-type and C113D in the absence of the ions.

4. Discussion

4-1. C113D mutation disarranges the basic triad in active loop of Pin1 PPIase domain

This work has demonstrated that C113D mutation destabilizes the catalytic site fold in Pin1 PPIase domain, which resulted in the allosteric change in the loop structure having the basic triad comprising of K63, R68 and R69. Among the basic triad, R69 showed the largest difference in the side chain orientation C113D mutant relative to the wild-type (Figure II-6C). The basic triad makes hydrogen bonds to phosphate moiety, as shown in the crystal structures [84, 113]. The molecular dynamics simulation of Pin1 in the complex with phosphorylated peptide demonstrated that the basic triad kept binding to substrate during isomerization; in particular, R69 and K63 form tighter interactions to phosphate group, while R68 is less crucial [144]. Therefore, disordering the basic triad structure, especially R69 side chain reorientation, explains the severely reduced substrate binding ability of C113D mutant, which was evidenced by the ITC experiments in this work (Figure II-2B).

C113D mutation reduces the isomerization rate for the Cdc25C phosphor-Ser peptide by 70-fold (Figure II-2A). In considering the above ITC experiments, the reduced isomerase activity of C113D mutant can be explained by its lowered affinity to the substrate. Since the first Pin1 crystal structure was reported, the role of SH group in C113 has been focused [128, 154]. These earlier proposals emphasizing the role of SH group as a catalyst in the *cis–trans* isomerization are now called into questions due to the several controversial results; one of which is the fact that C113D mutant does not

abolish its isomerization activity [128]. The present work demonstrated that C113 roles in keeping the catalytic site of PPIase in active fold, in particular, to maintain the functionally primed form of the basic triad.

4-2. Catalytic site fold was destabilized by C113D mutation

The allosteric structural change to the active loop could be propagated through the catalytic tetrad including C113, H59, H157, and T152 (Figure II-6D). The residues in the catalytic tetrad may form the hydrogen bonding network, as found in the crystal structure of Par14 [126]. In the present NMR analyses, no direct experimental validation was done to confirm the hydrogen bonding network. However, we could deduce the corresponding hydrogen bonding network exists in the catalytic site of PPIase for both the wild-type and C113D, because the defined imidazole ring flips for H59 and H157 and the spatial surrounding of C113/D113 and T152 in the NMR structures resemble the catalytic tetrad structure in Par14 (Figure II-6D). The hydrogen bonding network runs across the catalytic site of PPIase to connect the short helix having C113/D113 to the opposite side near the active loop.

The overall structure of C113D was similar to the wild-type structure (Figure II-6A), but the structural stability of C113D was significantly lower than that of the wild-type, as evidenced by the heat denaturing experiments (Figure II-18); the melting temperatures for the wild-type and C113D mutant were 49.4°C and 46.2°C, respectively. In addition, the less number of NOEs from imidazole rings of H59 and H157 in the catalytic site of C113D mutant

relative to the wild-type implicates the increased structural flexure of the histidines in the catalytic site (Figure II-6D).

In the mid of the catalytic tetrad, there are two conserved histidines, H59 and H157, which is referred to as “dual histidine motif”. The dual histidine motif is important for keeping the Pin1 fold; H59L mutation destabilized the protein, thus resulted in the faint isomerization activity [170]. Our study has shown that C113D mutation changed the strengths of the hydrogen bonds from H59 and H157 (Figure II-10). In the C113D mutant, H59 imidazole has a stronger hydrogen bond presumably to D113 side chain oxygen, whilst H59 has a tighter hydrogen bond to H157 imidazole in the wild-type, which were elucidate using H/D isotope effect on imidazole ^{15}N of the histidines (Figure II-10). The change in hydrogen bond is reminiscent of “tug-of-war” for H59 between the C113/D113 and H157 (Figures II-19A and II-19B). In considering the pivotal role of H59 in maintaining catalytic site fold, it is plausible that the imbalance in the tug-of-war for H59 in C113D mutant destabilizes the structure.

The sulfur atom in the SH moiety is a poor hydrogen bond acceptor [171]. The change from SH to OH group, therefore, strengthens the hydrogen bond between D113 and H59 $N^{\varepsilon 2}$ in C113D mutant with simultaneously weakening the hydrogen bond between H59 and H157 imidazole (Figures II-19A and II-19B). The weakened inter-histidine hydrogen bond in C113D mutant is consistent with the increased imidazole ring dynamics as shown by the decreased number of NOEs from the rings (Figure II-6D).

4-3. Allosteric structural change in the active site loop by C113D mutation

The allosteric structural change in the active loop, which disorganized the basic triad, could be probably caused by the reduced folding stability of the catalytic site. The reduced structural stability by C113D mutation was experimentally confident; the increased H/D exchange rates for the residues constituting the catalytic site (Figure II-11), and the elevated conformational exchange as elucidated by the increased values of $J_{eff}(0)$ (Figure II-15), in particular the residues 59 to 75 were apparent. The induced structural flexibility for the residues near H157 is also noticeable (Figures II-15).

4-4. C113 is sensitive to oxidation and C113D mimics the oxidized form Pin1

Pin1 PPIase domain has two cysteine residues, C57 and C113. The structure shows C57 is buried in the structure while C113 SH moiety is exposed to the solvent. As expected C113 has higher sensitivity to oxidation; the H_2O_2 oxidized specifically modified to C113, as assayed using maleimide fluorescence labeling and mass spectroscopy (Figure II-20). The excessive oxidation to SH group produces sulfonic acid group that structurally resembles carboxylic acid group as D113 in C113D mutant (Figure II-20). The C113D mutant could be supposed to mimic the oxidized form of Pin1 PPIase domain that happens inside cells under oxidative stress [133, 172]. The present study suggests the oxidized form of Pin1 PPIase domain reduces the binding activity to substrate, thus, has lowered isomerization activity.

5. Conclusions

In Chapter II, the present work has demonstrated a novel role of C113 in stabilizing the catalytic site fold. The change from SH to OH group disturbs the hydrogen bonding network formed by the catalytic tetrad because of unbalancing the tug-of-war for H59 between the residues at 113 and 157 (Figure II-19). Dual histidine motif comprising of the conserved H59 and H157 is important for keeping the catalytic site in an active fold. The imbalance of the tag-of-war in C113D mutant weakens the hydrogen bond among the dual histidine motif, thus destabilizes the catalytic site fold. The disturbed hydrogen bonding network in the catalytic tetrad leads to the allosteric disorder of the active loop including basic triad that binds to a phosphate moiety in the substrate, which explains the reduced substrate binding ability of C113D mutant. Pin1 oxidation happening in cells should reduce its isomerization activity through the alleviated binding to substrate, as anticipated from the work on C113D mutant PPIase domain being supposed to be a surrogate for the oxidized form of Pin1 PPIase domain.

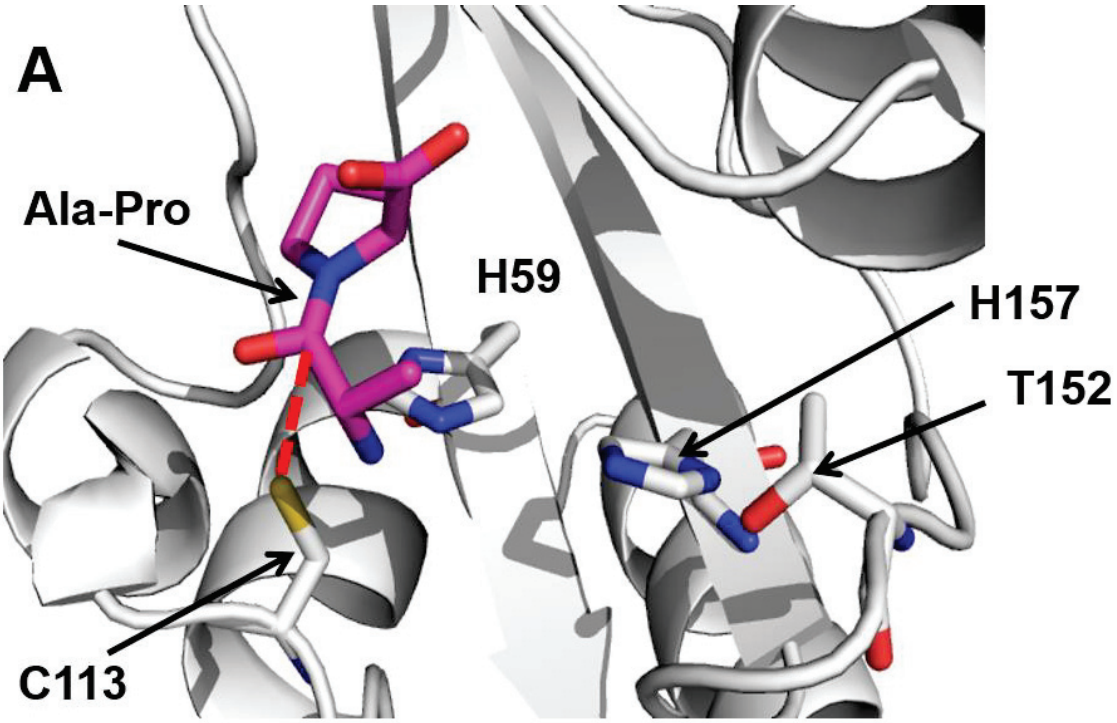
A
Ala-Pro
H59
H157
T152
C113

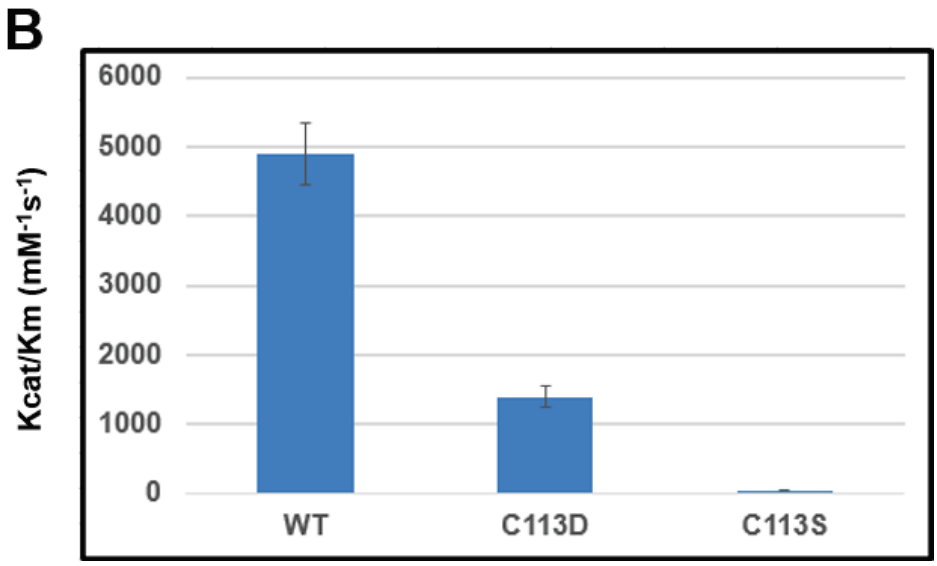
B
Kcat/Km (mM-1s-1)
6000
5000
4000
3000
2000
1000
0
WT
C113D
C113S

Figure II-1

(A) Nucleophilic addition mechanism is proposed from complex crystal structure of Pin1 and Ala-Pro peptide (PDB: 1PIN) [113]. Red: covalent bond between thiol of C113 and carbonyl carbon in the catalytic process. (B) Catalytic activity was measured for wild-type, C113D, and C113S [128]. Substrate: WFYpSPR-*p*NA.

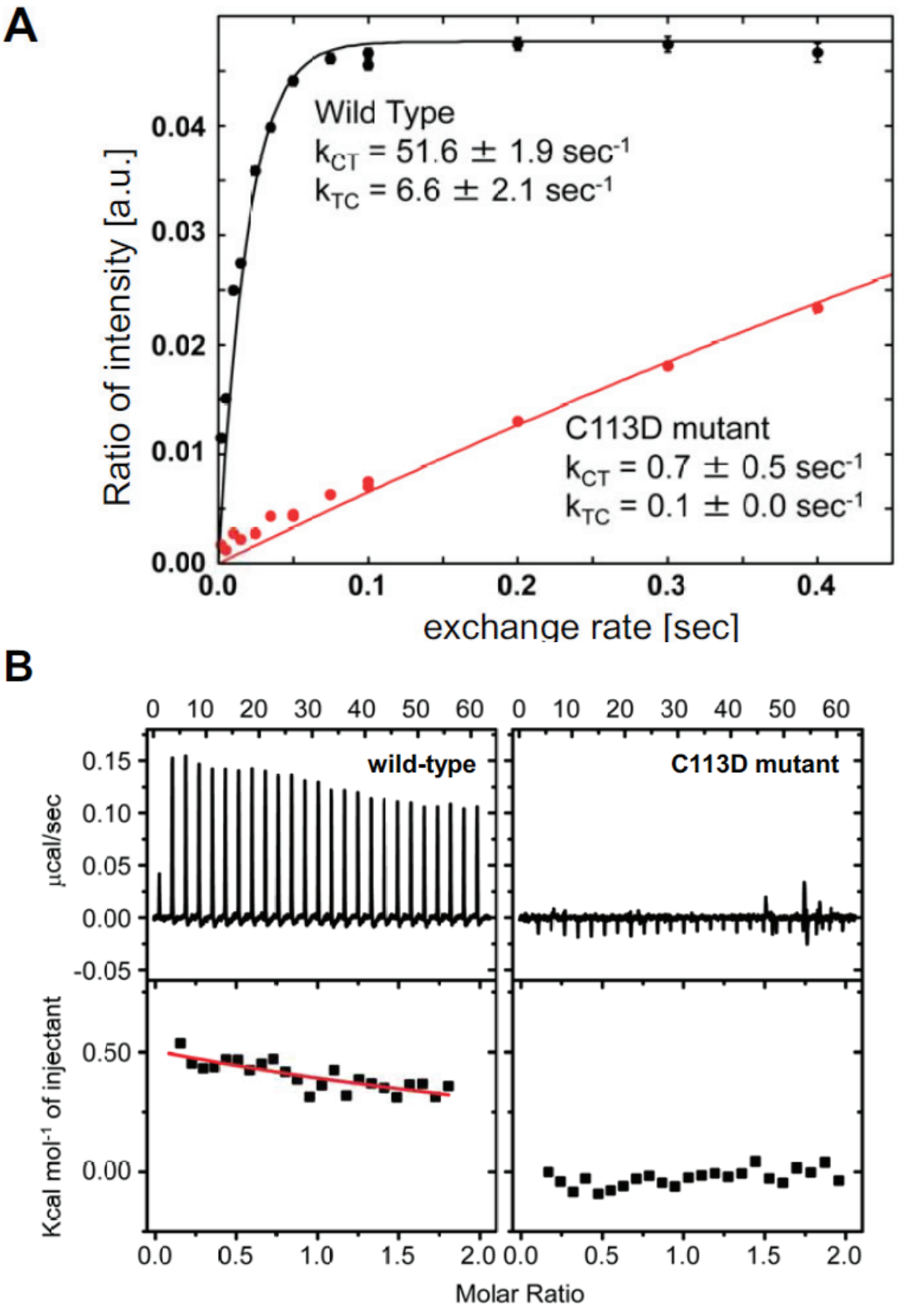
A
Wild Type
k_{CT} = 51.6 ± 1.9 sec^{-1}
k_{TC} = 6.6 ± 2.1 sec^{-1}
C113D mutant
k_{CT} = 0.7 ± 0.5 sec^{-1}
k_{TC} = 0.1 ± 0.0 sec^{-1}
Ratio of intensity [a.u.]
exchange rate [sec]
B
wild-type
C113D mutant
µcal/sec
Kcal mol^{-1} of injectant
Molar Ratio

Figure II-2

(A) Experimental rate constants for the wild-type and C113D mutant were measured by EXSY with Cdc25C phosphorylated peptide at varying exchange times. (B) Isothermal titration calorimetric data for the wild-type (left) and C113D mutant (right) PPIase domains at 298 K. Each peak corresponds to 1.5 μl injection of Cdc25C phosphorylated peptide substrate solution. The red full line drawn in the wild-type ΔH plot (left bottom) is the best-fit model function assuming 1:1 protein–substrate stoichiometry.

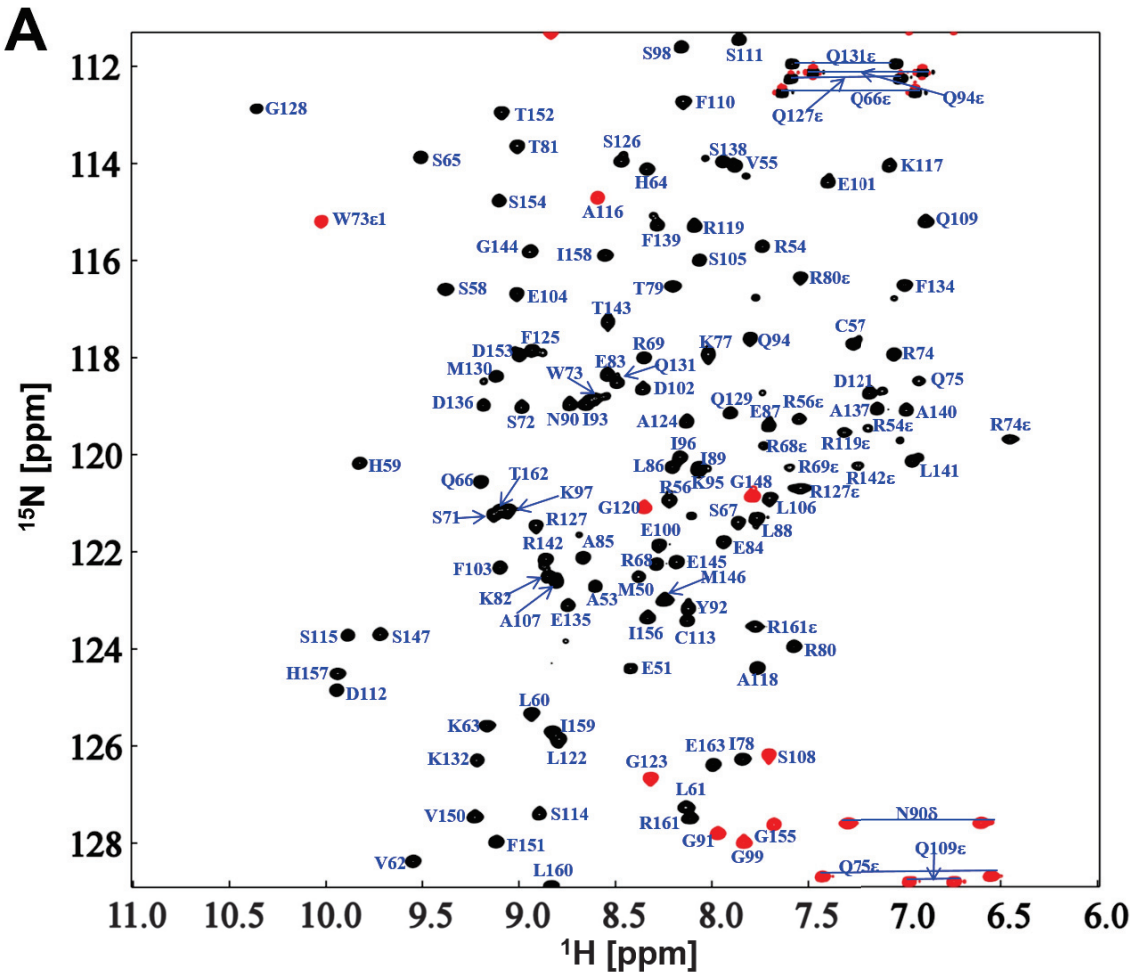
A
15N [ppm]
1H [ppm]
112
114
116
118
120
122
124
126
128
11.0
10.5
10.0
9.5
9.0
8.5
8.0
7.5
7.0
6.5
6.0
S98
S111
Q131ε
Q66ε
Q94ε
Q127ε
G128
T152
F110
S126
T81
S65
S138
V55
K117
H64
E101
S154
A116
W73ε1
Q109
F139
R119
G144
I158
R54
S105
R80ε
S58
E104
T79
F134
T143
C57
F125
R69
K77
Q94
D153
R74
M130
W73
F83
Q131
Q75
D102
D121
D136
Q129
E87
R56ε
A137
A140
S72
N90
I93
A124
R54ε
R74ε
I96
R68ε
R119ε
H59
L86
I89
R69ε
L141
Q66
T162
R56
K95
G148
R142ε
K97
R127ε
S71
R127
G120
S67
L106
E100
L88
R142
A85
E84
F103
R68
E145
M146
K82
M50
A53
Y92
A107
E135
I156
C113
R161ε
S115
S147
R80
E51
H157
A118
D112
L60
K63
I159
E163
I78
S108
K132
L122
G123
L61
V150
S114
R161
N90δ
G91
GI55
F151
G99
Q109ε
V62
Q75ε
L160

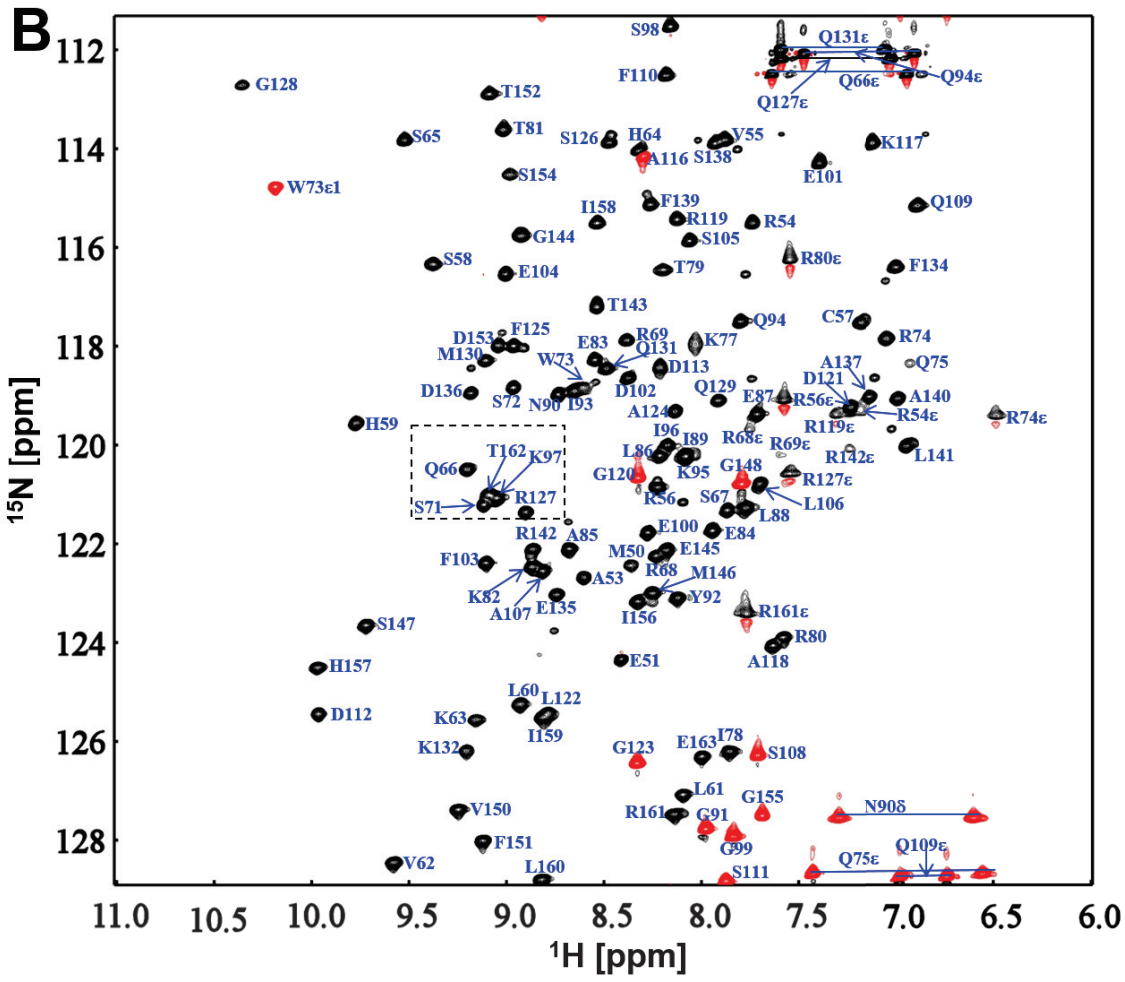
B
15N [ppm]
1H [ppm]
112
114
116
118
120
122
124
126
128
11.0
10.5
10.0
9.5
9.0
8.5
8.0
7.5
7.0
6.5
6.0
S98
Q131ε
F110
Q66ε
Q94ε
Q127ε
G128
T152
T81
S65
S126
H64
V55
K117
A116
S138
E101
W73ε1
S154
I158
F139
Q109
R119
R54
G144
S105
S58
E104
T79
R80ε
F134
T143
Q94
C57
D153
F125
R69
R74
M130
E83
Q131
K77
Q75
W73
D113
A137
D121
D136
S72
N90
I93
D102
Q129
E87
R56ε
A140
A124
R54ε
R74ε
H59
I96
I89
R68ε
R69ε
R119ε
T162
K97
L86
R142ε
L141
Q66
G120
K95
G148
R127ε
R127
R56
S67
L106
S71
L88
E100
E84
R142
A85
M50
E145
F103
R68
M146
A53
K82
Y92
R161ε
A107
E135
I156
S147
R80
E51
A118
H157
L60
L122
D112
K63
I159
K132
G123
E163
I78
S108
L61
G155
N90δ
V150
R161
G91
F151
G99
Q109ε
Q75ε
V62
L160
S111

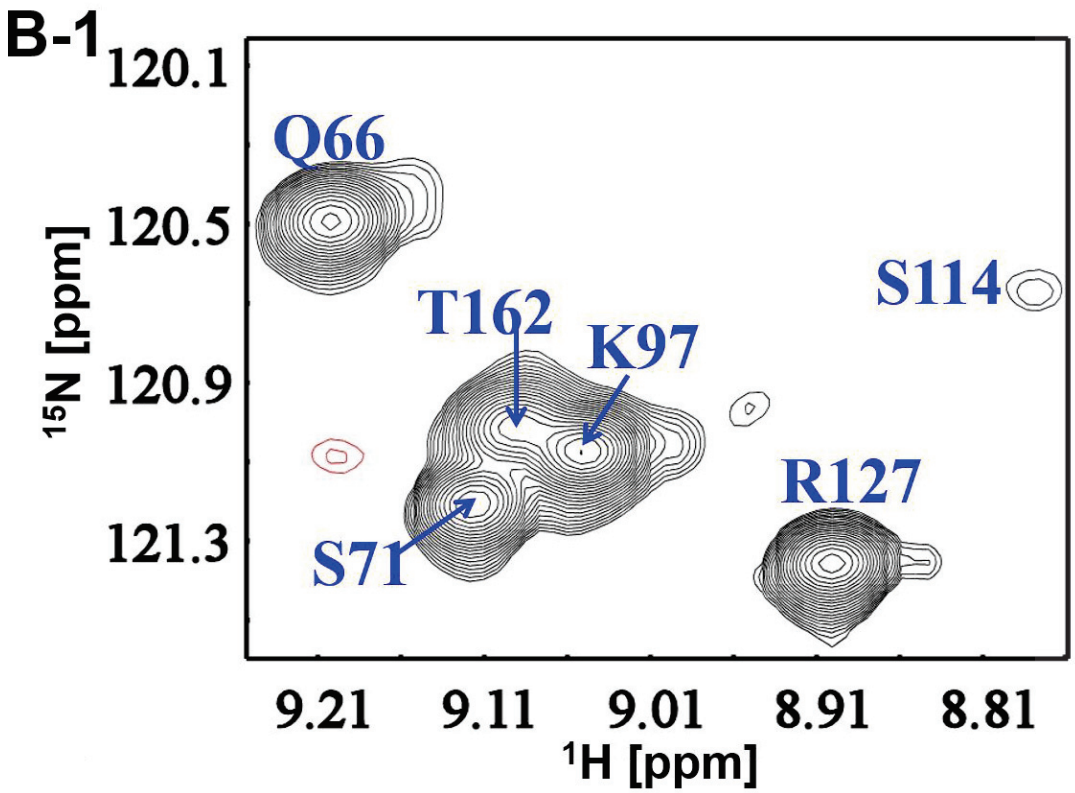

Figure II-3

Backbone resonance assignment for PPIases drawn on the ^{1}N-^{15}N HSQC spectrum with ions. (A) wild-type, amide groups of 109 residues (95.61%) were assigned except four prolines and E30. (B) C113D mutant, amide groups of 108 residues (94.74%) were assigned except four prolines, E30, and S115. (B-1) Backbone resonance assignment for residues in the box of (B).

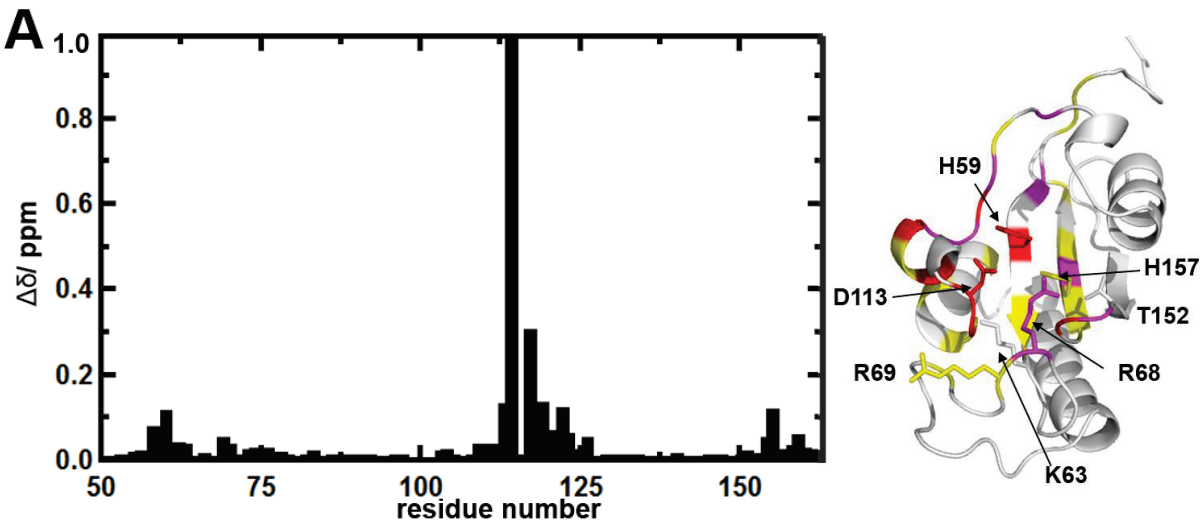
A
1.0
0.8
0.6
0.4
0.2
0.0
Δδ/ ppm
50
75
100
125
150
residue number
H59
H157
D113
T152
R69
R68
K63

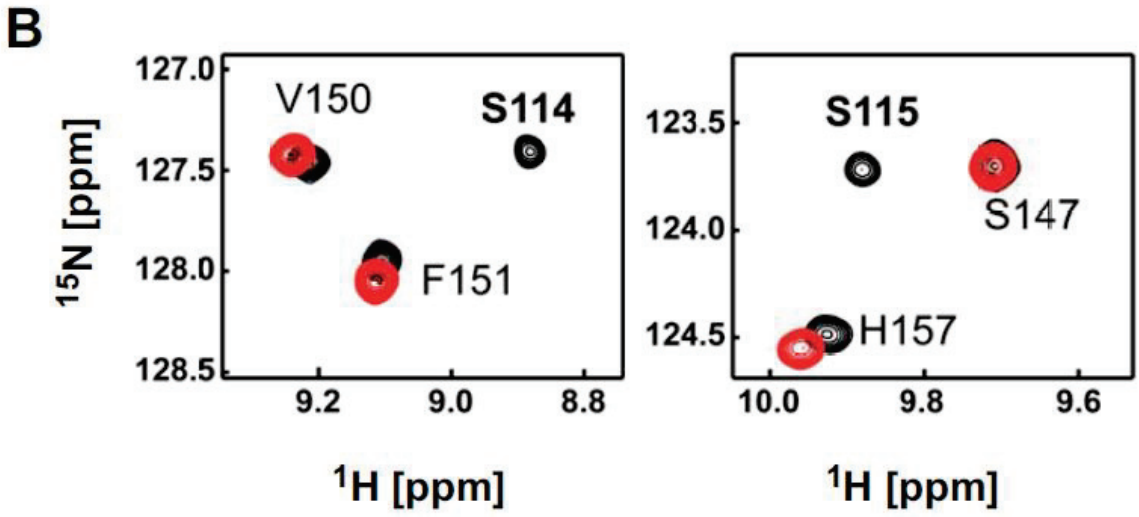
B
127.0
127.5
128.0
128.5
15N [ppm]
V150
S114
F151
9.2
9.0
8.8
1H [ppm]
123.5
124.0
124.5
S115
S147
H157
10.0
9.8
9.6
1H [ppm]

Figure II-4

(A) Residue-wise plot for the normalized chemical shift differences between the wild-type and C113D mutant in the presence of sulfate and phosphate ions. The normalized chemical shift difference for each residue is defined as, $\Delta\delta = \sqrt{(\Delta\delta^{1}\mathrm{H})^2 + (\Delta\delta^{15}\mathrm{N}/5)^2}$, where $\Delta\delta^{1}$H and $\Delta\delta^{15}$N are the chemical shift difference in ^{1}H and ^{15}N dimensions, respectively [173]. According to the magnitude of $\Delta\delta$, the residues in the C113D mutant structure were colored differently: over $\Delta\delta_{ave}$ + 1 σ (red), over $\Delta\delta_{ave}$ + 0.5σ (purple), and over $\Delta\delta_{ave}$ + 0.25 σ (yellow), where $\Delta\delta_{ave}$ is the average value for $\Delta\delta$ and σ is the standard deviation of $\Delta\sigma$ calculated over the entire residues. (B) The overlaid presentation of the parts of the ^{1}H-^{15}N spectra for the wild-type (black) and C113D mutant (red) in the presence of sulfate and phosphate ions, which show the signals for S114 (left) and S115 (right) have disappeared on the spectrum for C113D mutant. The S114 signal was observed far from the displayed spectral region with very weak intensity while the S115 resonance was not observed in anywhere on the spectrum for C113D mutant.

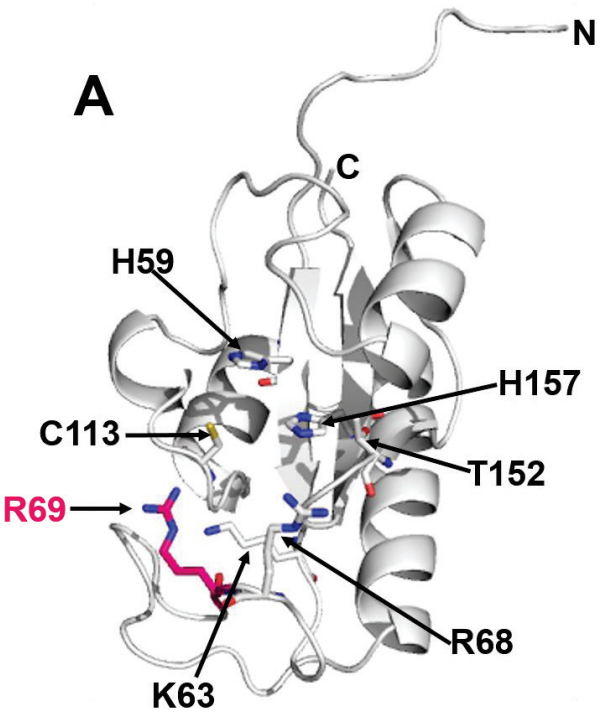
A
N
C
H59
H157
C113
T152
R69
R68
K63

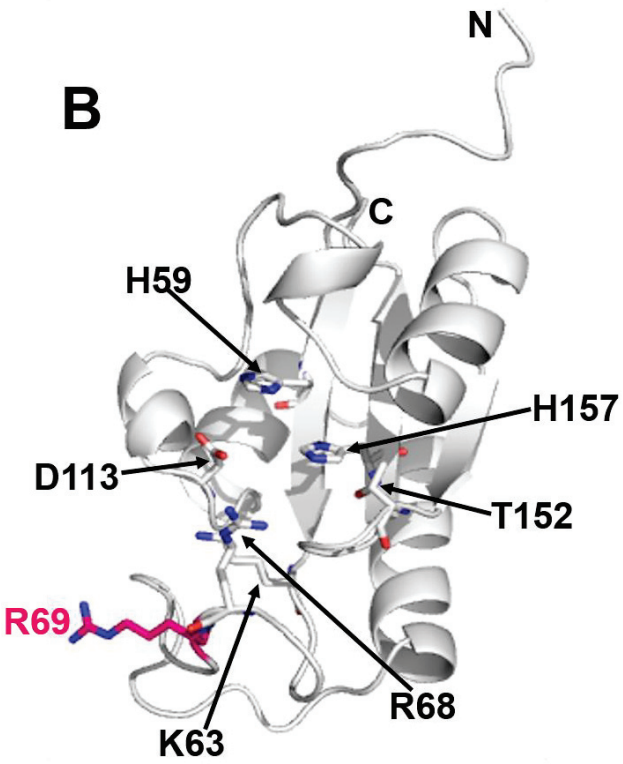
B
N
C
H59
H157
D113
T152
R69
R68
K63

Figure II-5

(A) Three dimensional solution structure for wild-type PPIase domain. (B) Three dimensional solution structure for C113D mutant PPIase domain. Obvious structural changes could be observed between wild-type and C113D mutant PPIase domains.

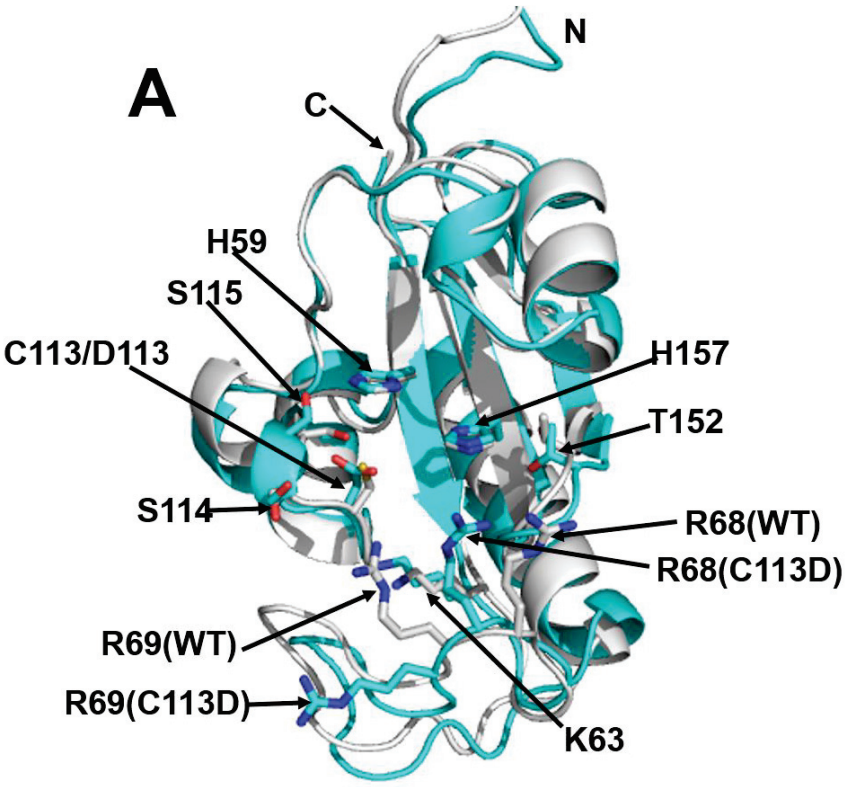
A
N
C
H59
S115
C113/D113
H157
T152
S114
R68(WT)
R68(C113D)
R69(WT)
R69(C113D)
K63

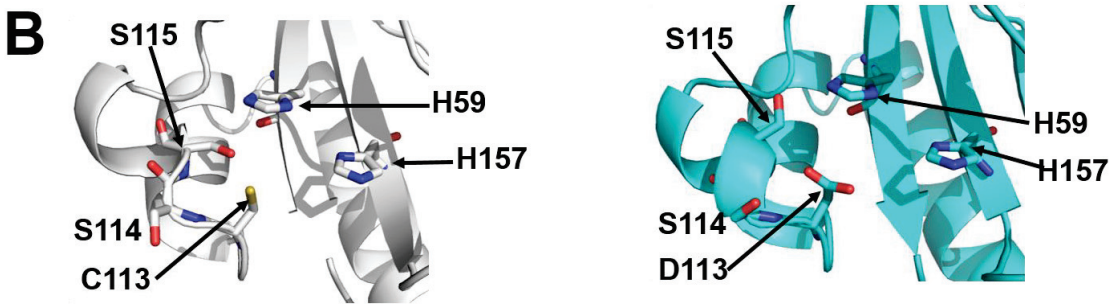
B
S115
H59
H157
S114
C113
S115
H59
H157
S114
D113

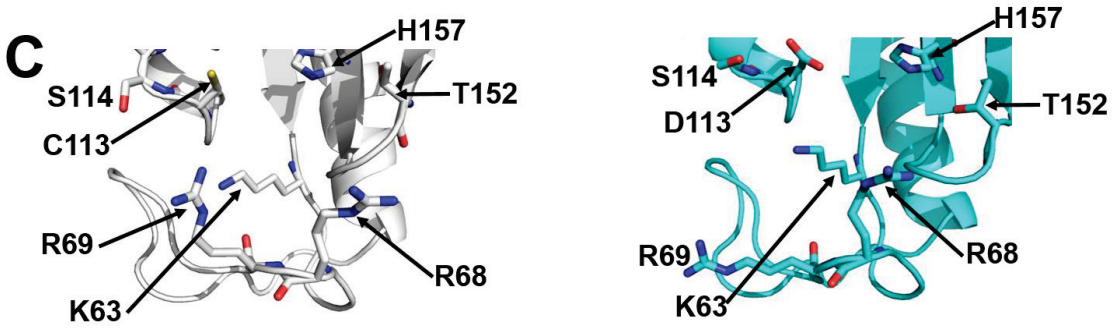
C
S114
C113
H157
T152
R69
K63
R68
S114
D113
H157
T152
R69
K63
R68

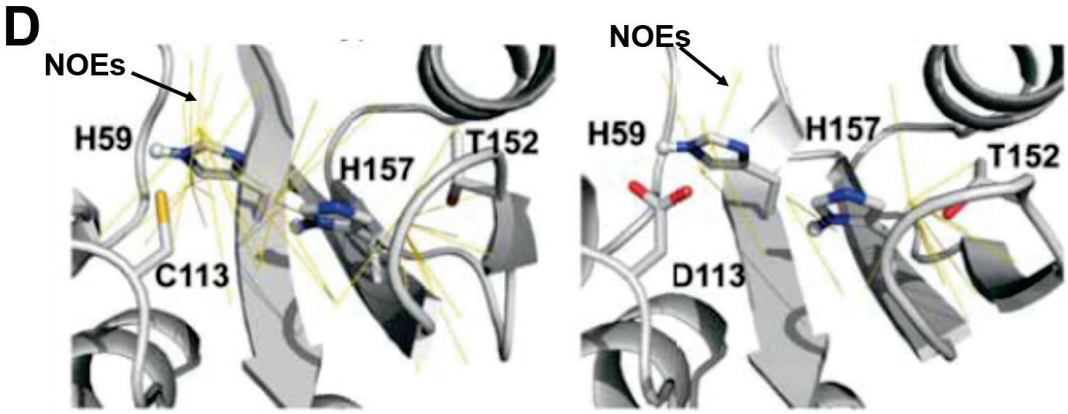
D
NOEs
H59
H157
T152
C113
NOEs
H59
H157
T152
D113

Figure II-6

(A) Structure overlap between the wild-type (gray) and C113D mutant (cyan) PPIase domains determined in this work. (B) Close up view of the structures near the mutation site of the wild-type (left, gray) and C113D mutant (right, cyan). (C) The active loop structure comprising of the basic tetrad, K63, R68 and R69; the wild-type (left, gray) and C113D mutant (right, cyan). (D) The observed NOEs from the imidazole ring protons are drawn in yellow lines; the wild-type (left) and C113D (right). All figures were built by the program PyMOL (Schrödinger, LLC).

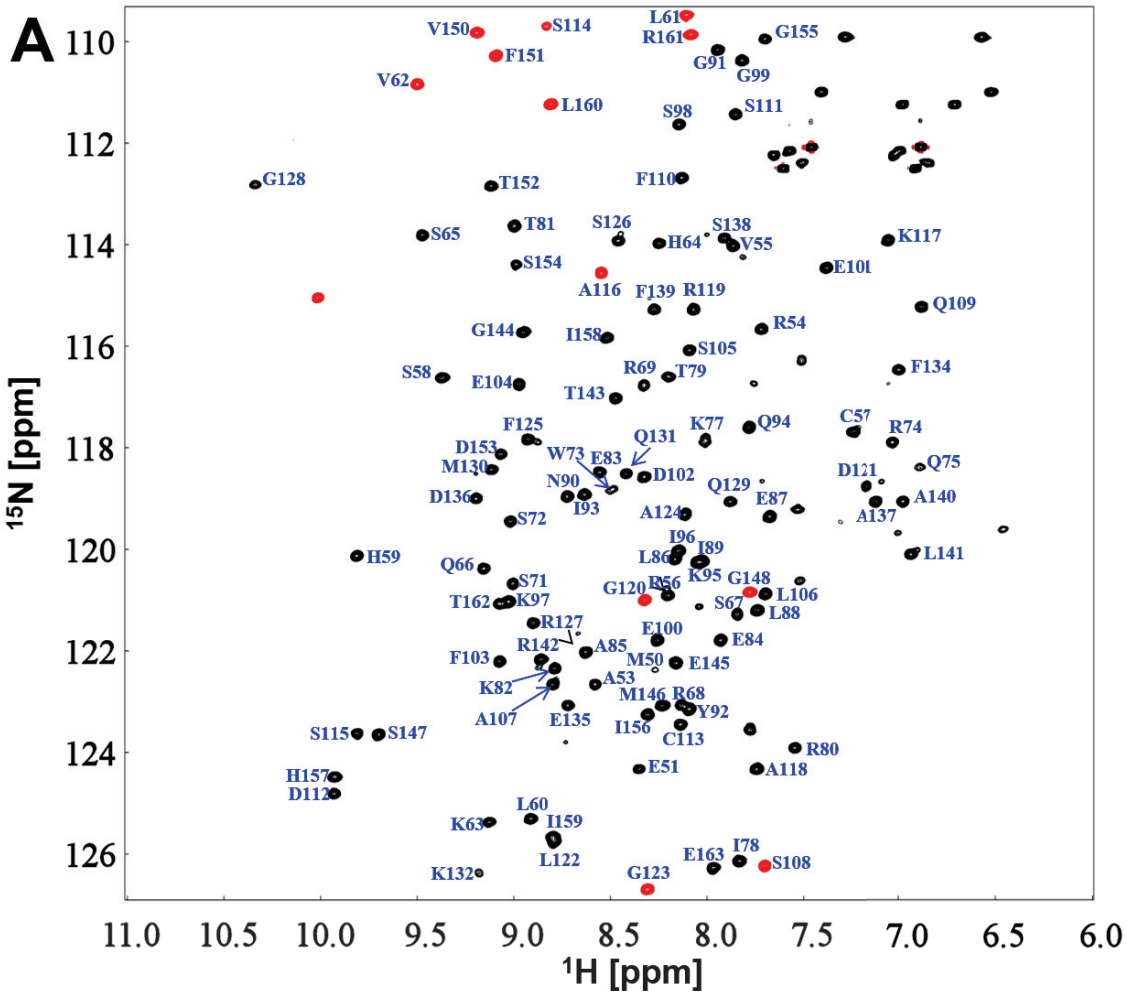
A
110
112
114
116
118
120
122
124
126
15N [ppm]
11.0
10.5
10.0
9.5
9.0
8.5
8.0
7.5
7.0
6.5
6.0
1H [ppm]
V150
S114
L61
R161
G155
F151
G91
G99
V62
L160
S98
S111
G128
T152
F110
S65
T81
S126
S138
H64
V55
K117
S154
E101
A116
F139
R119
Q109
R54
G144
I158
S105
S58
E104
R69
T79
F134
T143
F125
K77
Q94
C57
R74
D153
Q131
W73
E83
M130
D102
Q75
N90
Q129
E87
D121
D136
I93
A124
A140
S72
A137
I96
I89
H59
L86
L141
Q66
K95
G148
S71
G120
R56
T162
K97
S67
L106
L88
R127
E100
R142
A85
E84
F103
M50
E145
A53
K82
M146
R68
Y92
A107
E135
I156
C113
S115
S147
R80
E51
A118
H157
D112
L60
K63
I159
L122
E163
I78
S108
K132
G123

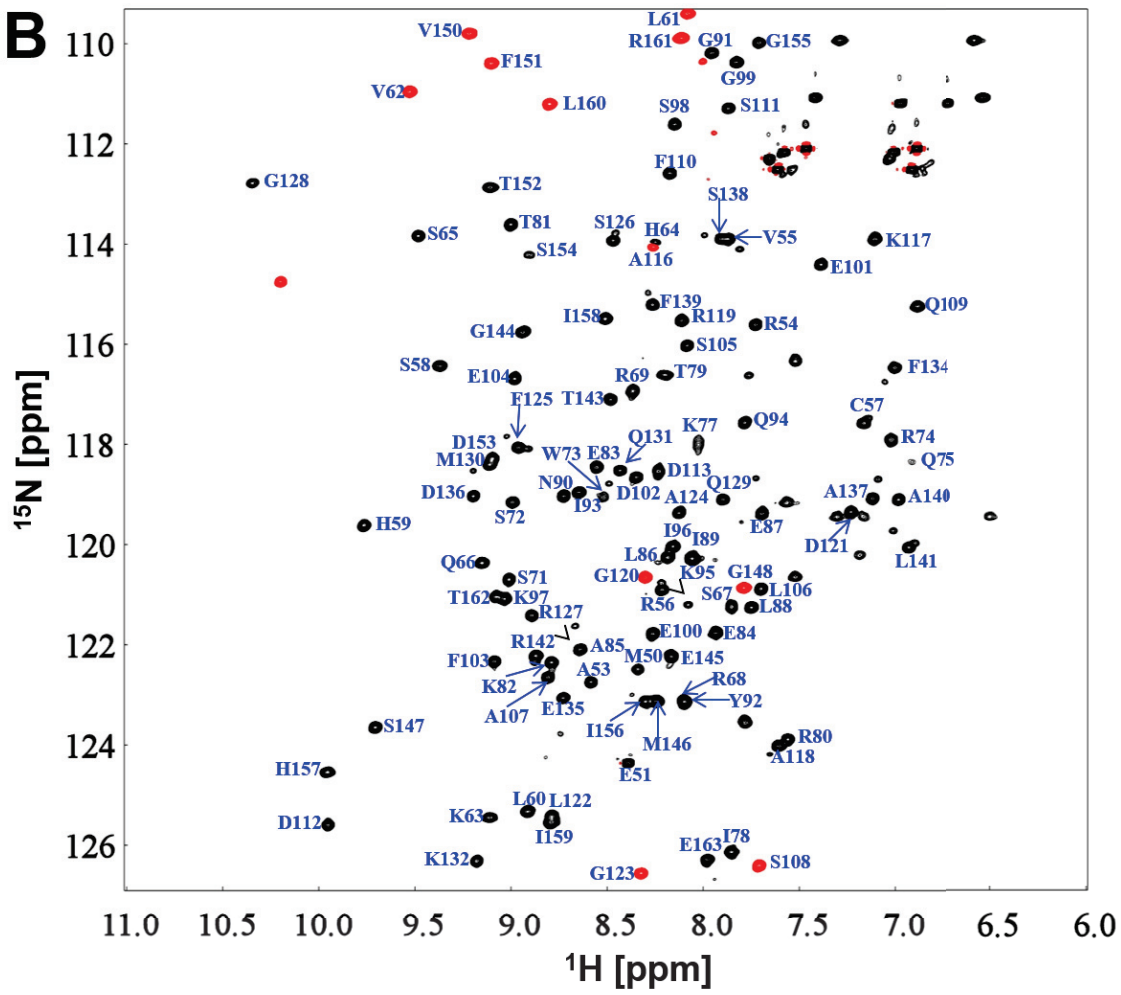
B
110
112
114
116
118
120
122
124
126
15N [ppm]
11.0
10.5
10.0
9.5
9.0
8.5
8.0
7.5
7.0
6.5
6.0
1H [ppm]
V150
L61
R161
G91
G155
F151
G99
V62
L160
S98
S111
F110
G128
T152
S138
T81
S126
H64
V55
K117
S65
S154
A116
E101
F139
Q109
I158
R119
R54
G144
S105
S58
E104
R69
T79
F134
F125
T143
C57
K77
Q94
D153
Q131
R74
M130
W73
E83
D113
Q75
N90
Q129
D136
D102
A124
A137
A140
I93
S72
E87
H59
I96
I89
D121
L86
L141
Q66
K95
G148
S71
G120
S67
L106
T162
K97
R56
L88
R127
E100
E84
R142
A85
M50
E145
F103
A53
R68
K82
Y92
E135
A107
I156
S147
M146
R80
A118
H157
E51
L60
L122
K63
D112
I159
E163
I78
K132
S108
G123

Figure II-7

Backbone resonance assignment for PPIases drawn on the ^{1}N-^{15}N HSQC spectrum without ions. (A) wild-type, amide groups of 109 residues (95.61%) were assigned except four prolines and E30. (B) C113D mutant, amide groups of 107 residues (93.86%) were assigned except four prolines, E30, S114, and S115.

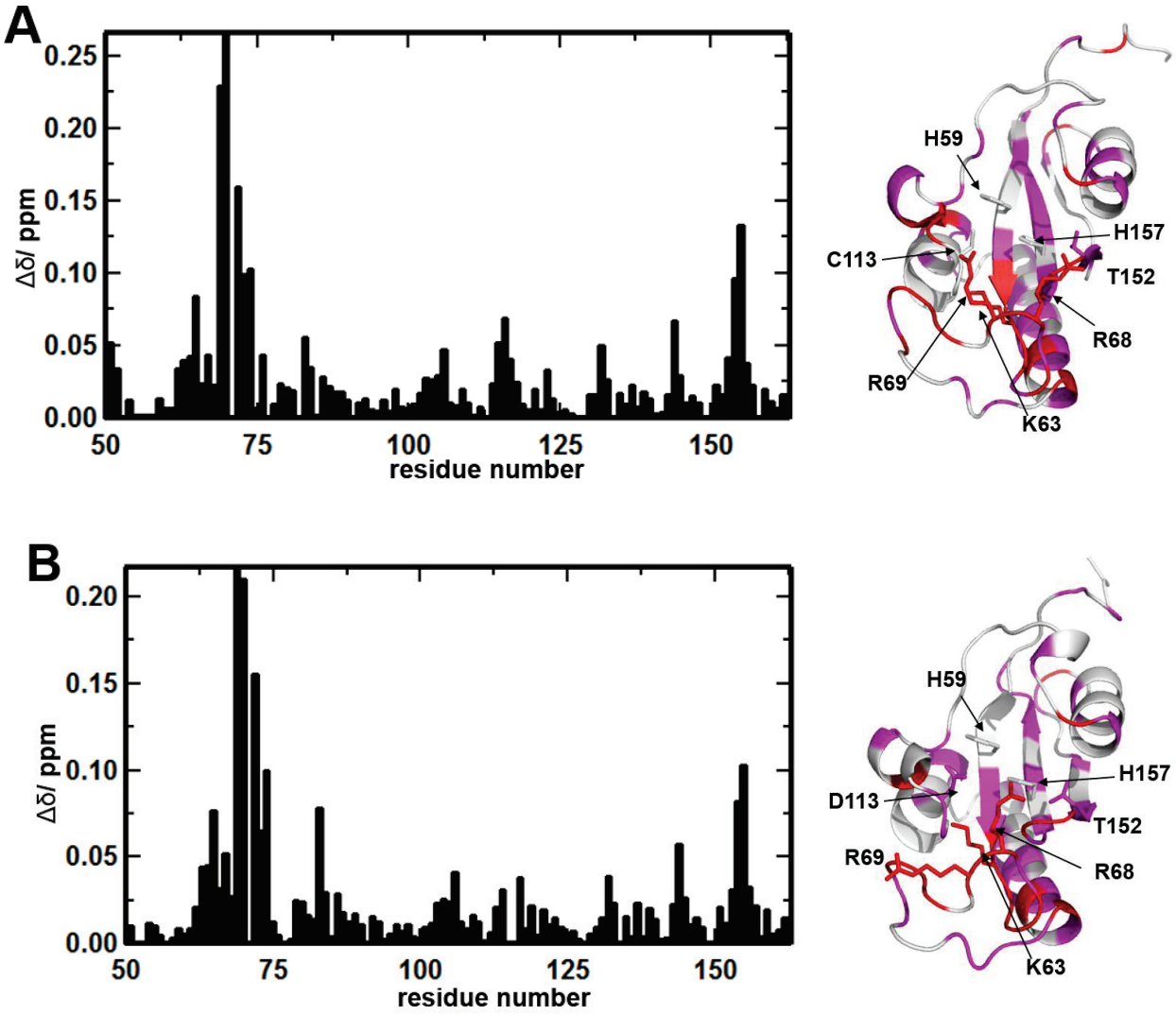
A
0.25
0.20
0.15
0.10
0.05
0.00
Δδ/ ppm
50
75
100
125
150
residue number
H59
H157
C113
T152
R68
R69
K63
B
0.20
0.15
0.10
0.05
0.00
Δδ/ ppm
50
75
100
125
150
residue number
H59
H157
D113
T152
R69
R68
K63

Figure II-8

Plot of the normalized chemical shift differences for the backbone chemical shifts between the presence and absence of sulfate and phosphate ions. (A) The wild-type and (B) C113D mutant. According to the magnitude of the normalized chemical shift difference, which is defined as $\Delta\delta = \sqrt{(\Delta\delta^{1}\mathrm{H})^2 + (\Delta\delta^{15}\mathrm{N}/5)^2}$, where $\Delta\delta^{1}$H and $\Delta\delta^{15}$N are the chemical shift difference in ^{1}H and ^{15}N dimensions, respectively, the residues in the wild-type and C113D mutant PPIase domain structures were colored differently (right): over $\Delta\delta_{ave}$ + 1 σ (red), over $\Delta\delta_{ave}$ + 0.5σ (purple), and over $\Delta\delta_{ave}$ + 0.25 δ (yellow), where $\Delta\delta_{ave}$ is the average value for $\Delta\delta$ and σ is the standard deviation of $\Delta\sigma$ calculated over the entire residues.

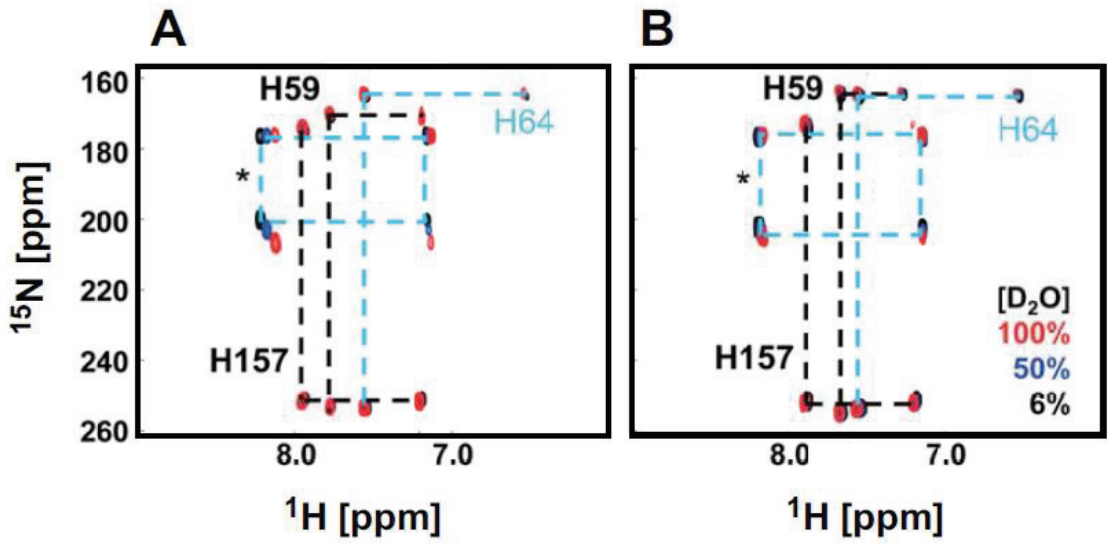

Figure II-9

^{1}H-^{15}N HSQC spectra for the imidazole rings of histidines in Pin1. (A) The wild-type and (B) C113D mutant. A set of signals marked with asterisks come from the histidine residue at position 0 in the segment comprising of GSH sequence, which was attached to the N-terminus due to the reason of plasmid construction

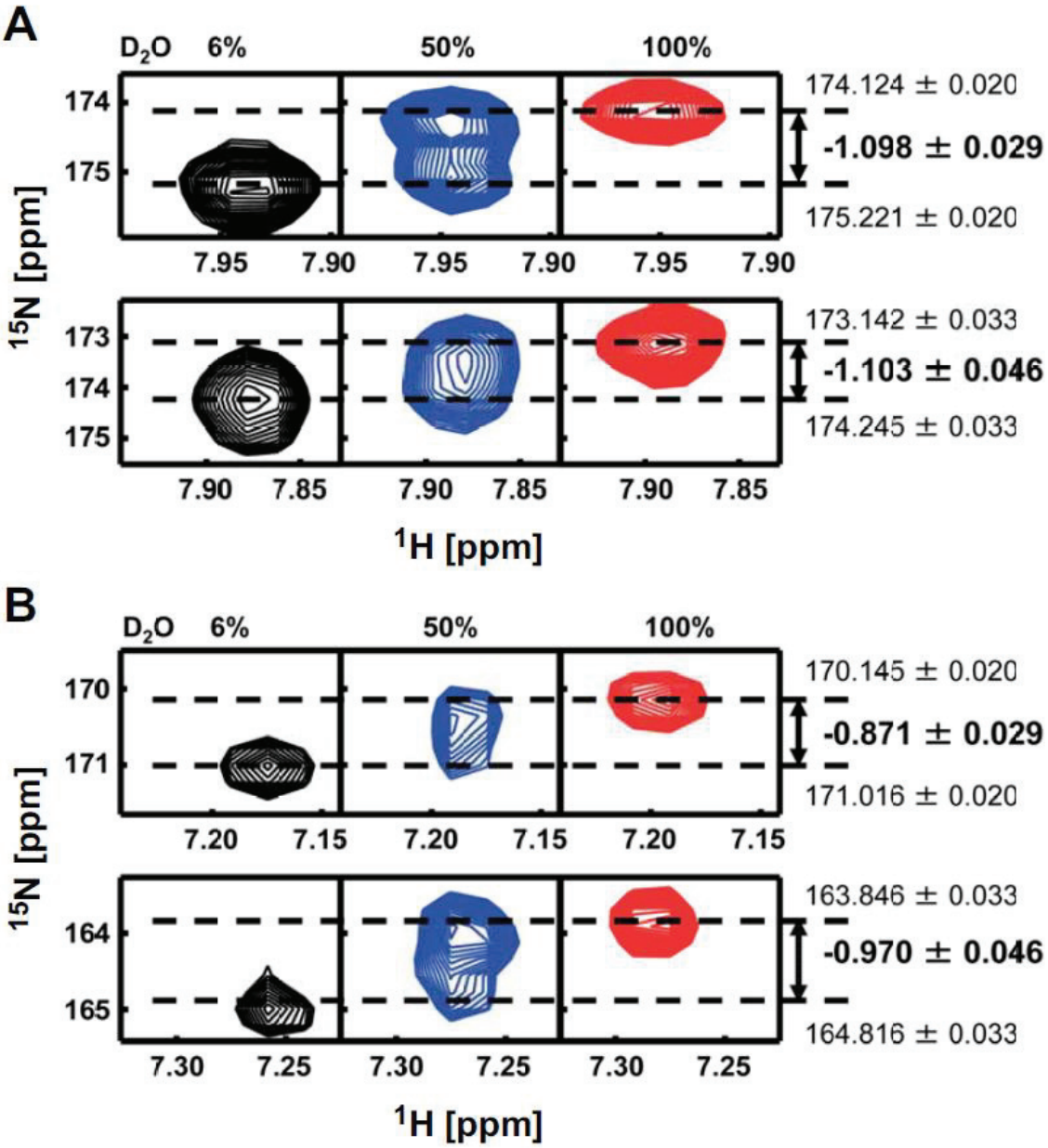
A
D2O 6%
50%
100%
174
175
15N [ppm]
7.95 7.90 7.95 7.90 7.95 7.90
174.124 ± 0.020
-1.098 ± 0.029
175.221 ± 0.020
173
174
175
7.90 7.85 7.90 7.85 7.90 7.85
173.142 ± 0.033
-1.103 ± 0.046
174.245 ± 0.033
1H [ppm]
B
D2O 6%
50%
100%
170
171
15N [ppm]
7.20 7.15 7.20 7.15 7.20 7.15
170.145 ± 0.020
-0.871 ± 0.029
171.016 ± 0.020
164
165
7.30 7.25 7.30 7.25 7.30 7.25
163.846 ± 0.033
-0.970 ± 0.046
164.816 ± 0.033
1H [ppm]

Figure II-10

H/D isotope effects on the chemical shifts for ^{15}N nuclei in the histidine imidazole ring were measured in the solutions having different D_2O contents. (A) The ^{1}H-$^{15}N^{\delta 1}$ HSQC signals for H157 collected in the solution containing 6% (black, left), 50% (blue, middle), and 100% (red, right); data in the upper and lower panels are for the wild-type and C113D mutant, respectively. (B) The same data set for ^{1}H-$^{15}N^{\varepsilon 2}$ signals for H59 of the wild-type (upper) and C113D mutant (lower).

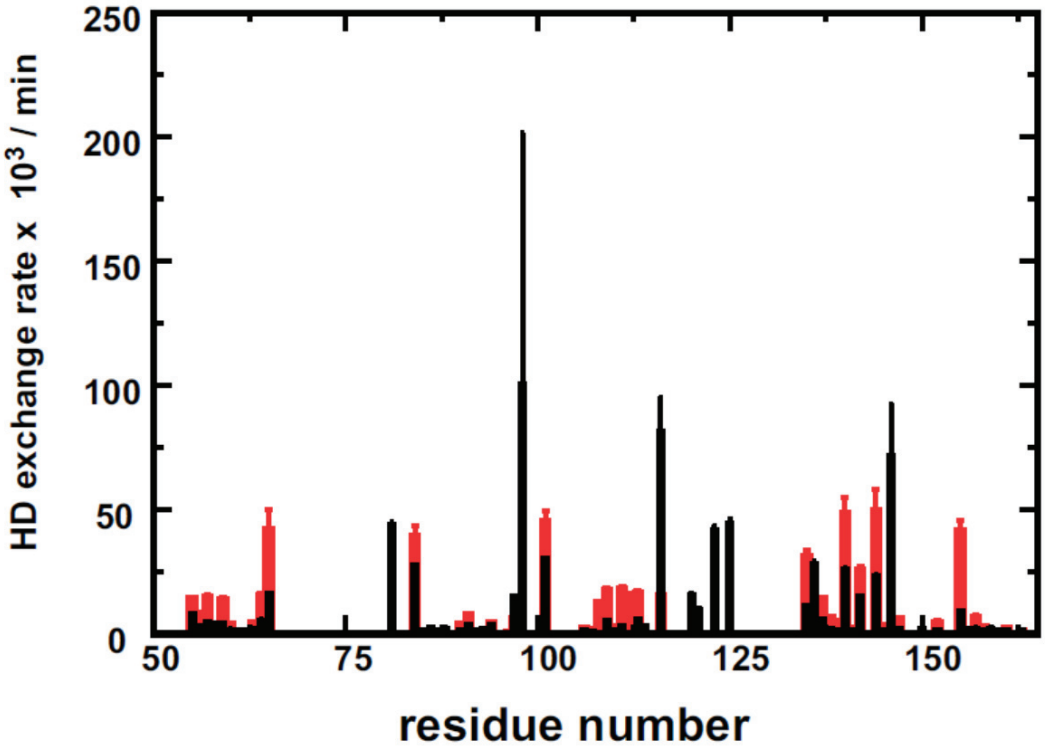

Figure II-11

H/D exchange rates for the residues in the wild-type (black) and C113D (red) mutant. The residues without exchange rates showed no observable peaks on the first ^{1}H-^{15}N HSQC spectrum in a series of data collection, implying their amide protons have rapidly exchanged to deuterons within about 10 min.

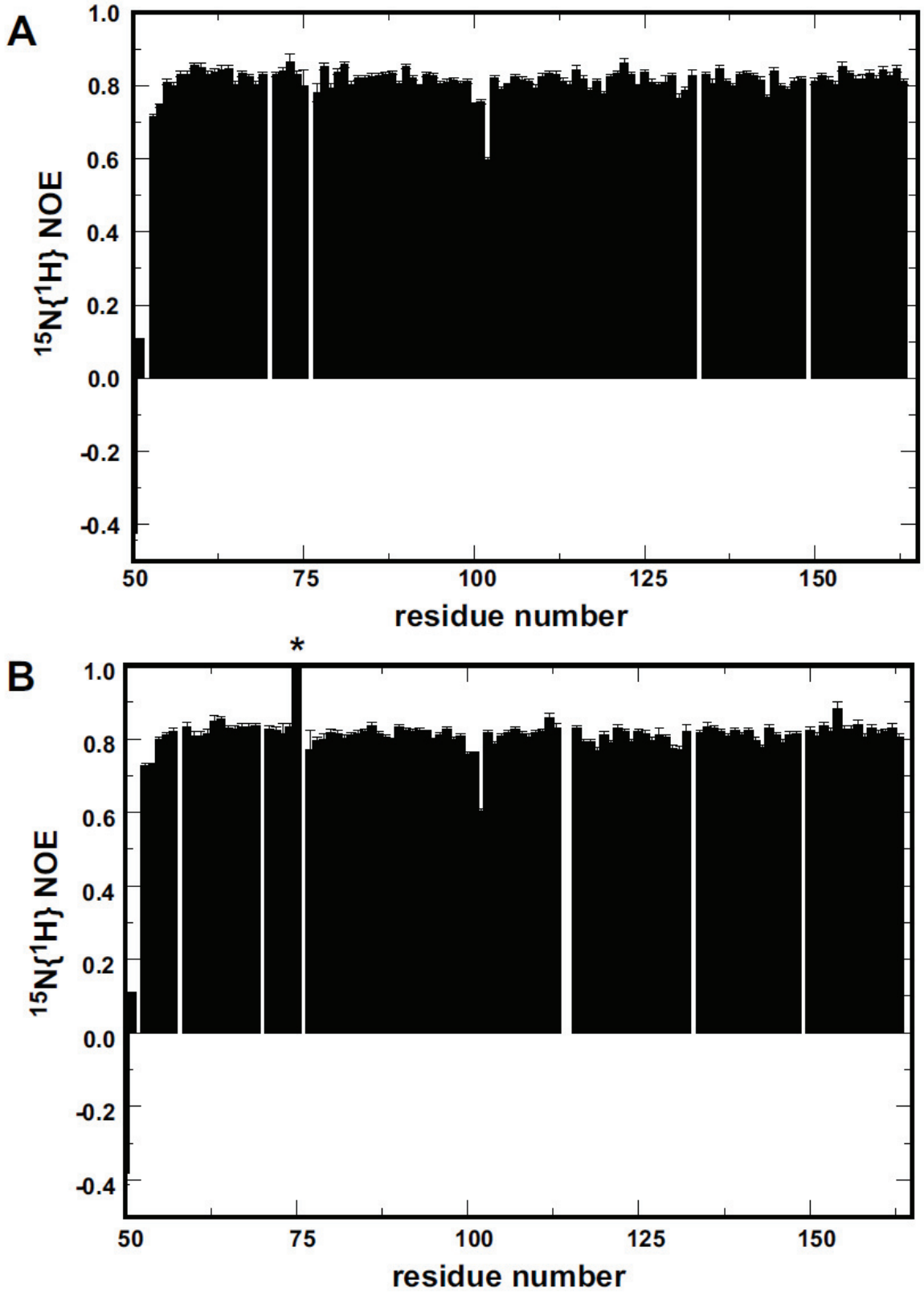
A
1.0
0.8
0.6
0.4
0.2
0.0
-0.2
-0.4
15N{1H} NOE
50
75
100
125
150
residue number
*
B
1.0
0.8
0.6
0.4
0.2
0.0
-0.2
-0.4
15N{1H} NOE
50
75
100
125
150
residue number

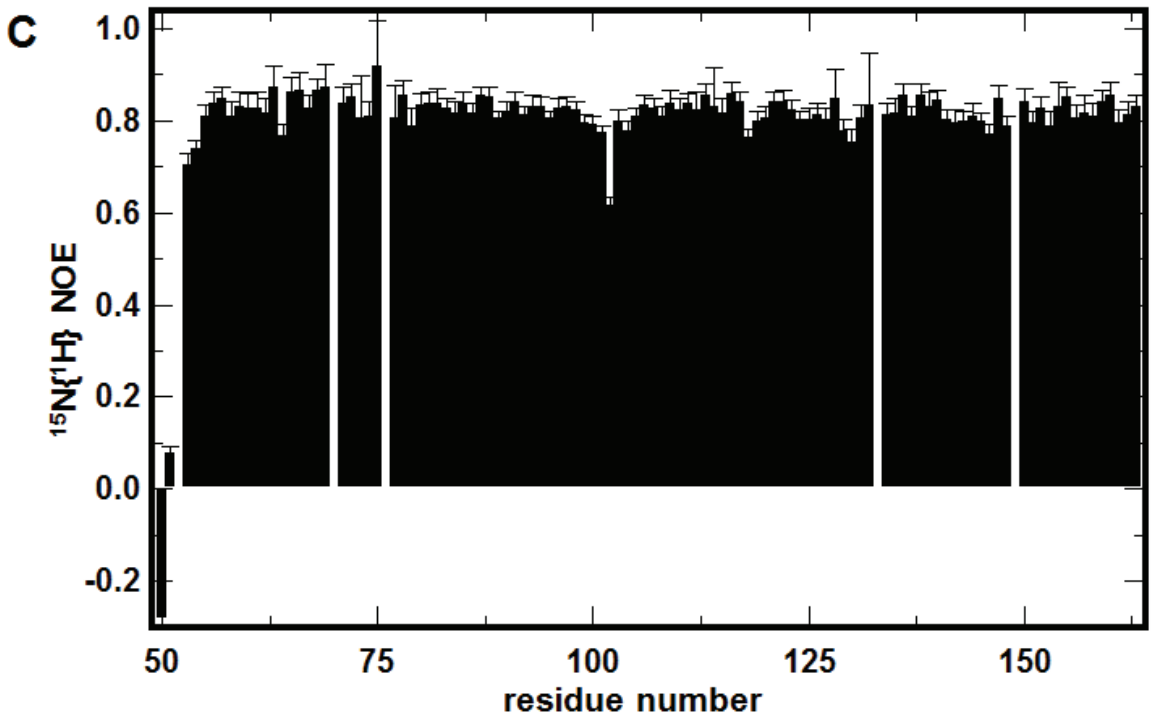
C
1.0
0.8
0.6
0.4
0.2
0.0
-0.2
$^{15}N\{^1H\}$ NOE
50
75
100
125
150
residue number

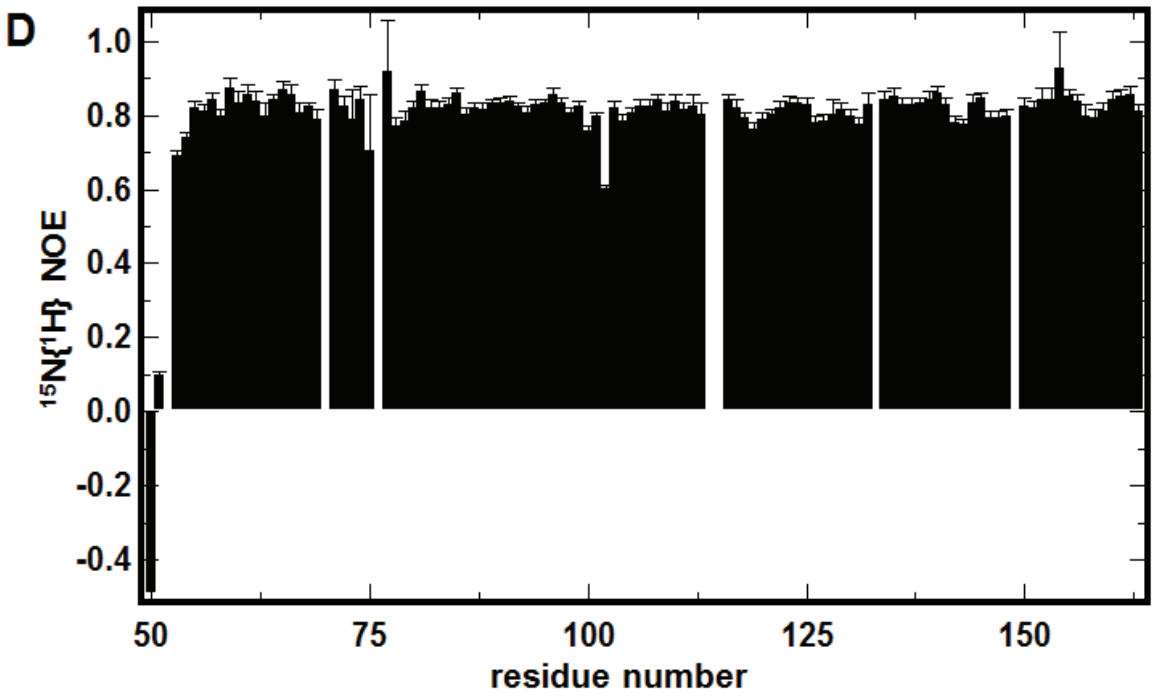
D
1.0
0.8
0.6
0.4
0.2
0.0
-0.2
-0.4
$^{15}N\{^1H\}$ NOE
50
75
100
125
150
residue number

Figure II-12

Heteronuclear NOE (hNOE) values plot against the residue number. (A) wild-type, (B) C113D mutant. The value marked with an asterisk is less reliable because the residue showed very small signal intensity even under non-saturating condition. (A) and (B) were finished in the presence of sulfate and phosphate ions. (C) wild-type, (D) C113D mutant. (C) and (D) were finished in the absence of sulfate and phosphate ions.

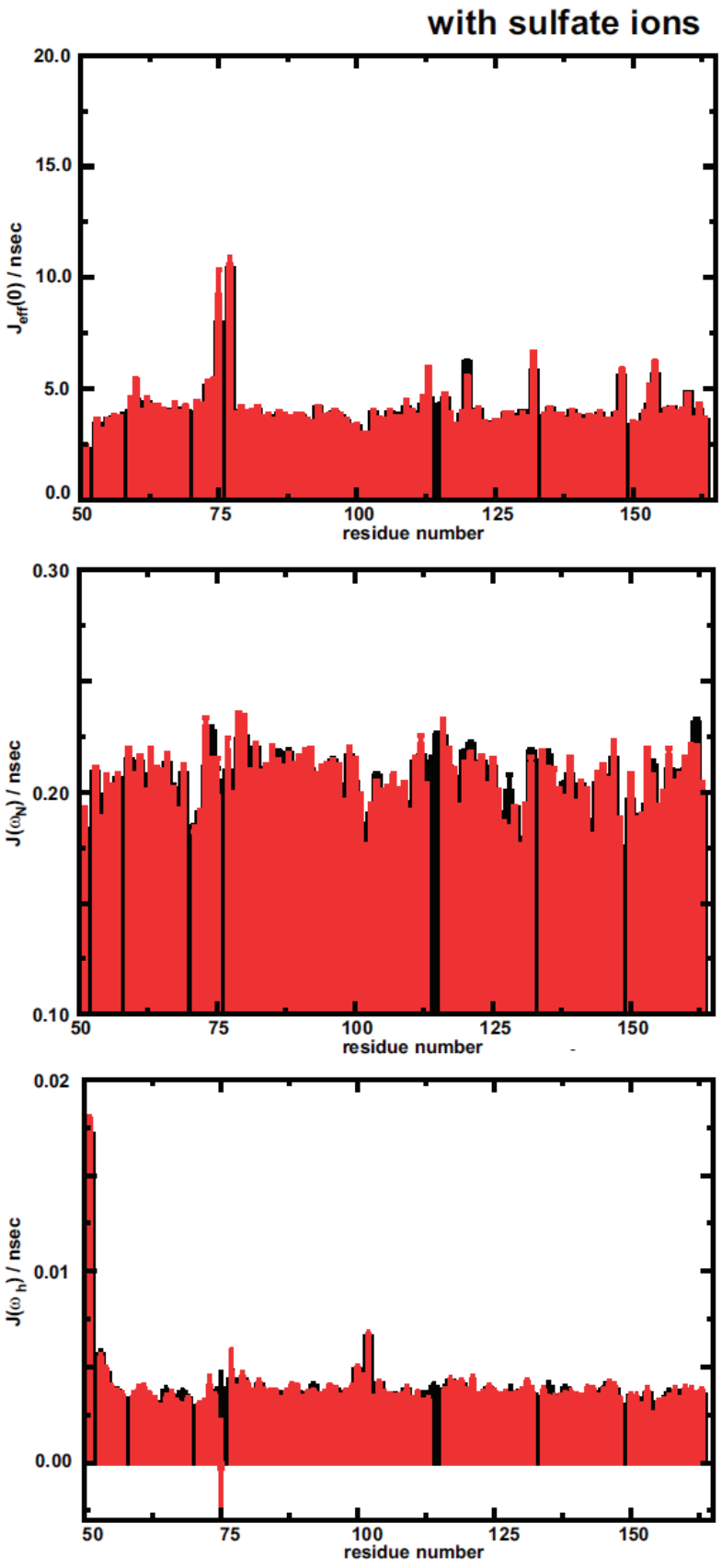
with sulfate ions
20.0
15.0
10.0
5.0
0.0
$J_{eff}(0)$ / nsec
50
75
100
125
150
residue number
0.30
0.20
0.10
$J(\omega_N)$ / nsec
50
75
100
125
150
residue number
0.02
0.01
0.00
$J(\omega_h)$ / nsec
50
75
100
125
150
residue number

Figure II-13

The comparison of the reduced spectral density function values of $J_{eff}(0)$, $J(\omega_N)$, and $J(\omega_h) = J(\omega_H) = J(\omega_H-\omega_N) = J(\omega_H+\omega_N)$ for the data collected in the presence of sulfate and phosphate ions. The bars in red are data for the C113D mutant, and the black bars are those for the wild-type.

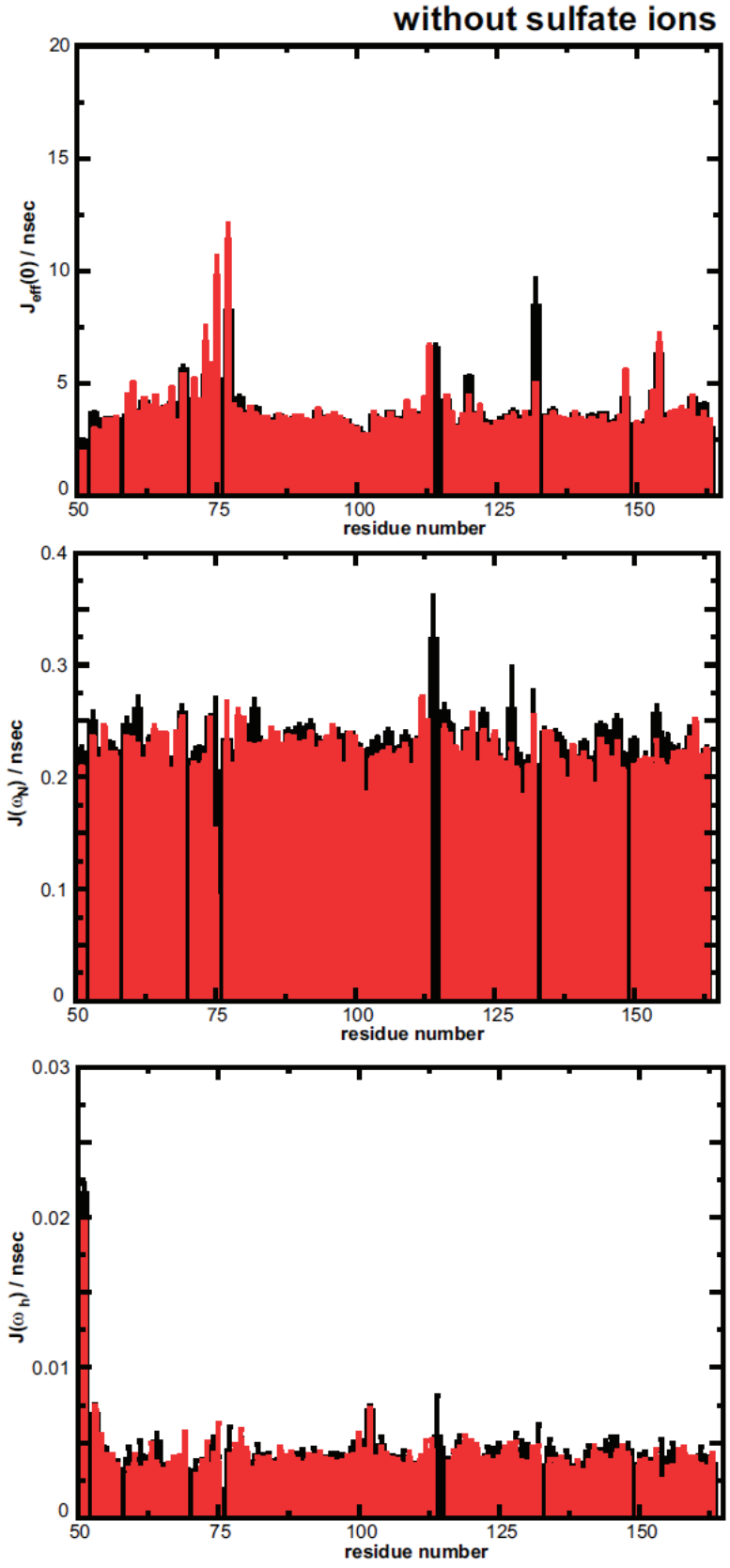
without sulfate ions
$J_{eff}(0)$ / nsec
residue number
$J(\omega_N)$ / nsec
residue number
$J(\omega_h)$ / nsec
residue number

Figure II-14

The comparison of the reduced spectral density function values of $J_{eff}(0)$, $J(\omega_N)$, and $J(\omega_h)$ for the data collected in the absence of sulfate and phosphate ions. The bars in red are data for the C113D mutant and the black bars are those for the wild-type.

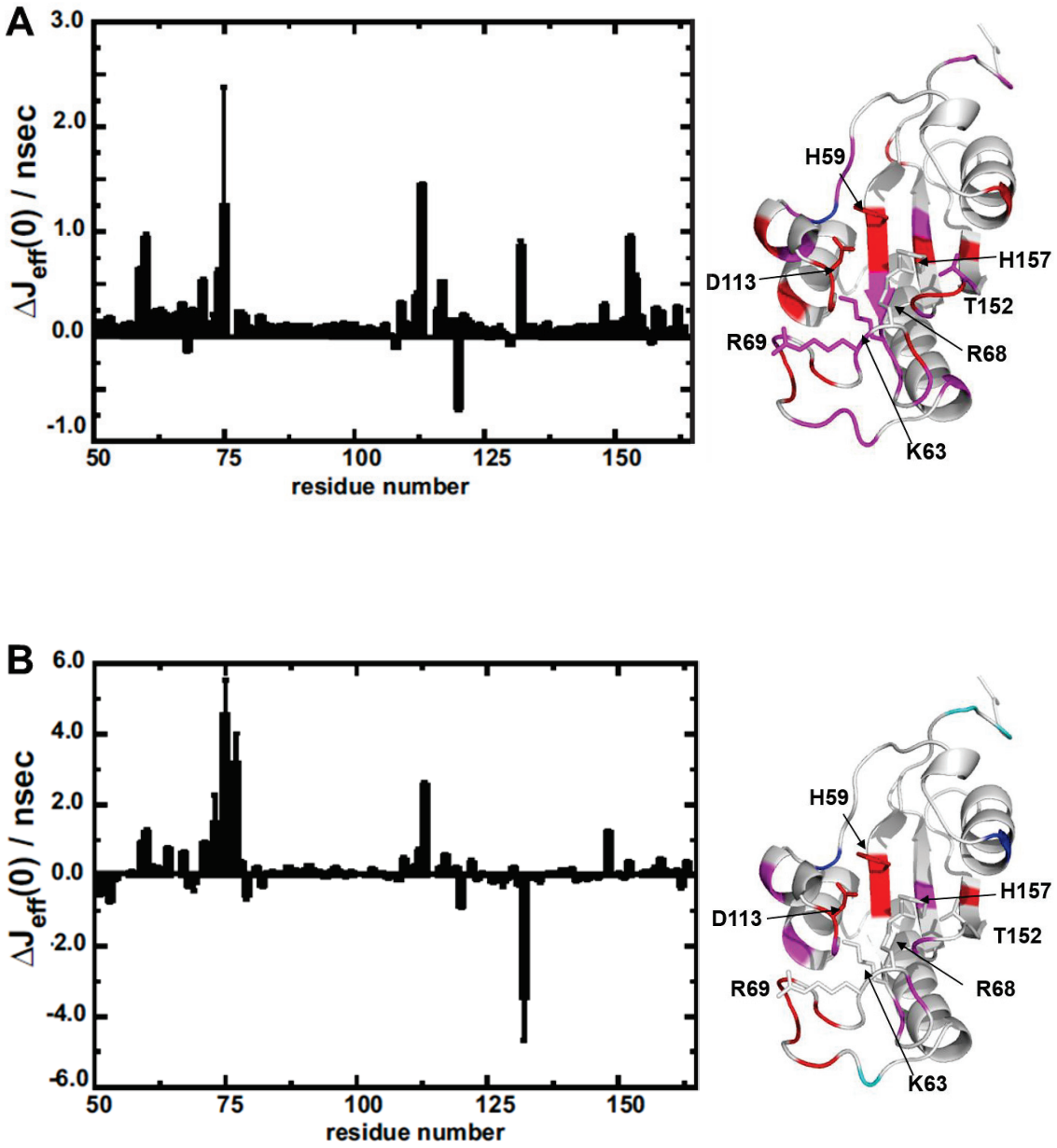
A
3.0
2.0
1.0
0.0
-1.0
$\Delta J_{eff}(0)$ / nsec
50
75
100
125
150
residue number
H59
H157
D113
T152
R69
R68
K63
B
6.0
4.0
2.0
0.0
-2.0
-4.0
-6.0
$\Delta J_{eff}(0)$ / nsec
50
75
100
125
150
residue number
H59
H157
D113
T152
R69
R68
K63

Figure II-15

The residue-wise difference plot for $J_{\mathrm{eff}}(0)$ for the data collected in the presence of sulfate and phosphate ions (A) and in the absence of the ions (B). $\Delta J_{\mathrm{eff}}(0)$ was calculated from the value for C113D mutant minus that for the wild-type. The difference was calculated for each residue as $\Delta J_{eff}(0) = J_{eff}(0)^{C113D} - J_{eff}(0)^{wild-type}$, where $J_{\mathrm{eff}}(0)^{\mathrm{C113D}}$ and $J_{\mathrm{eff}}(0)^{\text{wild-type}}$ the values for C113D mutant and the wild-type, respectively. The residues in the C113D mutant structure are colored according to the magnitude of the $\Delta J_{\mathrm{eff}}(0)$ value; over $\Delta J_{\mathrm{eff}}(0)_{\mathrm{ave}} + 1\sigma$ (red), over $\Delta J_{\mathrm{eff}}(0)_{\mathrm{ave}} + 0.5\sigma$ (magenta), less than $\Delta J_{\mathrm{eff}}(0)_{\mathrm{ave}} - 1\sigma$ (blue) and less than $\Delta J_{\mathrm{eff}}(0)_{\mathrm{ave}} - 0.5\sigma$ (cyan).

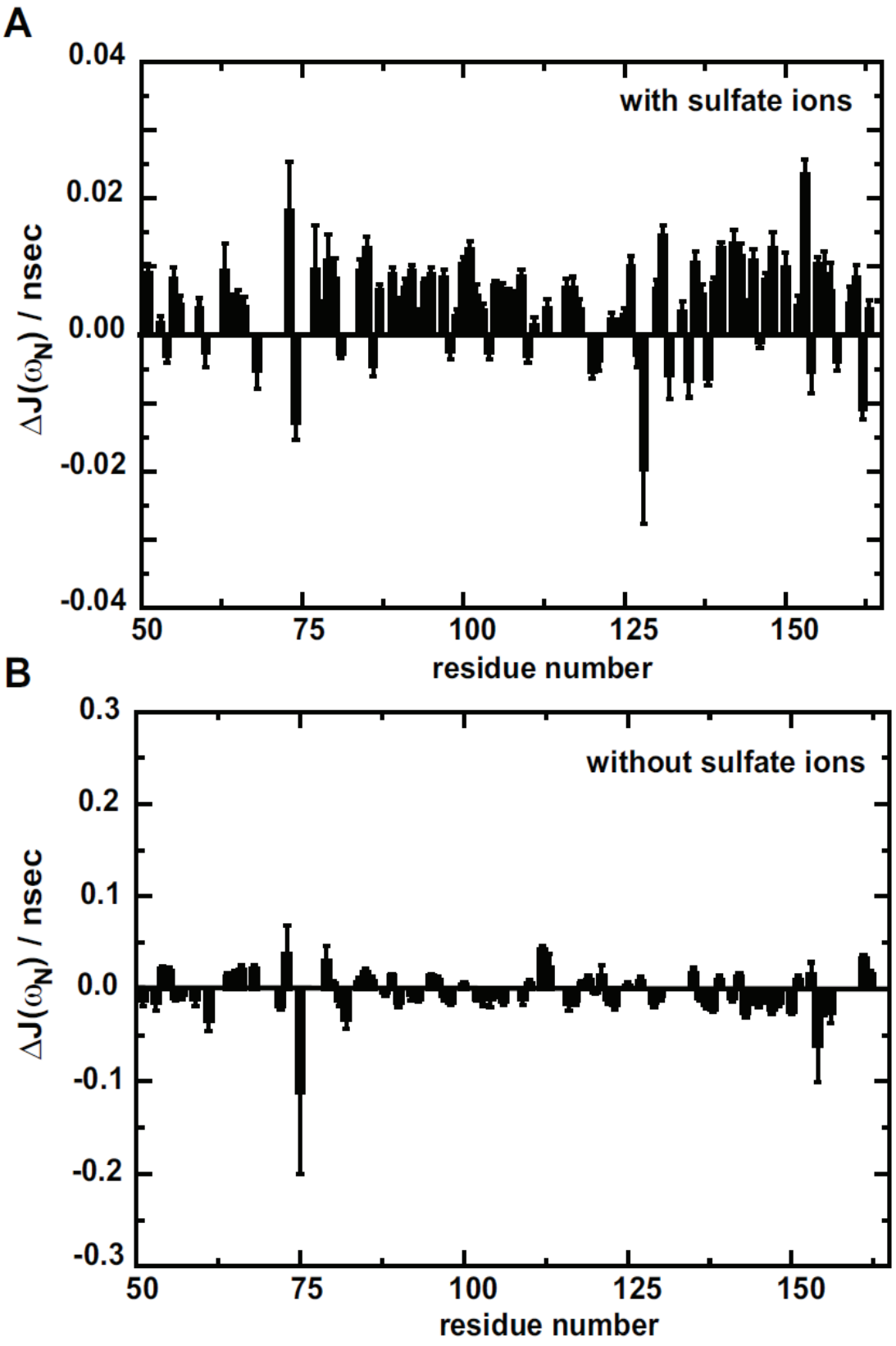
A
with sulfate ions
0.04
0.02
0.00
-0.02
-0.04
ΔJ(ωN) / nsec
50
75
100
125
150
residue number
B
without sulfate ions
0.3
0.2
0.1
0.0
-0.1
-0.2
-0.3
ΔJ(ωN) / nsec
50
75
100
125
150
residue number

Figure II-16

The residue-wise difference plot for $J(\omega_N)$ for the data collected in the presence of sulfate and phosphate ions (A) and in the absence of the ions (B). $\Delta J(\omega_N)$ was calculated from the value for C113D mutant minus that for the wild-type.

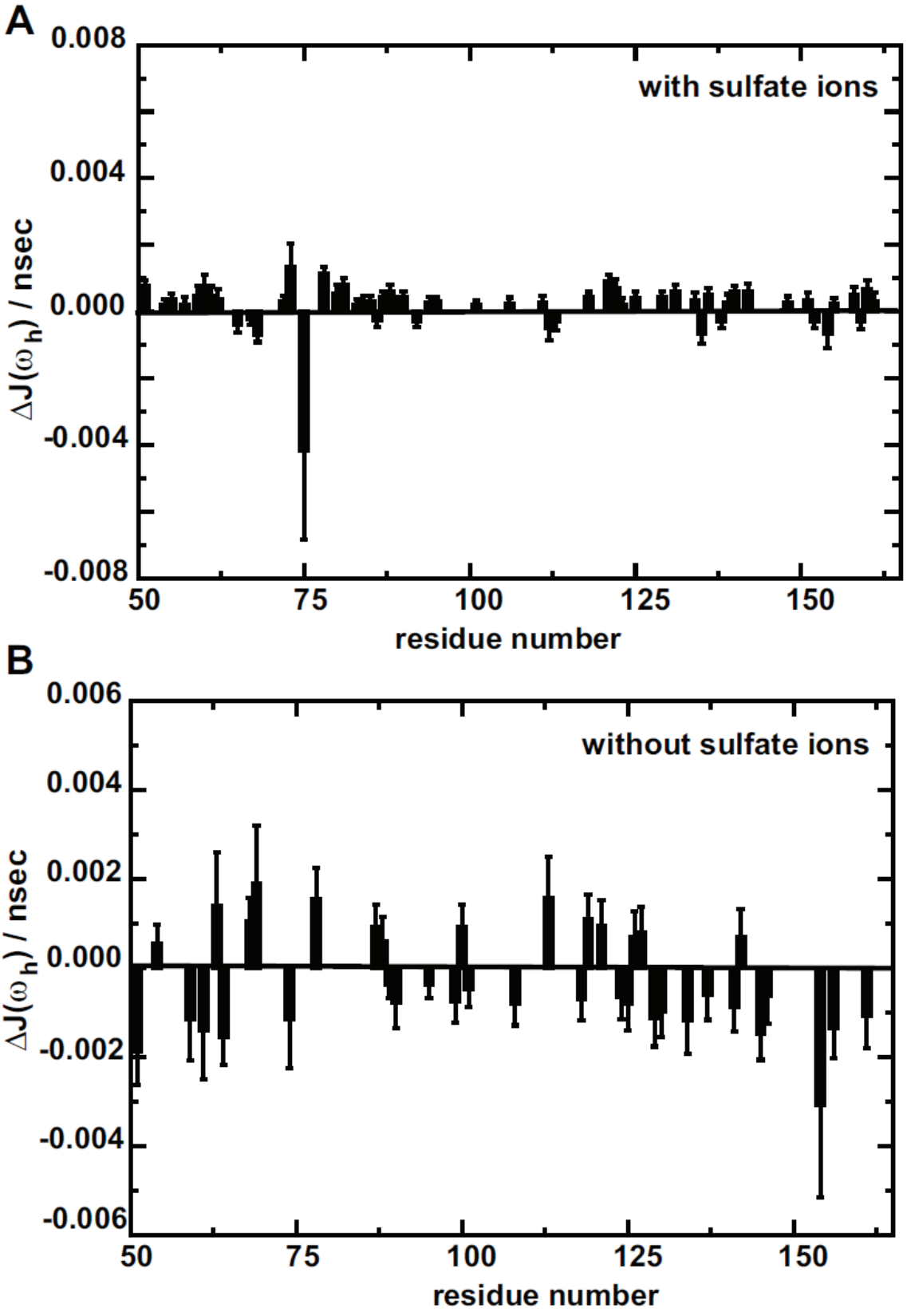
A
0.008
0.004
0.000
-0.004
-0.008
with sulfate ions
ΔJ(ω_h) / nsec
50
75
100
125
150
residue number
B
0.006
0.004
0.002
0.000
-0.002
-0.004
-0.006
without sulfate ions
ΔJ(ω_h) / nsec
50
75
100
125
150
residue number

Figure II-17

The residue-wise difference plot for $\mathcal{J}(\omega_h)$ for the data collected in the presence of sulfate and phosphate ions (A) and in the absence of the ions (B). $\Delta\mathcal{J}(\omega_h)$ was calculated from the value for C113D mutant minus that for the wild-type.

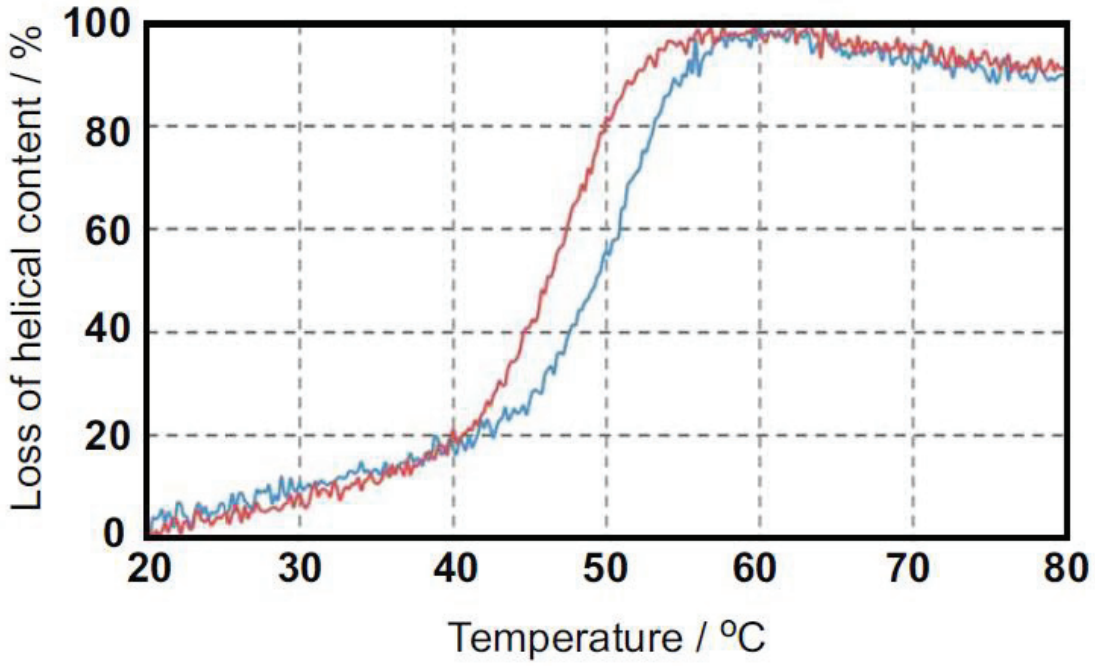

Figure II-18

The heat induced protein denaturing measured by CD molar ellipticity at 222 nm. Blue line indicates the profile for the wild-type Pin1 PPIase domain, while the red line is for C113D mutant.

A

Wild type

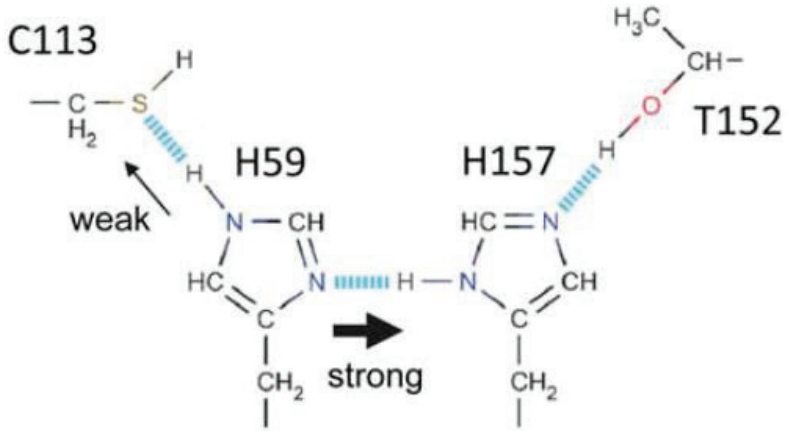

B

C113D mutant D113

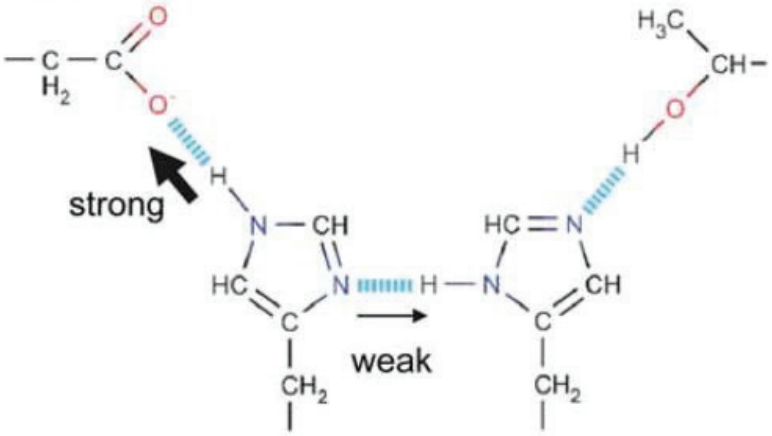

C

oxidized C113 oxC113

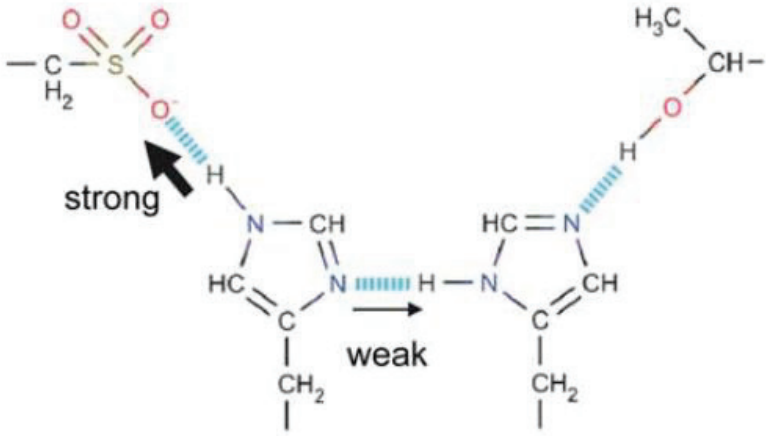

Figure II-19

Hydrogen bonding network and the tag-of-war for H59. (A) The wild-type PPIase domain, H59 forms stronger hydrogen bond to H157. (B) In the C113D mutant, H59 strengthen the hydrogen bonding to C113 with weakening the hydrogen bond to H157. (C) Oxidation to Pin1 PPIase preferentially converts C113 thiol group to sulfonate moiety, which resembles D113 side chain structure. Oxygen atom in sulfonate group plays as a better hydrogen bond acceptor than the sulfur atom in thiol of C113. The oxidized C113 would strengthen the hydrogen bond from H59 with weakening hydrogen bond between H59 and H157, as in C113D mutant. The oxidized Pin1 would be inactivated to the comparable level of C113D mutant Pin1.

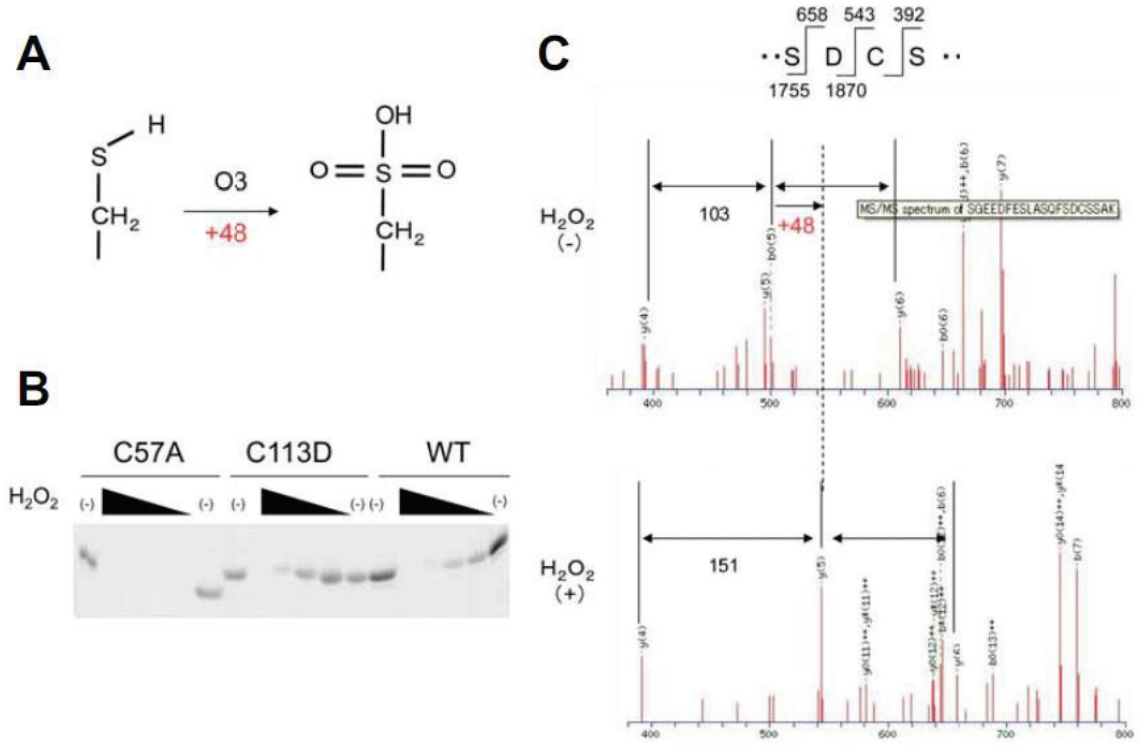

Figure II-20

Oxidation of the cysteine residues in Pin1. (A) Complete oxidation of a thiol group of cysteine leads to forming cysteic acid. The difference in the mass between them should be forty-eight corresponding to three oxygen. (B) Maleimide assay revealed the preferred reactivity of C113 in Pin1. Cysteine modification blocked the labeling of Pin1 proteins by rhodamine-maleimide. Increasing amount of H_2O_2 blocked the maleimide labeling of Pin1 (right). C113 in C57A mutant protein showed more sensitive (left), but C57 in C113D mutant protein showed less sensitive to oxidation (center). (C) Mass spectroscopic analysis revealed the existence of cysteic acid at the position of C113 in H_2O_2-treated Pin1. In the control peptide, C113 showed 103 molecular mass in MS/MS analysis (upper panel). On the contrary, in the H_2O_2-treated Pin1 protein, corresponding C113 showed 151 suggesting the formation of sulfonic acid as shown in A.

Table II-1

Structural statistics of the each final 10 structures of the wild-type (WT) and C113D mutant (C113D) PPIase domains of human Pin1

	WT	C113D
RMSDs from NOE upper distance restraints (Å)		
Intra-residual ($\|i-j\| = 0$) (539 for WT, and 540 for C113D)	0.000±0.004	0.000 ± 0.010
Medium-range ($1 \leq \|i-j\| \leq 4$) (1140, and 969)	0.006 ± 0.048	0.008 ± 0.052
Long-range ($\|i-j\| > 4$) (1062, and 881)	0.012 ± 0.069	0.013 ± 0.088
Total (2741, and 2390)	0.007 ± 0.053	0.008 ± 0.063
RMSDs from dihedral angle restraints (φ and ψ) (°) (88 for WT, and 82 for C113D)[a]	0.068 ± 0.178	0.143 ± 0.396
RMSDs from ideal stereochemistry		
Bonds (Å)	0.005 ± 0.000	0.005 ± 0.000
Angles (º)	0.510 ± 0.007	0.534 ± 0.010
Impropers (º)	0.793 ± 0.052	0.776 ± 0.040
Ramachandran plot[b] (%)		
Residues in most favored regions	87.1	87.8
Residues in additional allowed regions	12.8	11.8
Residues in generously allowed regions	0.1	0.3
Residues in disallowed regions	0.0	0.1
Average RMSDs to the mean structure (Å)[c]		
Backbone (N,CA,C',O)	0.68 ± 0.15	0.74 ± 0.16
All non-hydrogen	1.18 ± 0.19	1.23 ± 0.21

[a] The angle restraints were from TALOS+ with the angle ranges ±30°.

[b] For the residues R54-R161 in the 10 lowest energy structures.

[c] For the residues in the secondary structured parts (residues R54-V62, K82-K97, F103-Q109, S114-A118, D121-S126, K132-S138, V150-F151, and G155-R161 for wild-type, and R54-V62, K82-K97, F103-Q109, S114-A118, A124-S126, K132-F139, M146-F151, and G155-R161 for C113D mutant, respectively).

Table II-2

Conformational exchange in Pin1 PPIase domains for the wild-type and C113D mutant

Sample	Residues in a Group [a]		R_{ex} / sec^{-1} [b]
Wild-type (with ions)	C57 E104 F125 T143		651 ± 48
Wild-type (without ions)	C57 E83 Q94 E104 F134 T143		1099 ± 154
C113D mutant (with ions)	C57 Q94 T143		773 ± 71
C113D mutant (without ions)	LF [c]	Q94 E104 T143 D153	710 ± 63
	HF [c]	C57 R69 E83 F125 M130 Q131	1660 ± 124

[a] The residues in a group were subjected to the global fitting to determine the unique R_{ex} value for the grouped residues.

[b] Values of Rex were calculated from the fits of data to the Caver-Richards equation in the fast-exchange regime.

[c] The residues in the C113D mutant were classified into two classes showing different conformation exchange; LF and HF are the groups comprising the residues showing the higher- and lower conformational exchange rate, respectively.

Chapter III

General conclusions

1. C113D mutant with partial cis-trans isomerization rate is against nucleophilic attack mechanism

In nucleophilic attack mechanism for human Pin1 PPIase domain, C113 sulfur will form covalent bond to the carbonyl carbon of the substrate to facilitate the isomerization process. It is known that the carboxyl group of D113 in C113D mutant does not form covalent bond with the carbonyl carbon, however, our work shows that C113D mutant still has partial *cis-trans* isomerization rate, not the abolished catalytic function. This phenomenon is against previous proposed nucleophilic attack mechanism. In twisting amide bond mechanism, C113 sulfur was suggested to be far from methylene carbon in transition state. However, twisting amide bond mechanism did not show the role of C113 in the catalytic process. The present work has shown that C113 has a role in maintaining the catalytic site in an active fold, challenging the catalytic role of C113 in the catalytic process. In C113D mutant, the binding pocket residues show the allosteric changes and the active loop reveals reduced structurally stability, indicating decreased binding ability for the peptide, which may explain the decreased *cis-trans* isomerization rate.

2. Oxidized Pin1 in Alzheimer's disease

Our work has shown that C113D mutant mimics the oxidized form of Pin1. Oxidized Pin1 is proposed to have the reduced catalytic activity which is

ascribed to the low binding ability for substrate. Tau protein is one substrate of Pin1 in the cells and tau is hyper-phosphorylated and accumulated in Alzheimer's disease [134], which was thought to be related with oxidized Pin1 [172]. It is speculated that oxidized Pin1 loses the binding ability for tau protein and thus cannot isomerize tau protein, which induces the tau protein to be abnormal formation in Alzheimer's disease.

C113D mutant shows a reduced structural stability that is evidenced by H/D exchange and CD spectrum experiments. It is proposed that the oxidized Pin1 also has reduced structural stability; thus, the hydrophobic region of oxidized Pin1 has the higher possibility to be exposed to solvent relative to wild-type. Hydrophobic area of oxidized Pin1 is prone to interact with each other to form the accumulation compared with wild-type. Previous study showed that Pin1 was observed to be accumulated that may be related with Alzheimer's disease, although the role of accumulation was still elusive [174]. Hence, our work provides new insights into the Pin1 accumulation mechanism in the Alzheimer's disease.

References

[1] Farley, A. R., and Link, A. J. (2009) Identification and quantification of protein posttranslational modifications, *Methods Enzymol 463*, 725-763.

[2] Walsh, C. T., Garneau-Tsodikova, S., and Gatto, G. J. Jr. (2005) Protein posttranslational modifications: the chemistry of proteome diversifications, *Angew Chem Int Ed Engl 44,* 7342-7372.

[3] Cohen, P. (2002) The origins of protein phosphorylation, *Nat Cell Biol 4*, E127-E130.

[4] Cieśla, J., Frączyk, T., and Rode, W. (2011) Phosphorylation of basic amino acid residues in proteins: important but easily missed, *Acta Biochim Pol 58*, 137-148.

[5] Towler, D. A., and Gordon, J. I. (1988) The biology and enzymology of eukaryotic protein acylation, *Ann Rev Biochem 57,* 69-99.

[6] Goldston, A. M., Sharma, A. I., Paul, K. S., and Engman, D. M. (2014) Acylation in trypanosomatids: an essential process and potential drug target, *Trends Parasitol 30*, 350-360.

[7] Shaw, P. E. (2007) Peptidyl-prolyl cis/trans isomerase and transcription: is there a twist in the tail? *EMBO Rep 8*, 40-45.

[8] Ramachandran, G. N., and Mitra, A. K. (1976) An explanation for the rare occurrence of *cis* peptide units in proteins and polypeptides, *J Mol Biol 107*, 85-92.

[9] Craveur, P., Joseph, A. P., Poulain, P., de Brevern, A. G., and Rebehmed, J. (2013) Cis-trans isomerization of omega dihedrals in proteins, *Amino Acids 45*, 279-289.

[10] Stewart, D. E., Sarkar, A., and Wampler, J. E. (1990) Occurrence and role of *cis* peptide bonds in protein structures, *J Mol Biol 214*, 253-260.

[11] MacArthur, M. W., and Thornton, J. M. (1991) Influence of proline residues on protein conformation, *J Mol Biol 218*, 397-412.

[12] Weiss, M. S., Jabs, A., and Hilgenfeld, R. (1998) Peptide bonds revised, *Nat Struct Biol 5*, 676.

[13] Lu, K. P., Finn, G., Lee, T. H., and Nicholson, L. K. (2007) Prolyl cis-trans isomerization as a molecular timer, *Nat Chem Biol 10*, 619-629.

[14] Andreotti, A. H. (2003) Native state proline isomerization: an intrinsic molecular switch, *Biochemistry 42*, 9515-9524.

[15] Joseph, A. P., Srinivasan, N., and de Brevern, A. G. (2012) Cis-trans peptide variations in structurally similar proteins, *Amino Acids 43*, 1369-1381.

[16] Morgan, A. A., and Rubenstein, E. (2013) Proline: the distribution, frequency, positioning, and common functional roles of proline and polyproline sequences in the human proteome, *PLoS One 8*, e53785.

[17] Hutchinson, E. G., and Thornton, J. M. (1994) A revised set of potentials for beta-turn formation in proteins, *Protein Sci 3*, 2207-2216.

[18] Krieger, F., Möglich, A., and Kiefhaber, T. (2005) Effect of proline and glycine residues on dynamics and barriers of loop formation in polypeptide chains, *J Am Chem Soc 127*, 3346-3352.

[19] Wedemeyer, W. J., Welker, E., and Scheraga, H. A. (2002) Proline cis-trans isomerization and protein folding, *Biochemistry 41*, 14637-14644.

[20] Fischer, G., and Schmid, F. X. (1990) The mechanism of protein folding. Implications of in vitro refolding models for de novo protein folding and translocation in the cell, *Biochemistry 29*, 2205-2212.

[21] Juminaga, A., Wedemeyer, W. J., Garduño-Júarez, R., McDonald, M. A., and Scheraga, H. A. (1997) Tyrosyl interactions in the folding and unfolding of bovine pancreatic ribonuclease A: a study of tyrosine-to-phenylalanine mutants, *Biochemistry 36*, 10131-10145.

[22] Schmid, F. X. (1986) proline isomerization during refolding of ribonuclease A is accelerated by the presence of folding intermediates, *FEBS Lett 198*, 217-220.

[23] Neira, J. L, and Rico, M. (1997) Folding studies on ribonuclease A, a model protein, *Fold Des 2*, R1-R11.

[24] Raines, R. T. (1998) Ribonuclease A, *Chem Rev 98*, 1045-1065.

[25] Wlodawer, A., Svensson, L. A., Sjölin, L., and Gilliland, G. L. (1988) Structure of phosphate-free ribonuclease A refined at 1.26 Å, *Biochemistry 27*, 2705-2717.

[26] Juminaga, A., Wedemeyer, W. J., and Scheraga, H. A. (1998) Proline isomerization in bovine pancreatic ribonuclease A. 1. Unfolding condition, *Biochemistry 37*, 11614-11620.

[27] Kiefhaber T[1], Grunert HP, Hahn U, and Schmid FX. (1990) Replacement of a cis proline simplifies the mechanism of ribonuclease T1 folding, *Biochemistry 29*, 6475-6480.

[28] Schindler, T., Mayr, L. M., Landt, O., Hahn, U., and Schmid, F. X. (1996) The role of trans-folding mechanism of ribonuclease T1, *Eur J Biochem 241*, 516-524.

[29] George, R. A., and Heringa, J. (2003) An analysis of protein domain linkers: their classification and role in protein folding, *Protein Eng 15*, 871-879.

[30] Lee, G. R., Shin, W. H., Park, H., Shin, S., and Seok, C. (2012) Conformational sampling of flexible ligand-binding protein loops, *Bull Korean chem Soc 33*, 770-774.

[31] Abbate, F., Supuran, C. T., Scozzafava, A., Orioli, P., Stubbs, M. T., and Klebe, G. (2002) Nonaromatic sulfonamide group as an ideal anchor for potent human carbonic anhydrase inhibitors: role of hydrogen-bonding networks in ligand binding and drug design, *J Med Chem 45*, 3583-3587.

[32] Helm, C. A., Knoll, W., and Israelachvili, J. N. (1991) Measurement of ligand-receptor interactions, *Proc Natl Acad Sci U S A 88*, 8169-8173.

[33] Mallis, R. J., Brazin, K. N., Fulton, D. B., and Andreotti, A. H. (2002) Structural characterization of a proline-driven conformational switch within the Itk SH2 domain, *Nat Struct Biol 9*, 900-905.

[34] Bachmann, M. F., Littman, D. R., and Liao, X. C. (1997) Antiviral immune responses in Itk-deficient mice, *J Virol 71*, 7253-7257.

[35] Sahu, N., and August, A. (2009) ITK inhibitors in inflammation and immune-mediated disorders, *Curr Top Med Chem 9*, 690-703.

[36] Brazin, K. N., Mallis, R. J., Fulton, D. B., and Andreotti, A. H. (2001) Regulation of the tyrosine kinase Itk by the peptidyl-prolyl isomerase cyclophilin A, *Proc Natl Acad Sci U S A 99,* 1899-1904.

[37] Brazin, K. N., Fulton, D. B., and Andreotti, A. H. (2000) A Specific intermolecular association between the regulatory domains of a tec family kinase, *J Mol Biol 302*, 607-623.

[38] Gabashvili, I. S., Sokolowski, B. H. A., Morton, C. C., and Giersch, A. B. S. (2007) Ion channel gene expression in the inner ear, *J Assoc Res Otolaryngol 8*, 305-328.

[39] Tabassum, N., and Feroz, A. (2011) Ion channels and their modulation, *J App Pharm Sci 1*, 20-25.

[40] Voets, T., Droogmans, G., Wissenbach, U., Janssens, A., Flockerzi, V., and Nilius, B. (2004) The principle of temperature-dependent gating in cold- and heat-sensitive TRP channels, *Nature 430*, 748-754.

[41] Cesare, P., Moriondo, A., Vellani, V., and McNaughton, P. A. (1999) Ion channels gated by heat, *Proc Natl Acad Sci U S A 96,* 7658-7663.

[42] Sandoval, M., Burgos, J., Sepulveda, F. V., and Cid, L. P. (2011) Extracellular pH in restricted domains as a gating signal for ion channels involved in transepithelial transport, *Biol Pharm Bull 34*, 803-809.

[43] Chen, C. C., England, S., Akopian, A. N., and Wood, J. N. (1998) A sensory neuron-specific, proton-gated ion channel, *Proc Natl Acad Sci U S A 95,* 10240-10245.

[44] Zha, X. M. (2013) Acid-sensing ion channels: trafficking and synaptic function, *Mol Brain 6*, 1.

[45] Bagal, S. K., Brown, A. D., Cox, P. J., Omoto, K., Owen, R. M., Pryde, D. C., Sidders, B., Skerratt, S. E., Stevents, E. B., Storer, R. I., and Swain, N. A. (2012) Ion channels as therapeutic targets: a drug discovery perspective, *J Med Chem 56*, 593-624.

[46] Kaczorowski, G. J., McManus, O. B., Priest, B. T., and Garcia, M. L. (2008) Ion channels as drug targets: the next GPCRs, *J Gen Physiol 131*,399-405.

[47] Lummis, S. C., Beene, D. L., Lee, L. W., Lester, H. A., Broadhurst, R. W., and Dougherty, D. A. (2005) Cis-trans isomerization at a proline opens the pore of a neurotransmitter-gated ion channel, *Nature 438*, 248-252.

[48] Lummis, S. C. (2004) The transmembrane domain of the 5-HT3 receptor: its role in selectivity and gating, *Biochem Soc Trans 32,* 535-539.

[49] Meeus, N., and Lummis, S. C. R. (2003) Proline 307 in the mouse 5–-HT_{3a} receptor links binding and function, *pa2online 1*, 015P.

[50] Lorenz, S. H., Jakob, R. P., Weininger, U., Balbach, J., Dobbek, H., and Schmid, F. X. (2011) The filamentous phages fd and IF1 use different mechanisms to infect Escherichia coli, *J Mol Biol 405*, 989-1003.

[51] Lubkowski, J., Hennecke, F., Plückthun, A., and Wlodawer, A. (1999) Filamentous phage infection: crystal structure of g3p in complex with its coreceptor, the C-terminal domain of TolA, *Structure 7*, 711-722.

[52] Martin, A., and Schmid, F. X. (2003) A proline switch controls folding and domain interactions in the gene-3-protein of the filamentous phage fd, *J Mol Biol 331*, 1131-1140.

[53] Eckert, B., Martin, A., Balbach, J., and Schmid, F. X. (2005) Prolyl isomerization as a molecular timer in phage infection, *Nat Struct Mol Biol 12*, 619-623.

[54] Choichet, B. K., Baase, W. A., Kuroki, R., and Matthews, B. W. (1995) A relationship between protein stability and protein function, *Proc Natl Acad Sci U S A 92,* 452-456.

[55] Yue, P., Li, Z. L., and Moult, J. (2005) Loss of protein structure stability as a major causative factor in monogenic disease, *J Mol Biol 353*, 459-473.

[56] Moore, D. J., Zhang, L., Dawson, T. M., and Dawson, V. L. (2003) A missense mutation (L166P) in DJ-1, linked to familial Parkinson's disease, confers reduced protein stability and impairs homo-oligomerization, *J Neurochem 87*, 1558-1567.

[57] Truckses, D. M., Somoza, J. R., Prehoda, K. E., Miller, S. C., and Markley, J. L. (1996) Coupling between trans/cis proline isomerization and protein stability instaphylococcal nuclease, *Protein sci 5*, 1907-1916.

[58] Penela, P., Rivas, V, Salcedo, A., and Mayor, F. Jr. (2009) G protein-coupled receptor kinase 2 (GRK2) modulation and cell cycle progression, *Proc Natl Acad Sci U S A 107,* 1118-1123.

[59] Yoshida, N., Haga, K., and Haga, T. (2003) Identification of sites of phosphorylation by G-protein-coupled receptor kinase 2 in beta-tubulin, *Eur J Biochem 270*, 1154-1163.

[60] New, D. C., and Wong, Y. H. (2007) Molecular mechanisms mediating the G protein-coupled receptor regulation of cell cycle progression, *J Mol Signal 2,* 2.

[61] Pierce, K. L., Premont, R. T., and Lefkowitz, R. J. (2002) Seven-transmembrane receptors, *Nat Rev Mol Cell Biol 3,* 639-650.

[62] Zhou, X. Z., Lu, P. J., Wulf, G., and Lu, K. P. (1999) Phosphorylation-dependent prolyl isomerization: a novel signaling regulatory mechanism, *Cell Mol Life Sci 56,* 788-806.

[63] Ubersax, J. A., and Ferrell, J. E. Jr. (2007) Mechanisms of specificity in protein phosphorylation, *Nat Rev Mol Cell Biol 8*, 530-541.

[64] Arnesen, T. (2011) Towards a functional understanding of protein N-terminal acetylation, *PLoS Biol 9*, e1001074.

[65] Sriram, G., and Birge, R. B. (2010) Emerging roles for crk in human cancer, *Genes Cancer 1*, 1132-1139.

[66] Tsuda, M., and Tanaka, S. (2012) Roles for crk in cancer metastasis and invasion, *Genes Cancer 3*, 334-340.

[67] Sarkar, P., Reichman, C., Saleh, T., Birge, R. B., and Kalodimos, C. G. (2007) Proline cis-trans isomerization controls autoinhibition of a signaling protein, *Mol Cell 25*, 413-426.

[68] Nicholson, L. K., and Lu, K. P. (2007) Prolyl cis-trans Isomerization as a molecular timer in Crk signaling, *Mol Cell 25*, 483-485.

[69] Pauling, L., Corey, R. B., and Branson, H. R. (1951) The structure of proteins; two hydrogen-bonded helical configurations of the polypeptide chain, *Proc Natl Acad Sci U S A 37,* 205-211.

[70] Edison, A. S. (2001) Linus pauling and the planar peptide bond, *Nat Struct Biol 8*, 201-202.

[71] Gebauer, S., Friebe, S., Scherer, G., Gübitz, G., and Krauss, G. J. (1998) High Performance Liquid Chromatography on Calixarene-Bonded Silica Gels. III. Separations of *cis/trans* Isomers of Proline-Containing Peptides, *J Chromatogr Sci 36*, 388-394.

[72] Fischer, S., Dunbrack, R. L. Jr. and Karplus, M. (1994) Cis-trans imide isomerization of the proline dipeptide, *J Am Chem Soc 116*, 11931-11937.

[73] Harding, M. W., and Handschumacher, R. E. (1988) Cyclophilin, a primary molecular target for cyclosporine. Structure and functional implications, *Transplantation 46*, 29S-35S.

[74] Stamnes, M. A., and Zuker, C. S. (1990) Peptidyl-prolyl cis-trans isomerases, cyclophilin, FK506-binding protein, and ninaA: four of a kind, *Curr Opin Cell Biol 2*, 1104-1107.

[75] Jordens, J., Janssens, V., Longin, S., Stevens, I., Martens, E., Bultynck, G., Engelborghs, Y., Lescrinier, E., Waelkens, E., Goris, J., and Van Hoof, C. (2006) The protein phosphatase 2A phosphatase activator is a novel peptidyl-prolyl cis/trans-isomerase, *J Biol Chem 281*, 6349-6357.

[76] Rulten, S., Thorpe, J., and Kay, J. (1999) Identification of eukaryotic parvulin homologues: a new subfamily of peptidylrpolyl cis-trans isomerase, *Biochem Biophys Res Commun 259,* 557-562.

[77] Schroeder, O. E., Carper, E., Wind, J. J., Poutsma, J. L., Etzkorn, F. A., and Poutsma, J. C. (2006) Theoretical and experimental investigation of the energetics of cis-trans proline isomerization in peptide models, *J Phys Chem 110*, 6522-6530.

[78] Reimer, U., el Mokdad, N., Schutkowski, M., and Fischer, G. (1997) Intramolecular assistance of cis/trans isomerization of the histidine-proline moiety, *Biochemistry 1997*, 13802-13808.

[79] Fischer, S., Michnick, S., and Karplus, M. (1993) A mechanism for rotamase catalysis by the FK506 binding protein (FKBP), *Biochemistry 32*, 13830-13837.

[80] Cox, C., Young, V. G. Jr., and Lectka, T. (1997) Intramolecular catalysis of amide isomerization, *J Am Chem Soc 119*, 2307-2308.

[81] Cox, C., and Lectka, T. (1998) Intramolecular Catalysis of amide isomerization: kinetic consequences of the 5-NH- -Na hydrogen Bond in prolyl peptides, *Biochemistry 120*, 10660-10668.

[82] Hur, S., and Bruice, T. C. (2002) The Mechanism of Cis-Trans Isomerization of Prolyl Peptides by Cyclophilin, *J Am Chem Soc 124*, 7303-7313.

[83] Rosen, M. K., Standaert, R. F., Galat, A., Nakatsuka, M., and Schreiber, S. L. (1990) Inhibition of FKBP rotamase activity by immunosuppressant FK506: twisted amide surrogate, *Science 248*, 863-866.

[84] Xu, G. G., Zhang, Y., Mercedes-Camacho, A. Y., and Etzkorn, F. A. (2011) A reduced-amide inhibitor of Pin1 binds in conformation resembling a twisted-amide transition state, *Biochemistry 50*, 9545-9550.

[85] Wang, P., and Heitman, J. (2005) The cyclohpilins, *Genome Biol 6*, 226.

[86] Fischer, G., Wittmann-Liebold, B., Lang, K., Kiefhaber, T., and Schmid, F. X. (1989) Cyclophilin and peptidyl-prolyl cis-trans isomerase are probably identical proteins, *Nature 337*, 476-478.

[87] Handschumacher, R. E., Harding, M. W., Rice, J., Drugge, R. J., and Speicher, D. W. (1984) Cyclophilin: a specific cytosolic binding protein for cyclosporin A, *Science 226*, 544-547.

[88] Rosoff, P. M., and Terres, G. (1986) Cyclosporine A inhibits Ca^{2+} -dependent stimulation of the Na^{+}/H^{+} antiport in human T cells, *J Cell Biol 103*, 457-463.

[89] Bosco, D. A., Eisenmesser, E. Z., Pochapsky, S., Sundquist, W. I., and Kern, D. (2002) Catalysis of cis/trans isomerization in native HIV-1 capsid by human cyclophilin A, *Proc Natl Acad Sci U S A 99,* 5247-5252.

[90] Liu, J., Albers, M. W., Chen, C. M., Schreiber, S. L., and Walsh, C. T. (1990) Cloning, expression and purification of human cyclophilin in Escherichia coli and assessment of the catalytic role of cysteines by site-directed mutagenesis, *Proc Natl Acad Sci U S A 87,* 2304-2308.

[91] Haendler, B., Keller, R., Hiestand, P. C., Kocher, H. P., Wegmann, G., and Movva, N. R. (1989) Yeast cyclophilin: isolation and characterization of the protein, cDNA and gene, *Gene 83*, 39-46.

[92] Harrison, R. K., and Stein, R. L. (1990) Mechanistic studies of peptidyl prolyl cis-trans isomerase: evidence for catalysis by distortion, *Biochemistry 29*, 1684-1689.

[93] Harrison, R. K., Caldwell, C. G., Rosegay, A., Melillo, D., and Stein, R. L. (1990) Confirmation of the secondary deuterium isotope effect for the peptidyl prolyl cis-trans isomerase activity of cyclophilin by a competitive, double-label technique, *J Am Chem Soc 112*, 7063-7064.

[94] Harrison, R. K., and Stein, R. L. (1991) Mechanistic studies of enzymic and nonenzymic prolyl cis-trans isomerization, *J Am Chem Soc 114*, 3464-3471.

[95] Kallen, J., and Walkinshaw, M. D. (1992) The X-ray structure of a tetrapeptide bound to the active site of human cyclophilin A, *FEBS Lett 300*, 286-290.

[96] Howard, B. R., Vajdos, F. F., Li, S., Sundquist, W. I., and Hill, C. P. (2003) Structural insights into the catalytic mechanism of cyclophilin A, *Nat Struct Biol 10*, 475-481.

[97] Zydowsky, L. D., Etzkorn, F. A., Chang, H. Y., Ferquson, S. B., Stolz, L. A., Ho, S. I., and Walsh, C. T. (1992) Active site mutants of human cyclophilin A separate peptidyl-prolyl isomerase activity from cyclosporine A binding and calcineurin inhibition, *Protein Sci 1*, 1092-1099.

[98] Sawada, S., Suzuki, G., Kawase, Y., and Takaku, F. (1987) Novel immunosuppressive agent, FK506. In vitro effects on the cloned T cell activation, *J Immunol 139*, 1797-1803.

[99] Clipstone, N. A., and Crabtree, G. R. (1993) Calcineurin is a key signaling enzyme in T lymphocyte activation and the target of the immunosuppressive drugs cyclosporin A and FK506, *Ann N Y Acad Sci 696*, 20-30.

[100] Siekierka, J. J., Hung, S. H., Poe, M., Lin, C. S., and Sigal, N. H. (1989) A cytosolic binding protein for the immunosuppressant FK506 has peptidyl-prolyl isomerase activity but is distinct from cyclophilin, *Nature 341*, 755-757.

[101] Trandinh, C. C., Pao, G. M., and Saier, M. H. Jr. (1992) Structural and evolutionary relationships among the immunophilins: two ubiquitous families of peptidyl-prolyl cis-trans isomerases, *FASEB J 6*, 3410-3420.

[102] Suzuki, R., Nagata, K., Yumoto, F., Kawakami, M., Nemoto, N., Furutani, M., Adachi, K., Maruyama, T., and Tanokura, M. (2003) Three-dimensional Solution Structure of an Archaeal FKBP with a Dual Function of Peptidyl Prolyl cis–trans Isomerase and Chaperone-like Activities, *J Mol Biol 328*, 1149-1160.

[103] Yamaguchi, T., Kurisaki, A., Yamakawa, N., Minakuchi, K., and Sugino, H. (2006) FKBP12 functions as an adaptor of the Smad7–Smurf1 complex on activin type I receptor, *J Mol Endocrinol 36*, 569-579.

[104] Van Duyne, G. D., Standaert, R. F., Karplus, P. A., Schreiber, S. L., and Clardy, J. (1991) Atomic structure of FKBP-FK506, an immunophilin-imunosuppressant complex, *Science 252*, 839-842.

[105] Jordens, J., Janssens, V., Longin, S., Stevens, I., Martens, E., Bultynck, G., Engelborghs, Y., Lescrinier, E., Waelkens, E., Goris, J., and Van Hoof, C. (2006) The protein phosphatase 2A phosphatase activator is a novel peptidyl-prolyl cis/trans-isomerase, *J Biol Chem 281*, 6349-6357.

[106] Cayla, X., Goris, J., Hermann, J., Hendrix, P., Ozon, R., and Merlevede, W. (1990) Isolation and characterization of a tyrosyl phosphatase activator from rabbit skeletal muscle and xenopus laevis oocytes, *Biochemistry 29*, 658-667.

[107] Van Hoof C, Janssens V, Dinishiotu A, Merlevede W, and Goris J. (1998) Functional analysis of conserved domains in the phosphotyrosyl phosphatase activator. Molecular cloning of the homologues from drosophila melanogaster and saccharomyces cereVisiae, *Biochemistry 37*, 12899-12908.

[108] Leulliot, N., Vicentini, G., Jordens, J., Quevillon-Cheruel, S., Schiltz, M., Barford, D., van Tilbeurgh, H., and Goris, J. (2006) Crystal Structure of the PP2A Phosphatase Activator: Implications for Its PP2A-Specific PPIase Activity, *Mol Cell 23*, 413-424.

[109] Mikol, V., Kallen, J., Pflügl, G., and Walkinshaw, M. D. (1993) X-ray structure of a monomeric cyclophilin A-cyclosporin A crystal complex at 2.1 Å resolution, *J Mol Biol 234*, 1119-1130.

[110] Rahfeld, J. U., Schierhorn, A., Mann, K., and Fischer, G. (1994) A novel peptidyl-prolyl cis/trans isomerase from Escherichia coli, *FEBS Lett 343*, 65-69.

[111] Lu, K. P., Hanes, S. D. and Hunter, T. (1996) A human peptidyl-prolyl isomerase essential for regulation of mitosis, *Nature 380*, 544-547.

[112] Landrieu. I., De Veylder, L., Fruchart, J. S., Odaert, B., Casteels, P., Portetelle, D., Van Montagu, M., Inzé, D., and Lippens, G. (2000) The Arabidopsis thaliana PIN1At Gene Encodes a Single-domain Phosphorylation-dependent Peptidyl Prolyl cis/trans Isomerase, *J Biol Chem 275*, 10577-10581.

[113] Ranganathan, R., Lu, K. P., Hunter, T., and Noel, J. P. (1997) Structural and Functional Analysis of the Mitotic Rotamase Pin1 Suggests Substrate Recognition Is Phosphorylation Dependent, *Cell 89*, 875-886.

[114] Terada, T., Shirouzu, M., Fukumori, Y., Fujimori, F., Ito, Y., Kigawa, T., Yokoyama, S., and Uchida. T. (2001) Solution structure of the human parvulin-like peptidyl prolyl cis/trans isomerase, hPar14, *J Mol Biol 305*, 917-926.

[115] Sekerina, E., Rahfeld, J. U., Müller, J., Fanghänel, J., Rascher, C., Fischer, G., and Bayer, P. (2000) NMR solution structure of hPar14 reveals similarity to the peptidyl prolyl cis/trans isomerase domain of the mitotic regulator hPin1 but indicates a different functionality of the protein, *J Mol Biol 301*, 1003-1017.

[116] Landrieu, I., Wieruszeski, J. M., Wintjens, R., Inzé, D., and Lippens G. (2002) Solution Structure of the Single-domain Prolyl Cis/ Trans Isomerase PIN1At from Arabidopsis thaliana, *J Mol Biol 320*, 321-332.

[117] Kühlewein, A,, Voll, G., Hernandez Alvarez, B., Kessler, H., Fischer, G., Rahfeld, J. U., and Gemmecker, G. (2004) Solution structure of Escherichia coli Par10: The prototypic member of the Parvulin family of peptidyl-prolyl cis/trans isomerases, *Protein Sci 13*, 2378-2387.

[118] Bitto, E., and McKay, D. B. (2002) Crystallographic structure of SurA, a molecular chaperone that facilitates folding of outer membrane porins, *Structure 10*, 1489-1498.

[119] Li, Z., Li, H., Devasahayam, G., Gemmill, T., Chaturvedi, V., Hanes, S. D., and Van Roey, P. (2005) The structure of the candida albicans Ess1 prolyl isomerase reveals a well-ordered linker that restricts domain mobility, *Biochemistry 44*, 6180-6189.

[120] Tossavainen, H., Permi, P., Purhonen, S. L., Sarvas, M., Kilpeläinen, I., and Seppala, R. (2006) NMR solution structure and characterization of substrate binding site of the PPIase domain of PrsA protein from *Bacillus subtilis, FEBS Lett 580,* 1822-1826.

[121] Heikkinen, O., Seppala, R., Tossavainen, H., Heikkinen, S., Koskela, H., Permi, P., and Kilpeläinen, I. (2009) Solution structure of the parvulin-type PPIase domain of *Staphylococcus aureus* PrsA – Implications for the catalytic mechanism of parvulins, *BMC Struct Biol 9,* 17.

[122] Jaremko, Ł., Jaremko, M., Elfaki, I., Mueller, J. W., Ejchart, A., Bayer, P., and Zhukov, I. (2011) Structure and dynamics of the first archaeal parvulin reveal a new functionally important loop in parvulin-type prolyl isomerases, *J Biol Chem 286*, 6554-6565.

[123] Sun, L., Wu, X., Peng, Y., Goh, J. Y., Liou, Y. C., Lin, D., and Zhao, Y. (2012) Solution structural analysis of the single-domain parvulin TbPin1, *PloS One 7*, e43017.

[124] Wang, Y., Liu, C., Yang, D., Yu, H., and Liou, Y. C. (2010) Pin1At encoding a peptidyl-prolyl cis/trans isomerase regulates flowering time in Arabidopsis, *Mol Cell 37*, 112-122.

[125] Uchida, T., Fujimori, F., Tradler, T., Fischer, G., and Rahfeld, J. U. (1999) Identification and characterization of a 14 kDa human protein as a novel parvulin-like peptidyl prolyl cis/trans isomerase, *FEBS Lett 446*, 278-282.

[126] Mueller, J. W., Link, N. M., Matena, A., Hoppstock, L., Rüppel, A., Bayer, P., and Blankenfeldt, W. (2011) Crystallographic proof for an extended hydrogen-bonding network in small prolyl isomerases, *J Am Chem Soc 133*, 20096-20099.

[127] Zhou, X. Z., Kops, O., Werner, A., Lu, P. J., Shen, M., Stoller, G., Küllertz, G., Stark, M., Fischer, G., and Lu, K. P. (2000) Pin1-dependent prolyl isomerization regulates dephosphorylation of Cdc25C and tau proteins, *Mol Cell 6*, 873-883.

[128] Behrsin, C. D., Bailey, M. L., Bateman, K. S., Hamilton, K. S., Wahl, L. M., Brandl, C. J, Shilton, B. H., and Litchfield, D. W. (2007) Functionally important residues in the peptidyl-prolyl isomerase Pin1 revealed by unigenic evolution, *J Mol Biol 365*, 1143-1162.

[129] Xu, G. G., Slebodnick, C., and Etzkorn, F. A. (2012) Cyclohexyl ketone inhibitors of Pin1 dock in a trans- diaxial cyclohexane conformation, *PLoS One 7*, e44226.

[130] Mercedes-Camacho, A. Y., Mullins, A. B., Mason, M. D., Xu, G. G., Mahoney, B. J., Wang, X., Peng, J. W., and Etzkorn, F. A. (2013) Kinetic isotope effects support the twisted amide mechanism of Pin1 peptidyl-prolyl isomerase, *Biochemistry 52*, 7707-7713.

[131] Lu, K. P. (2004) Pinning down cell signaling, cancer and Alzheimer's disease, *Trends Biochem Sci 29*, 200-209.

[132] Esnault, S., Shen, Z.-J., and Malter, J. S. (2008) Pinning Down Signaling in the Immune System: The Role of the Peptidyl-Prolyl Isomerase Pin1 in Immune Cell Function, *Crit Rev Immunol 28*, 45-60.

[133] Butterfield, D. A., Abdul, H. M., Opii, W., Newman, S. F., Joshi, G., Ansari, M. A., and Sultana, R. (2006) Pin1 in Alzheimer's disease, *J Neurochem 98*, 1697-1706.

[134] Lim J, and Lu, K. P. (2005) Pinning down phosphorylated tau and tauopathies, *Biochim Biophys Acta 1739*, 311-322.

[135] Balastik, M., Lim, J., Pastorino, L., and Lu, K. P. (2007) Pin1 in Alzheimer's disease: multiple substrates, one regulatory mechanism? *Biochim Biophys Acta 1772,* 422-429.

[136] Theuerkorn, M., Fischer, G., and Schiene-Fischer, C. (2011) Prolyl cis/trans isomerase signalling pathways in cancer, *Curr Opin Pharmacol 11*, 281-287.

[137] Cai, N., Li, M., Qu, J., Liu, GH., and Izpisua Belmonte, J. C. (2012) Post-translational modulation of pluripotency, *J Mol Cell Biol 4*, 262-265.

[138] Wilson, K. A., Bouchard, J. J., and Peng, J. W. (2013) Interdomain interactions support interdomain communication in human Pin1, *Biochemistry 52*, 6968-6981.

[139] Namanja, A. T., Wang, X. J., Xu, B., Mercedes-Camacho, A. Y., Wilson, K. A., Etzkorn, F. A., and Peng, J. W. (2011) Stereospecific gating of functional motions in Pin1, *Proc Natl Acad Sci U S A 108,* 12289-12294.

[140] Matena, A., Sinnen, C., van den Boom, J., Wilms, C., Dybowski, J. N., Maltaner, R., Mueller, J. W., Link, N. M., Hoffmann, D., and Bayer, P. (2013) Transient domain interactions enhance the affinity of the mitotic regulator Pin1 toward phosphorylated peptide ligands, *Structure 21*, 1769-1777.

[141] Peng, J. W., Wilson, B. D., and Namanja, A. T. (2009) Mapping the dynamics of ligand reorganization via ^{13}CH3 and ^{13}CH2 relaxation dispersion at natural abundance, *J Biomol NMR 45*, 171-183.

[142] Fanghanel, J., and Fischer, G. (2004) Insights into the catalytic mechanism of peptidyl prolyl cis/trans isomerases, *Front Biosci 9*, 3453-3478.

[143] Mueller, J. W., and Bayer, P. (2008) Small family with key contacts: Par14 and Par17 parvulin proteins, relatives of Pin1, now emerge in biomedical research, *Perspect Medicin Chem 2*, 22-20.

[144] Velazquez, H. A., and Hamelberg, D. (2013) Conformation-directed catalysis and coupled enzyme–substrate dynamics in Pin1 phosphorylation-dependent cis–trans isomerase, *J Phys Chem B 117,* 11509-11517.

[145] Velazquez, H. A., and Hamelberg, D. (2011) Conformational Selection in the Recognition of Phosphorylated Substrates by the Catalytic Domain of Human Pin1, *Biochemistry 50*, 9605-9615.

[146] Cavanagh, J., Fairbrother, W. J., Palmer III, A. G., and Skelton, N. J. (1996) *Heteronuclear NMR Experiments*, Academic Press, Inc., New York.

[147] Delaglio, F., Grzesiek, S., Vuister, G. W., Zhu, G., Pfeifer, J., and Bax, A. (1995) NMRPipe: A multidimensional spectral processing system based on UNIX pipes, *J Biomol NMR 6*, 277-293.

[148] Kobayashi, N., Iwahara, J., Koshiba, S., Tomizawa, T., Tochio, N., Güntert, P., Kigawa, T., and Yokoyama, S. (2007) KUJIRA, a package of integrated modules for systematic and interactive analysis of NMR data directed to high-throughput NMR structure studies, *J Biomol NMR 39,* 31-52.

[149] Johnson, B. (2004) Using NMRView to visualize and analyze the NMR spectra of macromolecules, In *Protein NMR Techniques* (Downing, A. K., Ed.), pp 313-352, Humana Press.

[150] Güntert, P. (2004) Automated NMR structure calculation with CYANA, In *Protein NMR Techniques* (Downing, A. K., Ed.), pp 353-378, Humana Press.

[151] Güntert, P. (2009) Automated structure determination from NMR spectra, *Eur Biophys J 38*, 129-143.

[152] Shen, Y., Delaglio, F., Cornilescu, G., and Bax, A. (2009) TALOS+: A hybrid method for predicting protein backbone torsion angles from NMR chemical shifts, *J Biomol NMR 44*, 213-223.

[153] Schwieters, C. D., Kuszewski, J. J., Tjandra, N., and Clore, G. M. (2003) The Xplor-NIH NMR molecular structure determination package, *J Magn Reson 160*, 65-73.

[154] Laskowski, R. A., Rullmannn, J. A, MacArthur MW, Kaptein R, and Thornton JM. (1996) AQUA and PROCHECK-NMR: Programs for checking the quality of protein structures solved by NMR, *J Biomol NMR 8*, 477 - 486.

[155] Jeener, J., Meier, B. H., Bachmann, P., and Ernst, R. R. (1979) Investigation of exchange processes by two-dimensional NMR spectroscopy, *J Chem Phys 71*, 4546-4553.

[156] d'Auvergne, E., and Gooley, P. (2008) Optimisation of NMR dynamic models I. Minimisation algorithms and their performance within the model-free and Brownian rotational diffusion spaces, *J Biomol NMR 40*, 107-119.

[157] d'Auvergne, E., and Gooley, P. (2008) Optimisation of NMR dynamic models II. A new methodology for the dual optimisation of the model-free parameters and the Brownian rotational diffusion tensor, *J Biomol NMR 40*, 121-133

[158] Walker, O., Varadan, R., and Fushman, D. (2004) Efficient and accurate determination of the overall rotational diffusion tensor of a molecule from ^{15}N relaxation data using computer program ROTDIF, *J Magn Reson 168*, 336-345.

[159] Long, D., Liu, M., and Yang, D. (2008) Accurately probing slow motions on millisecond timescales with a robust NMR relaxation experiment, *J Am Chem Soc 130*, 2432-2433.

[160] Carver, J. P., and Richards, R. E. (1972) A general two-site solution for the chemical exchange produced dependence of T2 upon the carr-Purcell pulse separation, *J Magn Reson 6*, 89-105.

[161] Price, K. V., Storn, R. M., and Lampinen, J. A. (2005) *Differential Evolution*, Springer-Verlag, Berlin.

[162] Shiraki, T., Kamiya, N., Shiki, S., Kodama, T. S., Kakizuka, A., and Jingami, H. (2005) Alpha,beta-unsaturated ketone is a core moiety of natural ligands for covalent binding to peroxisome proliferator-activated receptor gamma, *J Biol Chem 280*, 14145-14153.

[163] Kim, P. S., and Baldwin, R. L. (1982) Influence of charge on the rate of amide proton exchange, *Biochemistry 21*, 1-5.

[164] Neuhaus, D., and Williamson, M. P. (1989) *The nuclear Overhauser effect in structural and conformational analysis*, VCH Publishers Ltd., United Kingdom.

[165] Smirnov, S. N., Golubev, N. S., Denisov, G. S., Benedict, H., Schah-Mohammedi, P., and Limbach, H.-H. (1996) Hydrogen/Deuterium isotope effects on the NMR chemical shifts and geometries of intermolecular low-barrier hydrogen-bonded complexes, *J Am Chem Soc 118*, 4094-4101.

[166] Pelton, J. G., Torchia, D. A., Meadow, N. D., and Roseman, S. (1993) Tautomeric states

of the active-site histidines of phosphorylated and unphosphorylated III^{Glc}, a signal-transducing protein from Escherichia coli, using two-dimensional heteronuclear NMR techniques, *Protein Sci 2*, 543-558.

[167] Markus, M. A., Dayie, K. T., Matsudaira, P., and Wagner, G. (1996) Local mobility within villin 14T probed via heteronuclear relaxation measurements and a reduced spectral density mapping, *Biochemistry 35*, 1722-1732.

[168] Lipari, G., and Szabo, A. (1982) Model-free approach to the interpretation of nuclear magnetic resonance relaxation in macromolecules. 1. Theory and range of validity, *J Am Chem Soc 104*, 4546-4559.

[169] Labeikovsky, W., Eisenmesser, E. Z., Bosco, D. A., and Kern, D. (2007) Structure and dynamics of Pin1 during catalysis by NMR, *J Mol Biol 367*, 1370-1381.

[170] Bailey, M. L., Shilton, B. H., Brandl, C. J., and Litchfield, D. W. (2008) The dual histidine motif in the active site of Pin1 has a structural rather than catalytic role, *Biochemistry 47,* 11481-11489.

[171] Zhou, P., Tian, F., Lv, F., and Shang, Z. (2009) Geometric characteristics of hydrogen bonds involving sulfur atoms in proteins, *Proteins 76*, 151-163.

[172] Sultana, R., Boyd-Kimball, D., Poon, H. F., Cai, J., Pierce, W. M., Klein, J. B., Markesbery, W. R., Zhou, X. Z., Lu, K. P., and Butterfield, D. A. (2006) Oxidative modification and down-regulation of Pin1 in Alzheimer's disease hippocampus: A redox proteomics analysis, *Neurobiology of aging 27*, 918-925.

[173] Hall, D. A., Vander Kooi, C. W., Stasik, C. N., Stevens, S. Y., Zuiderweg, E. R., and Matthews, R. G. (2001) Mapping the interactions between flavodoxin and its physiological partners flavodoxin reductase and cobalamin-dependent methionine synthase, *Proc Natl Acad Sci U S A 98*, 9521-9526.

[174] Holzer, M., Gärtner, U., Stöbe, A., Härtig, W., Gruschka, H., Brückner, M. K., and Arendt, T. (2002) Inverse association of Pin1 and tau accumulation in Alzheimer's disease hippocampus, *Acta Neuropathol 104*, 471-481.

Acknowledgements

I acknowledge to Professor Shin-ichi Tate for giving me a chance to continue NMR study in Japan and having supervised me for three years. I came to Japan with no knowledge about NMR. Professor Shin-ichi Tate taught me from the beginning of the study-the basic backbone and side chain assignment. Here, I thank Mr. Shin-ichi Tate very much again!

I thank assistant professor Naoya Tochio for helping me in the past one and half years sincerely. I thank Professor Naohiro Kobayashi for providing the free useful software KUJIRA. I thank Professor Naoko Utsunomiya-Tate, Kazuhiko Igarashi, and Takuma Shiraki for the help in my research.

I thank associate Professor Katsuo Katayanagi and assistant Professor Eiji Ohmae in the lab. I thank Dr. Shogo Nakano for helping me study linux system. I thank Dr. Jun-ichi Uewaki for experiment support. I thank Yu Tamari working in one organic chemistry company for supporting perfect samples. I thank the members in my lab.

公表論文

(1). The C113D mutation in human Pin1 causes allosteric structural changes in the phosphate binding pocket of the PPIase domain through the tug of war in the dual-histidine motif

(ヒトPin1タンパク質C113D変位は二重ヒスチジンモチーフ中の綱引きによりアロステリックにPPIaseドメインのリン酸基結合ポケット構造を変化させる)

著者　Xu, N., Tochio, N., Wang, J., Tamari, Y., Uewaki, J., Utsnomiya-Tate, N., Igarashi, K., Shiraki, T., Kobayashi, N., and Tate, S.
(徐　宁, 栃尾尚哉，王　静，玉利　佑，上脇準一，楯（宇都宮）直子，五十嵐和彦，白木琢磨，小林直宏，楯　真一)

(学会誌) *Biochemistry*, **53** (34), (2014), 5568-5578.